DAMPIER PORT AUTHORITY: MARINE ENVIRONMENTAL MODELLING

Final Report

17th December 2009

Prepared for:
Dampier Port Authority

Document control form

Document draft	*Originated by*	*Edit & review*	*Authorized for release by*	*Date*
Draft 1 - Issued for internal review	*M. Zed* *M. Burling*			*25 Nov 2009*
Draft 2- issued for client review	*M. Zed* *M. Burling*	*M. Burling*	*M. Burling*	*30 Nov 2009*
Final Report- issued to client	*M. Zed* *M. Burling*	*M. Burling*	*M. Burling*	*17 Dec 2009*

Document name: APASA - DPA DredgeModelling.doc

APASA Project Number: J0056

APASA Project Manager: Murray Burling

DISCLAIMER:

This document contains confidential information that is intended only for use by the client and is not for public circulation, publication, nor any third party use without the approval of the client.

Readers should understand that modelling is predictive in nature and while this report is based on information from sources that Asia-Pacific ASA Pty Ltd. considers reliable, the accuracy and completeness of said information cannot be guaranteed. Therefore, Asia-Pacific ASA Pty Ltd., its directors, and employees accept no liability for the result of any action taken or not taken on the basis of the information given in this report, nor for any negligent misstatements, errors, and omissions. This report was compiled with consideration for the specified client's objectives, situation, and needs. Those acting upon such information without first consulting Asia-Pacific ASA Pty Ltd., do so entirely at their own risk.

Contents

Figures

Tables

EXECUTIVE SUMMARY

Asia-Pacific ASA (APASA) has been commissioned by the Dampier Port Authority (DPA) to undertake a marine modelling study to assess suspended sediment plumes, potential coastal impacts and oil spill risks associated with developing infrastructure for the expansion of its existing cargo wharf and port facilities in Dampier, Western Australia. The project, known as the Dampier Marine Services Facility project, involves dredging over 2.1 million cubic metres of material from the harbour and the construction of a reclamation area of approximately 248,000 m^2.

The sediment plume modelling has been conducted in a number of stages. The initial stages involved the analysis of environmental data and selection of two dredging simulation scenarios to represent the ambient and more energetic conditions likely to be experienced during operations. Current (HYDROMAP) and wave (SWAN) models were developed using these environmental forcing conditions and calibrated against available observations. A variety of current and wave parameters were included in the calibration process, with detailed investigations into the appropriate specification of wave and current dynamics specific to the site and its surrounding waters. As the dredging is proposed to occur over the cyclone season of November to March, three realistic cyclone events were included in the energetic scenario with their effects incorporated into the current and wave models. The models developed during the final calibration demonstrated a high level of agreement with field observations.

Two eight month hindcast databases were generated from the calibrated models, representing the ambient and energetic scenarios, for use in the ASA sediment fate modelling package, DREDGEMAP. Particle size distributions were determined through examining geotechnical work performed on bores extracted directly from the dredging zone. The resultant distribution used in the model was similar to that employed for the Pluto Dredge Modelling Project. The suspension rate from the cutterhead was set to a slightly more conservative value (0.5 % of the production rate) than previously used in the Pluto work. Outfall discharge concentration was provided by the DPA and set at 170 mg/l in the model, with this constituting only the fine, more dispersive materials present in the geotechnical analysis.

Downtime as a result of regular daily dredger maintenance, coral spawning periods, cyclone closure (energetic scenario only) and exceedance of limiting sea state conditions were included in real-time into the model using a designated start date of the 1st of November 2010. Taking into account the dredge volumes and cut paths (provided by the dredge consultant) and associated downtime it was estimated that under ambient and energetic conditions the dredging would take approximately 159 and 173 days respectively. Using this information, dredge dispersion modelling was then conducted for the entire duration of the dredging operations plus a period of time after cessastion of the works to assess longer term fate.

The dredge modelling has assessed total suspended solids (TSS) concentrations and sedimentation against the thresholds employed for the Pluto Dredging Project. These thresholds were considered appropriate for the present study following monitoring work

during and after the Pluto dredging operations that suggested that the thresholds represented substantially conservative levels for coral mortality.

The findings from the sediment fate modelling and analysis were:

- The suspended sediment plume is predicted to be relatively close to the Dampier coast, with concentrations above 20 mg/l restricted to the immediate region surrounding the dredge zone.
- Results for the ambient and energetic simulations show that the sediment plume is expected to be dominantly transported north-east, with movement southwards towards King Bay stronger during the ambient run.
- Both scenarios indicated that the plume would extend only as far as 4 to 5 km from the dredge zone with concentrations in excess of 5 mg/l above background.
- The highest sustained plume concentrations were within 200 m of the outfall discharge point along the northern reclamation wall, with concentrations in excess of 25 mg/l observed here 6-7 % of the time during both scenarios.
- Exceedance of the nearshore TSS threshold of 35 mg/l was predicted to occur primarily within the immediate vicinity of the outfall discharge site, and to a lesser degree within the dredge zone and adjacent BLB turning basin.
- Offshore exceedances were predicted during the energetic scenario as a result of resuspension during cyclone events, however, these are not expected to be significantly in excess of background rates.
- Exceedance of acute sedimentation thresholds are predicted to occur within the dredge zone and to a lesser extent within approximately 100 m of its perimeter.
- The most severe acute exceedances are predicted to occur within 200 m of the outfall discharge zone, where more than 50 days of exceedance was predicted during the dredging operations.
- Exceedance of the medium and chronic term thresholds are expected to be restricted to the extents of the dredge zone and predicted to be exceeded less than 15 days over the entire dredge operation.
- Areas more than 5 km from the DMSF development site are predicted to remain below the designated TSS and sedimentation thresholds for the entire dredging operation under ambient conditions.

An assessment of the sedimentation level expected to occur within the Pluto turning basin immediately north of the proposed dredge area was also completed. An assessment of the overall bottom thickness increase as a result of dredging indicated an average increase of 0.6 to 1.6 mm over the entire turning basin, with a maximum increase of 11 mm along the south-western extent.

Oil spill dispersion modelling was conducted to assess the exposure risk of an accidental hydrocarbon release at the port. The trajectory, dispersion and weathering of four oil spill

scenarios have been modelled using ASA's oil spill fates and effects model, SIMAP. This included a summer and winter simulation of both a 50,000 litre heavy fuel oil spill off the face of the wharf and 2,500 litre diesel fuel spill from alongside the wharf. A variety of thresholds were employed when examining the surface oil, shore stranded oil and entrained oil exposure with each set at conservative levels based on their documented environmental impacts.

The findings from the oil spill modelling are:

- Weathering analysis of heavy fuel oil indicated only a 10 % reduction in its mass would occur over a period of 5 days, whilst 40 % of the diesel fuels mass will evaporate over the first two days of exposure.
- The heavy fuel oil would likely drift north-east against the Burrup Peninsula toward Angel Sound during summer and west toward East and West Lewis Islands during winter.
- Probabilities of surface oil thicknesses harmful to seabirds in excess of 40 % were restricted to 5-6 km in a northeast direction from the spill site during summer and 3-4 km directly offshore during winter.
- The model predicts that the heavy oil will contact the shoreline somewhere within Mermaid Sound, with an 83 % probability that this will occur to the immediate north of the release site during summer and 57% probability of contact to the eastern shoreline of East Lewis Island during winter.
- Simulations indicated there would be no build up of entrained heavy fuel oil underneath slicks.
- There were no slicks predicted to reach levels detrimental to seabirds for the diesel fuel spill, with exceedances of lower thresholds only moderate even in exposed areas.
- Prevailing winds during summer again moved the diesel slicks northeast along the Burrup Peninsula, with winter characterised by offshore movement as with the heavy fuel oil scenarios.
- During winter, shoreline exposure to the Burrup Peninsula near the release site has a probability of 60 %,with a 30 % probability of shoreline exposure for East Lewis Island.
- The highest probability of entrained diesel concentrations being above 1 ppb is predicted to be lower than 40 %, relevant only for the waters in close vicinity of the release site and in Withnell Bay during summer.
- During winter, the predicted probability of entrained diesel concentrations above 1 ppb was below 20 %.

An assessment of the changes to the beach dynamics to the immediate north of the site was also conducted with the key findings being:

- The proposed development will have only a minor effect on the current and wave conditions at the beach to the immediate north of the DMSF site, with its effect on tides negligible.
- The reclamation zone construction and dredging is expected to marginally alter the current and wave energy at the beach zone, with an expected reduction in the overall magnitude at the southern extents of the beach.
- This effect on the beach dynamics is highly localised with impacts north of the beach expected to be negligible.

1 INTRODUCTION

The Dampier Port Authority (DPA) is seeking to expand the capacity of its operations in Dampier, Western Australia. The project, known as the Dampier Marine Services Facility (DMSF) project, involves the expansion of the existing Dampier Cargo Wharf (DCW) and Port facilities. The expansion includes dredging approximately 2.1 million cubic metres (in-situ volume) of sand, clay and rock material from the harbour and the construction of a reclamation area of approximately 248,000 m^2. Following the completion of the reclamation area, a piled jetty will be constructed with part of the reclamation wall converted to sheet piling for use as additional berthing space.

Before dredging commences a rock wall of slope 1:1.5 will be constructed at the perimeter of the reclamation area, with up to two flow-out weir boxes placed along this wall. Dredged material will be mobilised by the action of the cutterhead and pumped directly into the reclamation area through a discharge pipe (no trailer utilised). Dredging is expected to take approximately 4 to 6 months to complete and is programmed to start on the 1st of November 2010 and continue to mid 2011.

The DPA has undertaken a number of stages of assessment and review and arrived at an offshore option for the development. The location of the proposed development and harbour layout is shown in drawing 42906759-037-B (reproduced in Appendix A). Asia-Pacific ASA (APASA) has been commissioned to model suspended sediment plumes that could be generated by the dredging operations and filling of reclamation areas relevant to this option. Oil spill modelling has also been completed for four scenarios.

This report documents the existing marine conditions, the setup of the required models and the model outcomes.

1.1 Scope of Work

The scope of work included:

- Source and format available wind and wave data for use in model development, validation and analysis.
- Modifying the existing APASA hydrodynamic and wave models that were used for the Pluto Dredging project to represent the proposed port expansion layout. Perform additional runs and further validation against recent current and wave measurements made at the site and offshore. The models developed for the Pluto project were used with the permission of Woodside Energy Limited (WEL).
- Produce a model hindcast database over two separate 8 month periods, representing ambient and above-average conditions (herein referred to as the energetic scenario) scenarios. As the dredging is proposed to occur over the cyclone season (expected to be late 2010 to mid 2011) up to three cyclones were included in the energetic scenario.

- Sediment fate modelling to determine the likely effects of the proposed dredging programme:
    - Calculate cumulative suspended sediment concentrations (SSC) and sedimentation values.
    - Generate contour maps of SSC and sedimentation.
    - Undertake percentile analysis for SSC and sedimentation rates.
    - Perform threshold analysis based on values used in the Pluto Dredging Project and considered appropriate for this study.
- Model the fate of four oil spill scenarios.
- Assessment of the construction related sedimentation expected to occur within the Woodside turning basin to investigate WEL concerns.
- Analysis of changes to the current, wave and tide conditions at the beach to the immediate north of the study site.

1.2 Study Datums

Water depths and levels presented in this report are with respect to Mean Sea Level (MSL) unless otherwise stated and are in units of meters.

Positions are satellite derived from the Global Positioning System using the WGS 1984 datum, unless stated otherwise. Position units are in latitude/longitudes in decimal degrees.

All units are in standard SI units.

2 METOCEAN CHARACTERISTICS OF THE SITE

2.1 Metocean Data Sources and Assumptions

Meteorological and oceanographic data for this study was obtained from a number of sources, including wind stations, ocean buoys and recent Acoustic Doppler Current Profiler (ADCP) measurements made by APASA. The wind stations and offshore measurement stations used in the study are illustrated in Figure 2-1.

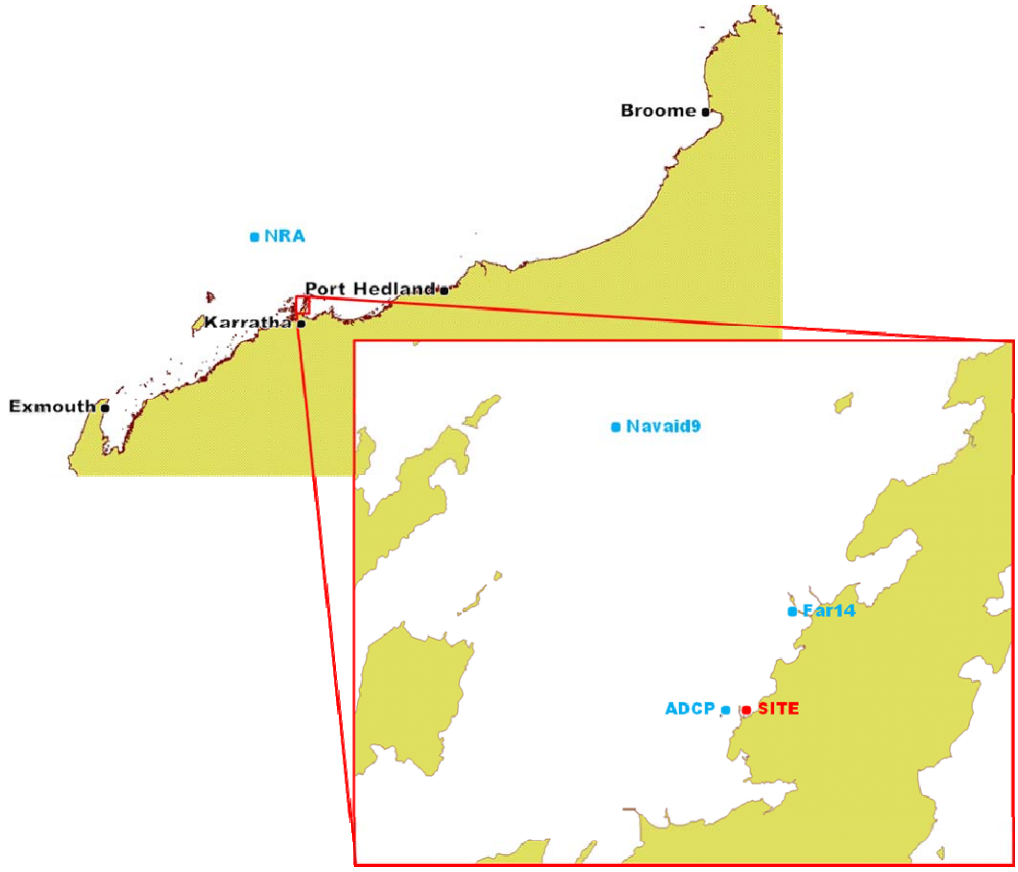

Figure 2-1 Location of observational wave and current data obtained for the study. Measurement stations are shown in blue. DPA site is annotated in red.

The geographical coordinates of each of these stations along with their record depths (or elevation in the case of the wind measurements), period of record and data source are summarised in Table 2-1.

Table 2-1 Details of measurement stations

Station	Location	Depth	Period of Record	Data Source
NRA	116.1667 E, 19.6153 S	125 m	January 2005 - August 2009	RPS MetOcean/WEL
Navaid9	116.7164 E, 20.5464 S	16 m	January 2005 - August 2009	RPS MetOcean/WEL
Far14	116.7627 E, 20.5898 S	35 m ASL	January 2005 - August 2009	RPS MetOcean/WEL
ADCP	116.7441 E, -20.6150 S	12 m	May 2009 - June2009	APASA

All datasets were analysed and converted to standard SI units where necessary. Any unrealistic outliers were removed as part of a quality control process to maintain accuracy in the subsequent model development and validation. Publicly available global model output and online tide and cyclone databases were also utilised for model development and validation. These are further described in Sections 3 and 4.

2.2 Tides

Tides at Dampier are semi-diurnal (two highs and two lows per day) with a mean spring tidal range of 3.7 m (ANTT, 2008). The tidal plane information is given in Table 2-2.

Table 2-2 Tidal planes at King Bay, Dampier (after ANTT, 2008)

Tidal Plane	Elevation Above Datum (m)
HAT (Highest Astronomical Tide)	5.0
MHWS (Mean High Water Springs)	4.4
MHWN (Mean High Water Neaps)	3.1
MSL (Mean Sea Level)	2.6
MLWN (Mean Low Water Neaps)	2.1
MLWS (Mean Low Water Springs)	0.7
LAT (Lowest Astronomical Tide)	0.1

A typical tidal elevation time-series is shown in Figure 2-2. Note the transition from spring to neaps to springs again occurring at intervals of 14.5 days, approximately half the length of the lunar (synodic) cycle.

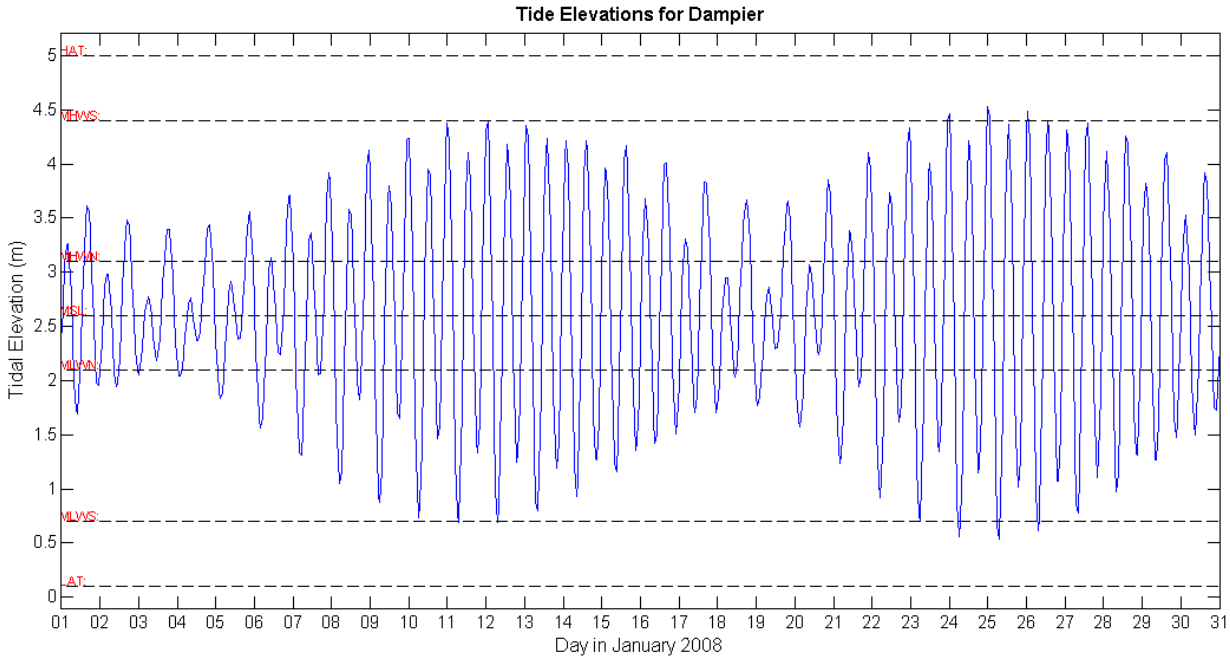

Figure 2-2 Typical tidal elevation time-series at Dampier. Period shown is 1 January 2008 to 30 January 2008 and elevation is shown as metres above datum, which is Lowest Astronomical Tide (LAT).

2.3 Winds

Wind measurements were taken approximately 3km northeast of the site at the WEL Far14 wind station located just offshore from their LPG jetty. This was extremely useful as it was expected to capture localised seabreeze effects that were not likely to be as pronounced at the Bureau of Meteorology Karratha wind station.

Analysis of this wind dataset indicated that the dominant wind direction at the site oscillated during the year from WSW during spring and summer to ESE in winter as illustrated in the seasonal wind rose plots in Figure 2-3.

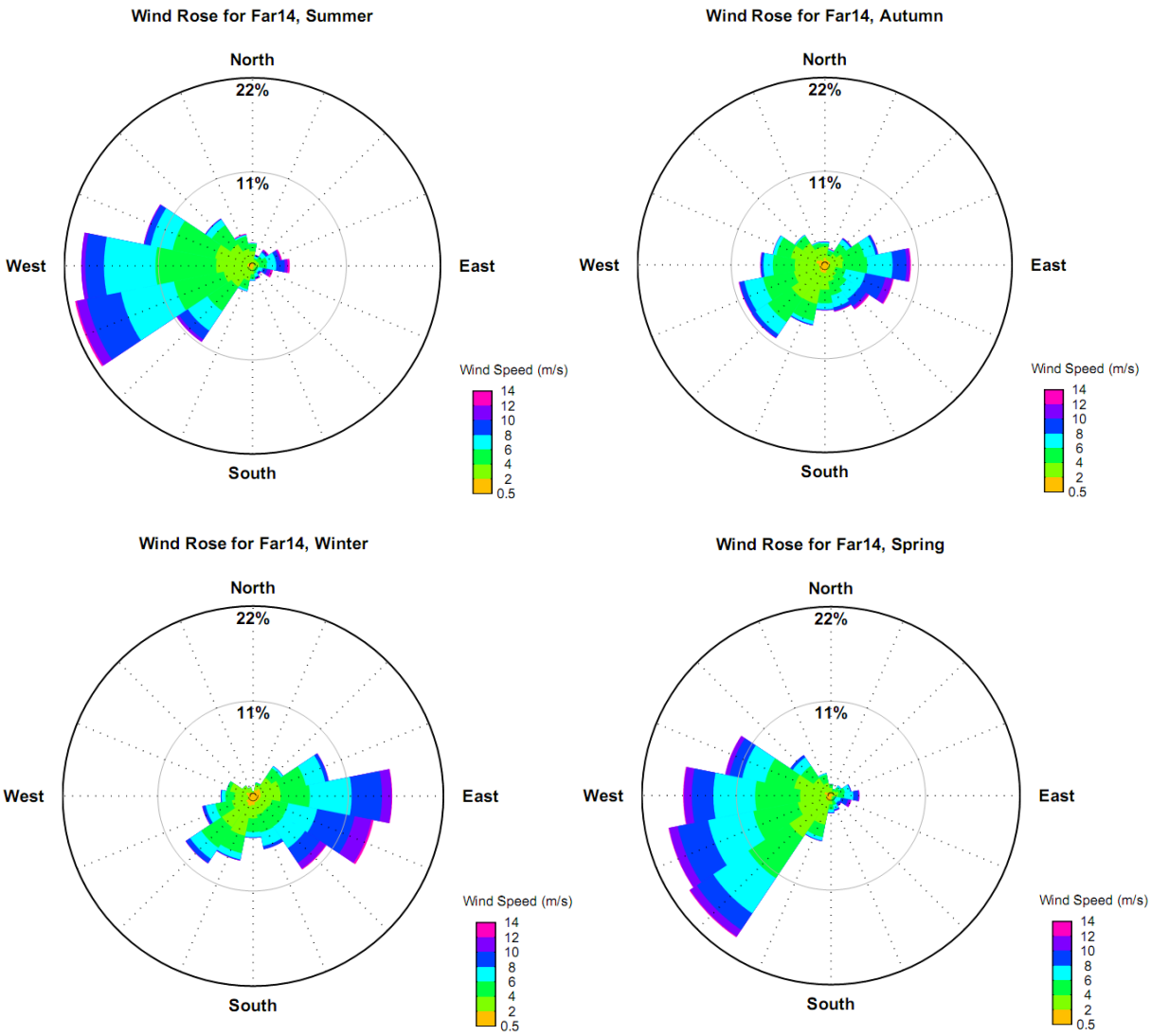

Figure 2-3 Seasonal rose plots of wind speed and direction as measured at the Far14 wind station. Data shown includes measurements from January 2005 to August 2009. The roses show the percentage occurrence of wind direction (direction FROM) around the compass, with colour coding indicating the proportion in each speed class.

Wind magnitudes are relatively consistent throughout summer, winter and spring with winds in excess of 10 m/s (~20 knots) occurring approximately 4 to 5 % of the time during each of these seasons. The transitional season of autumn is characterised by calmer conditions with winds exceeding 10 m/s less than 3 % of the time with near equal portions occurring from the WSW and ESE directions. Although most of the winds during summer occur from the west to south-westerly directions, the strongest winds tend to occur from the east.

2.4 Currents

The nearshore hydrodynamics were investigated through an ADCP deployment completed by APASA from the 12th of May to the 9th of June 2009. The ADCP was deployed near the end of the DPA Bulk Liquids Berth (BLB) at 116.744 ^{o}E, 20.615 ^{o}S in approximately 12 m of water. The ADCP recorded measurements of current speed and direction at 0.5 m increments through the water column every 10 minutes. The records were analysed to identify variations through the water column in both speed and direction. Current roses derived from this analysis are presented below in Figure 2-4 for the seabed, mid-depth and surface depths.

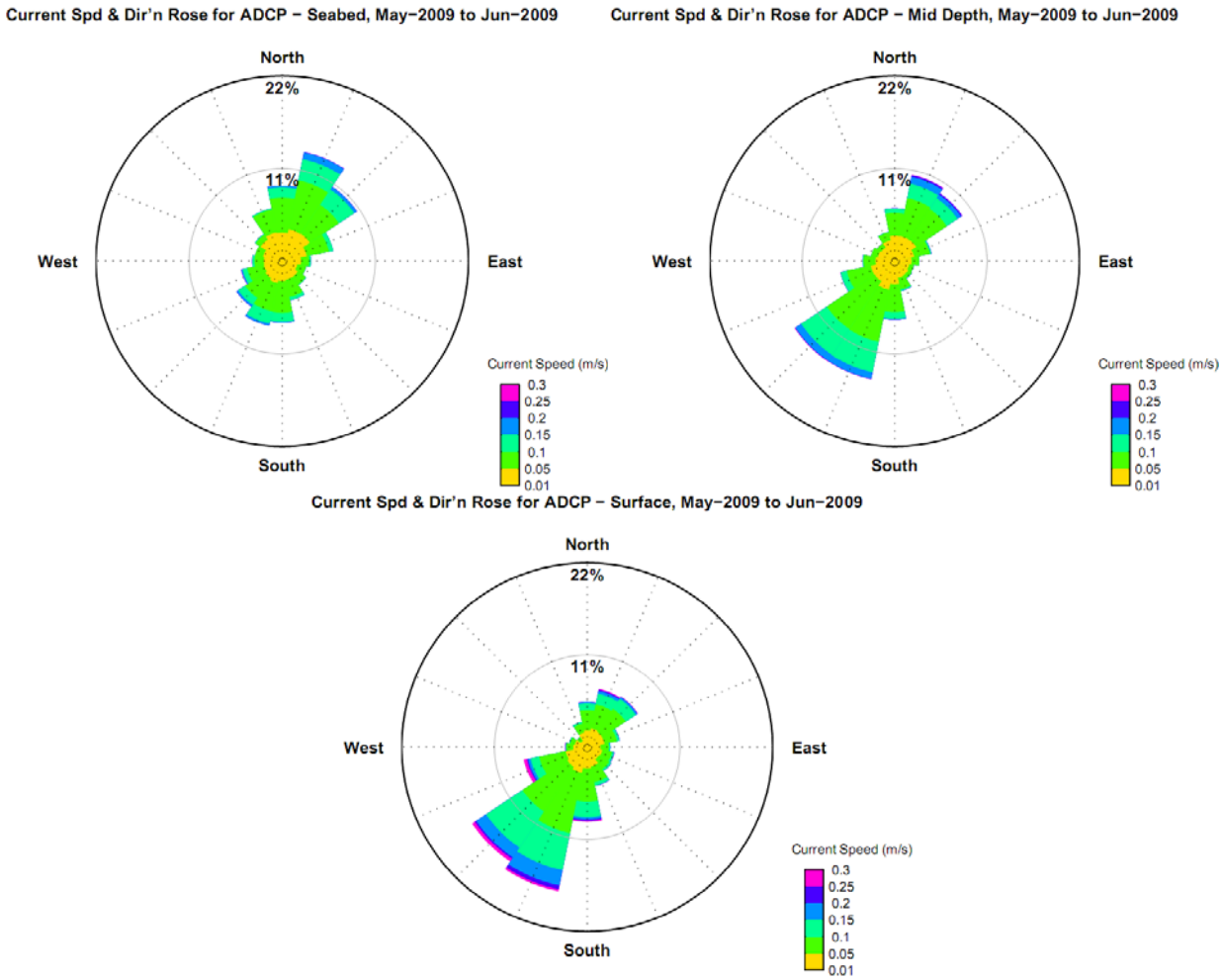

Figure 2-4 Current speed and direction rose plots extracted from the ADCP measurements at the seabed (top left), mid depth (top right) and surface (bottom) depths. The roses show the percentage occurrence of wind direction (direction TOWARDS) around the compass, with colour coding indicating the proportion in each speed class.

Data from the ADCP indicate that the dominant current direction is in the NNE and SSW directions throughout the entire water column, clearly indicating the dominance of the tidal (i.e. barotropic) component steered by the local bathymetry in the hydrodynamics near the site. Near surface currents show a larger portion of currents heading NNE (ebb dominated), with a transition occurring towards the seabed to SSW (flood) dominated currents. Current speeds

vary slightly through the water column with a maximum of 0.22 m/s recorded at the seabed and 0.29 m/s at the surface.

2.5 Waves

Wave information was obtained at three sites:

- Offshore at the WEL North-Rankin A (NRA) platform
- In central mermaid sound at Navaid 9
- The ADCP deployed near the site.

Each of these locations are presented graphically in Figure 2-1. The Navaid 9 and ADCP measurements have been analysed to define the offshore and local wave climate for the site. Rose plots of wave height and period against direction for the ADCP measurements are presented in Figure 2-5, with conditions assumed to be representative of the winter period.

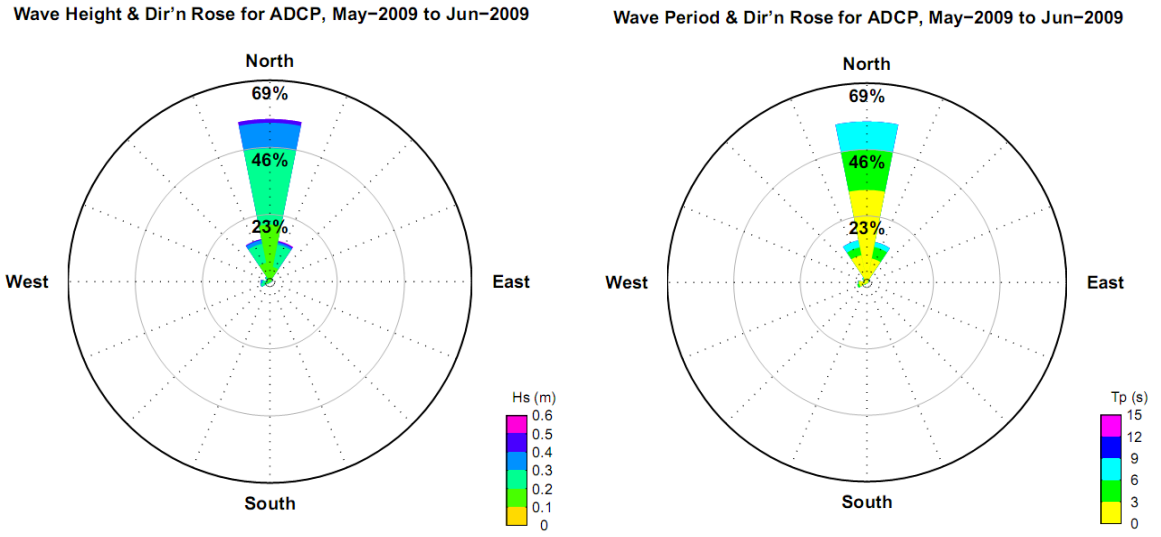

Figure 2-5 Rose plots of wave height and direction (left) and wave period and direction (right) from the ADCP measurements. The roses show the percentage occurrence of wind direction (direction FROM) around the compass, with colour coding indicating the proportion in each height, or period class as appropriate.

The ADCP wave measurements, containing the shortest data record of the three sources, clearly indicate the dominance of northerly waves at the site during the deployment period, with less than 5 % occurring from the SW direction. The wave climate is moderate with 99 % of waves incident at the site having a significant wave height (Hs) of less than 0.5 m and peak wave period (Tp) less than 9 s.

The offshore wave climate, within greater Mermaid Sound as defined by the Navaid 9 buoy, is illustrated by the wave height and direction roses in Figure 2-6. The Navaid 9 measurements again show the dominance of waves occurring from the north within Mermaid Sound. The more exposed location of the buoy means that larger swells are experienced as indicated in the plots, with Hs exceeding 0.5 m approximately 20 % of the time during a typical summer and 27 % of the time during winter. Overall the transitional seasons of spring and autumn are characterised by the lowest wave climate, with wave heights in excess of 0.5 m Hs occurring less than 15 % of the time.

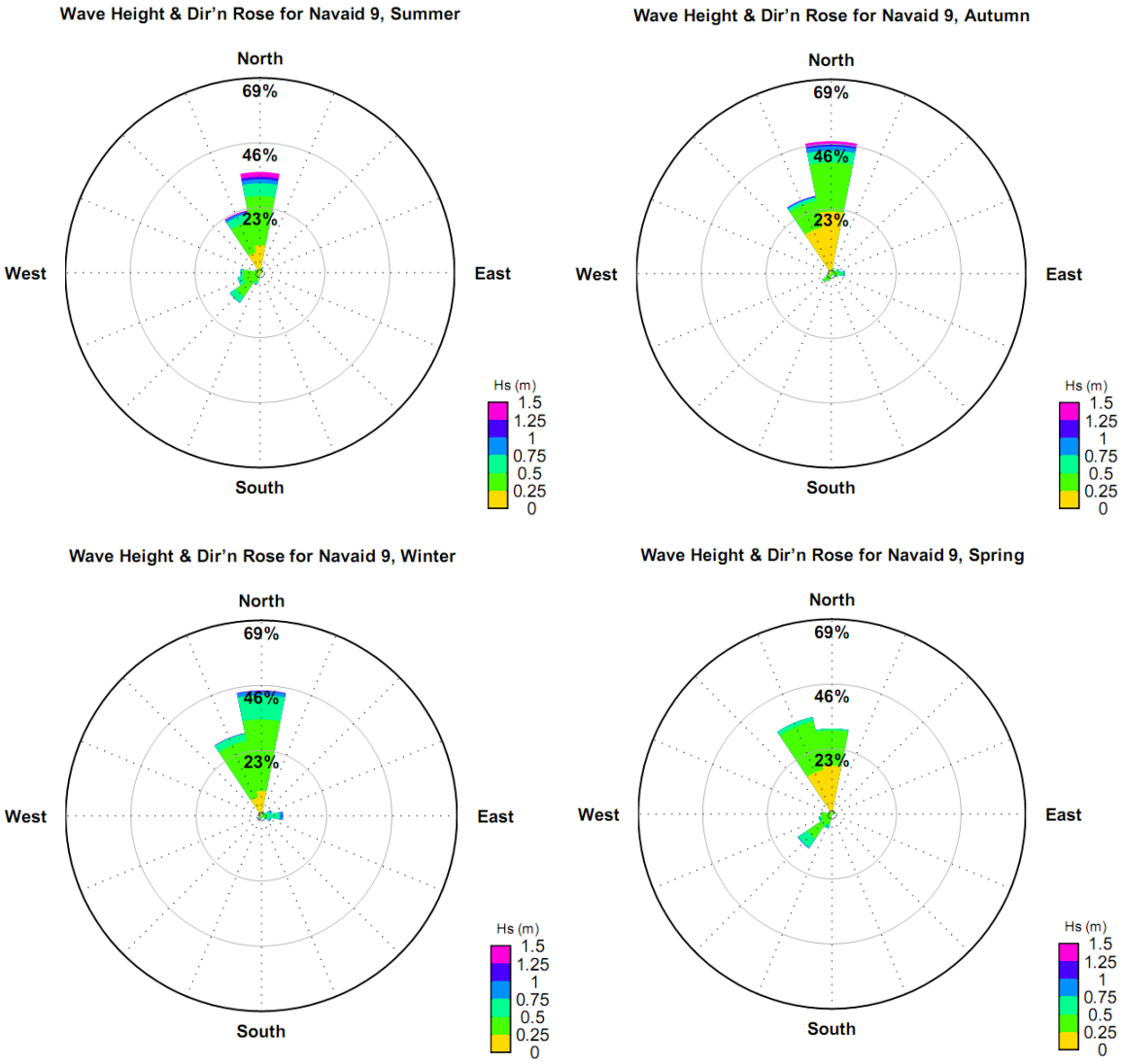

Figure 2-6 Seasonal rose plots of wave height and direction from Navaid 9 measurements. The roses show the percentage occurrence of wave direction (direction FROM) around the compass, with colour coding indicating the proportion in each height, or period class as appropriate. Data shown includes measurements from January 2005 to August 2009.

3 HYDRODYNAMIC MODELLING

3.1 Model Description

The three-dimensional currents were generated using a large scale ocean/coastal circulation model, HYDROMAP, which has been successfully applied in many regions around the world (Isaji et al., 2001, Zigic et al., 2003).

HYDROMAP is formulated to describe the locally induced flow field when tides and winds are the most important forcings. The HYDROMAP model solves for the three-dimensional Navier–Stokes equations under an incompressible flow assumption for Newtonian fluids with the inclusion of the Coriolis terms. The equations are solved using a Cartesian coordinate system and include the non-linear acceleration terms. The dominant frictional forces are assumed to be the vertical diffusion of momentum due to wind shear at the water surface, and friction at the sea bed. The horizontal diffusion of momentum is neglected. Also, vertical accelerations are neglected and the pressure distribution is assumed to be hydrostatic. These assumptions are valid for modelling the wind and tidal driven circulation over the area of interest.

The hydrodynamic equations of motion are solved using a finite difference grid in the horizontal (x,y) coordinates and the Galerkin method in the vertical (z) coordinate. The numerical solution methodology follows that of Davies (1977) with further developments for model efficiency by Owen (1980) and Gordon (1982) (Davies, 1977a, Gordon, 1982, Owen, 1980) and more recently by ASA. The finite difference scheme is fully explicit and uses a space staggered grid scheme with vertical velocities specified at the center of each grid cell, and the horizontal velocities given at the grid cell faces. To allow for time steps larger than the Courant-Friedrichs-Lewy (CFL) condition, the free-surface elevation is treated separately from the internal, three-dimensional flow variables. The scheme has been extensively tested through comparison with analytic solutions for:

- one-dimensional standing tidal wave in a rectangular basin;
- wind driven flow in a closed domain;
- cones test case for testing the advection scheme using a squared-shaped basin bounded by solid walls.

HYDROMAP has also been validated against measured currents and water elevations in hundreds of applications worldwide.

A detailed presentation of the model and applications can be found in Isaji and Spaulding (1984) and more detail on the extensive comparison with analytical solutions is found in Owen (1980) (Isaji and Spaulding, 1984).

3.2 Domain and Bathymetry

The model domain established for this study needed to be large enough to capture the full effects of wind and tidal induced forcing on the circulation within the coastal region near the site. As such, a large model domain was created, with extents illustrated in Figure 3-1, spanning approximately 70 km in an east west direction (Longitude 116.37 to 117.04 ^{O}E) and 63 km in a north south direction (Latitude 20.27 to 20.82 ^{O}S).

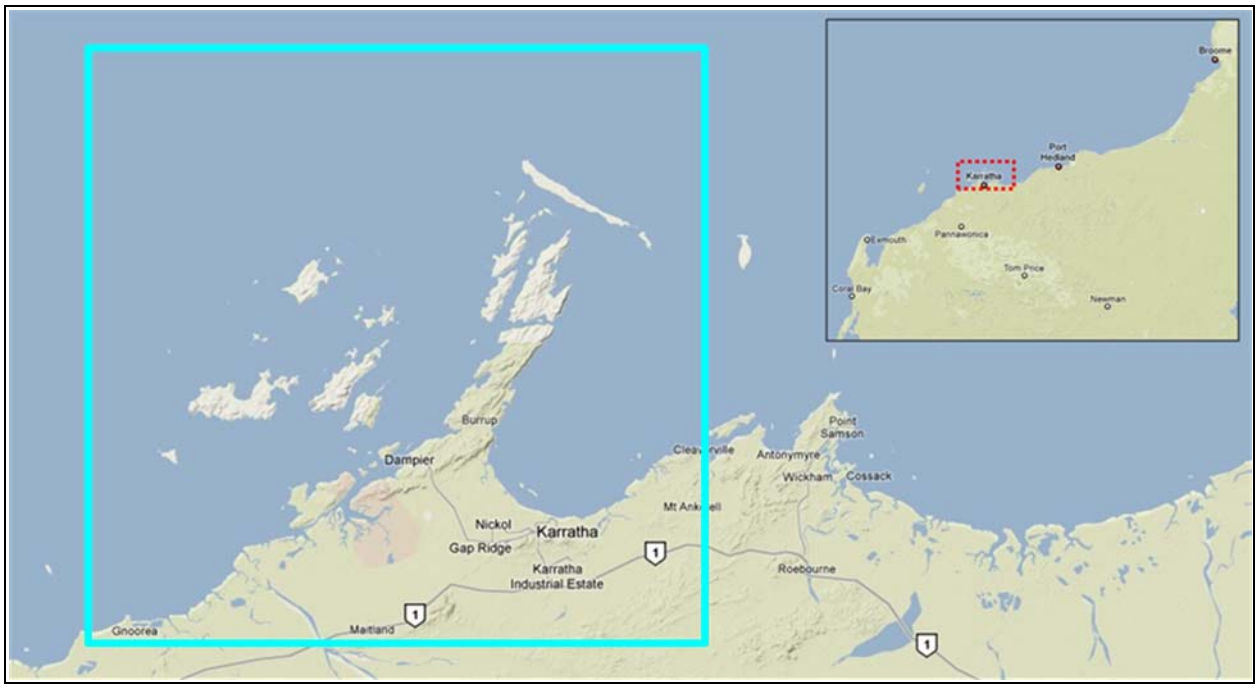

Figure 3-1 Locality map and Hydromap domain shown by the red box.

The hydrodynamic grid used a nested sub-gridding approach which allowed for higher resolution around areas of specific interest or where complex bathymetries or morphologies occur. Computational cell sizes (square) ranged from 1600 m at a coarse scale down to 100 m at the finest scale. Figure 3-2 shows examples of the variable grid resolution employed in the model. The final validated grid consisted of approximately 18,000 active computational water cells.

Bathymetry used in the model was obtained from multiple sources, including APASA's existing dataset from the earlier Pluto works and recent survey data of the waters near the site in July 2009. The bathymetry, as mapped onto the hydrodynamic grid, is illustrated in Figure 3-3.

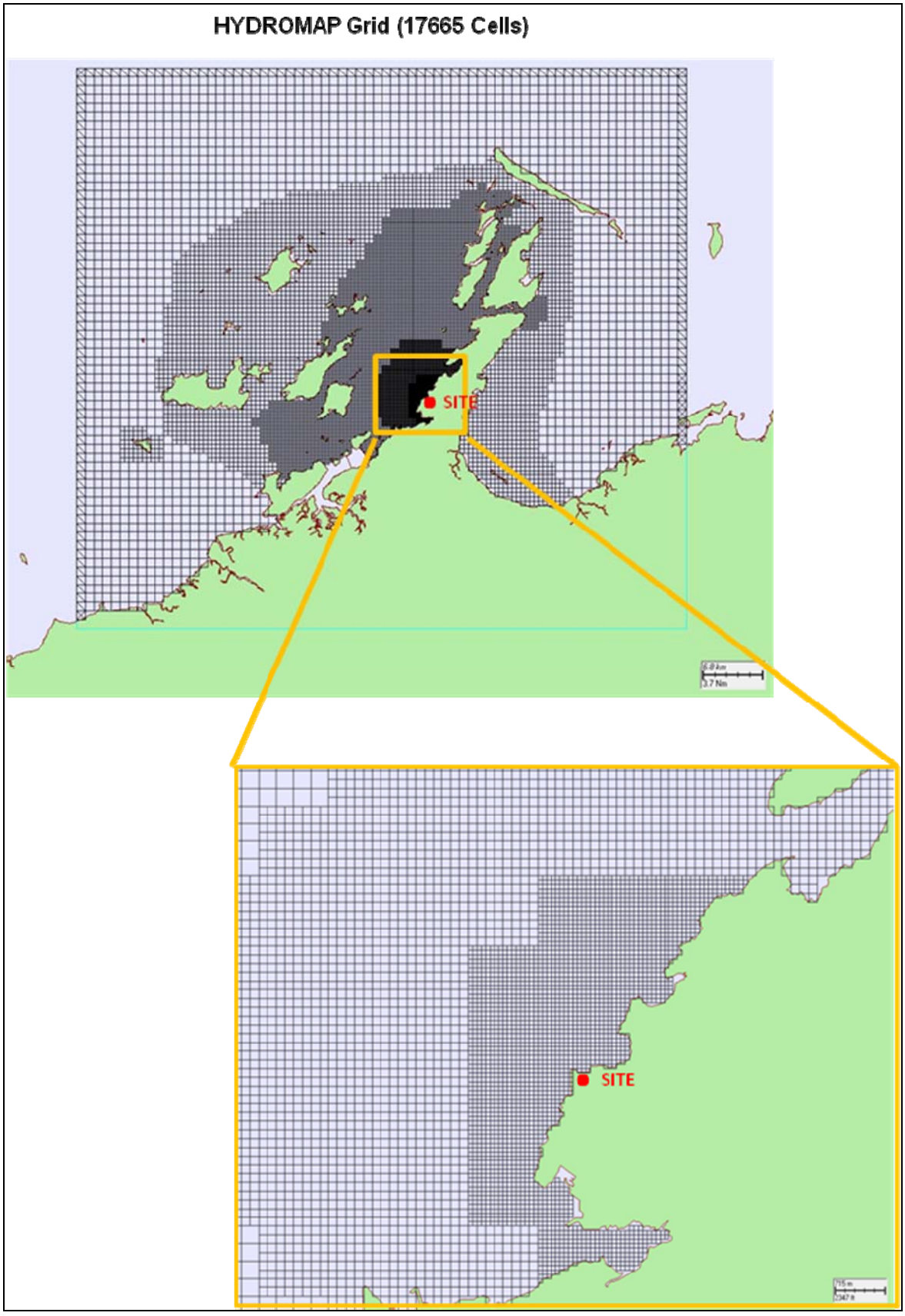

Figure 3-2 Hydrodynamic grid used in HYDROMAP. Second zoom highlights the transition from coarse resolution to fine resolution within the domain.

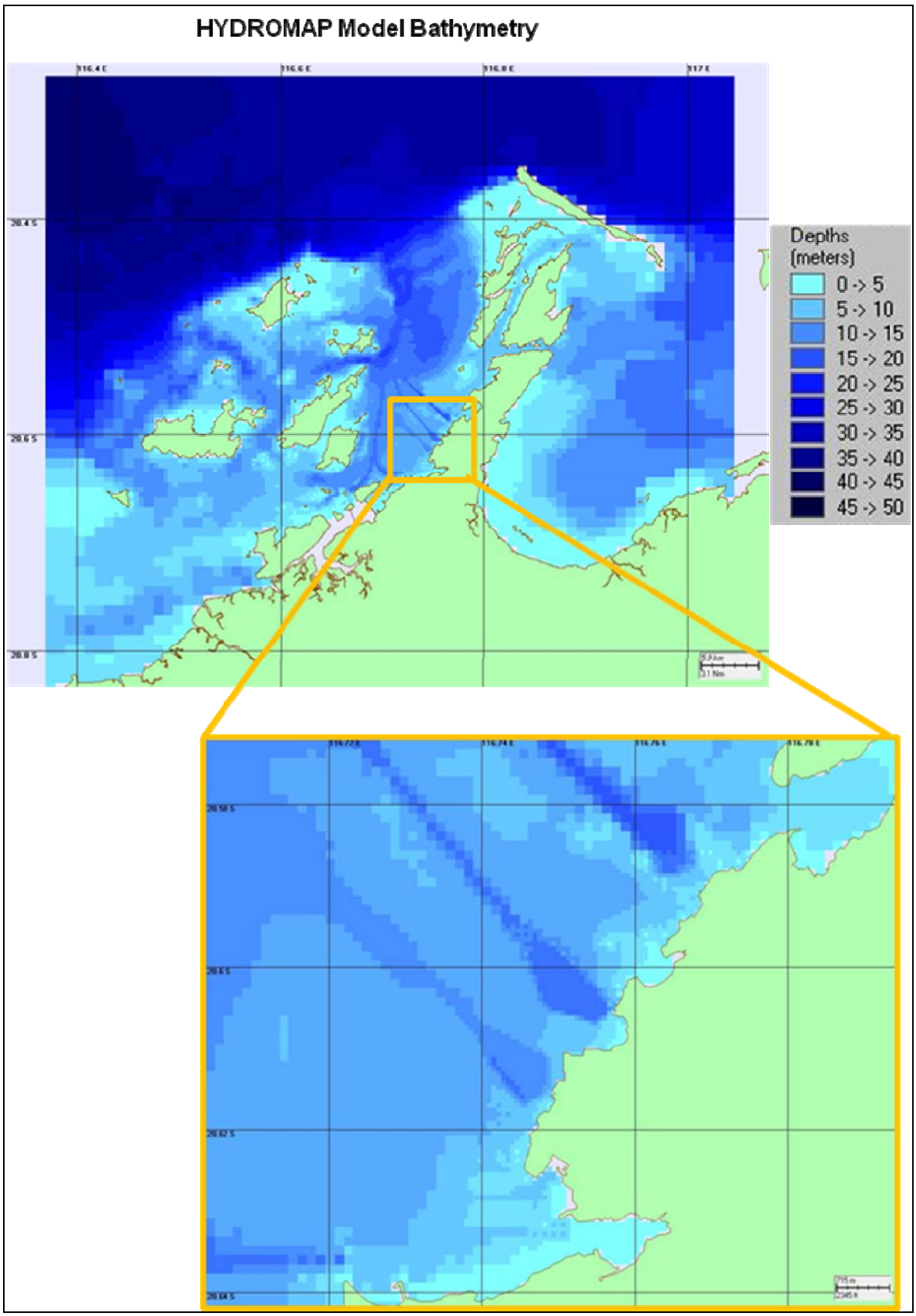

Figure 3-3 Bathymetry used in the hydrodynamic grid.

3.3 Tidal Forcing

The astronomical tides were included on all the open boundaries of the model, based on the tidal constituents provided by the Topex Poseidon global tidal set (TPX0 version 7.0; source: NOAA). The eight largest tidal constituents were used in the simulations: K2, S2, M2, N2, K1, P1, O1 and Q1. These eight constituents were selected as they account for the majority of the tidal amplitude. The values of the constituents vary over the latitude and longitude of the model boundary.

3.4 Wind Forcing

The appropriate wind forcing for the hydrodynamic model was selected as the dataset that best represented the wind conditions in Mermaid Sound. To determine which of the available datasets are the most appropriate, the hindcast wind database from the National Centers for Environmental Prediction (NCEP) global wind model (the same winds used to force the WaveWatch III model further discussed in Section 4.4.2) and the winds measured at the Far14 wind station were compared. This enabled any spatial variability in the winds to be identified, as the NCEP data was extracted at an offshore location (116.25 ^{o}E, 20 ^{o}S), and to ensure that the Far14 wind station was an accurate predictor of the offshore wind speed and direction.

The results of this analysis are illustrated in the wind speed and direction comparison illustrated in Figure 3-4. The period shown was selected to coincides with the period of the ADCP deployment.

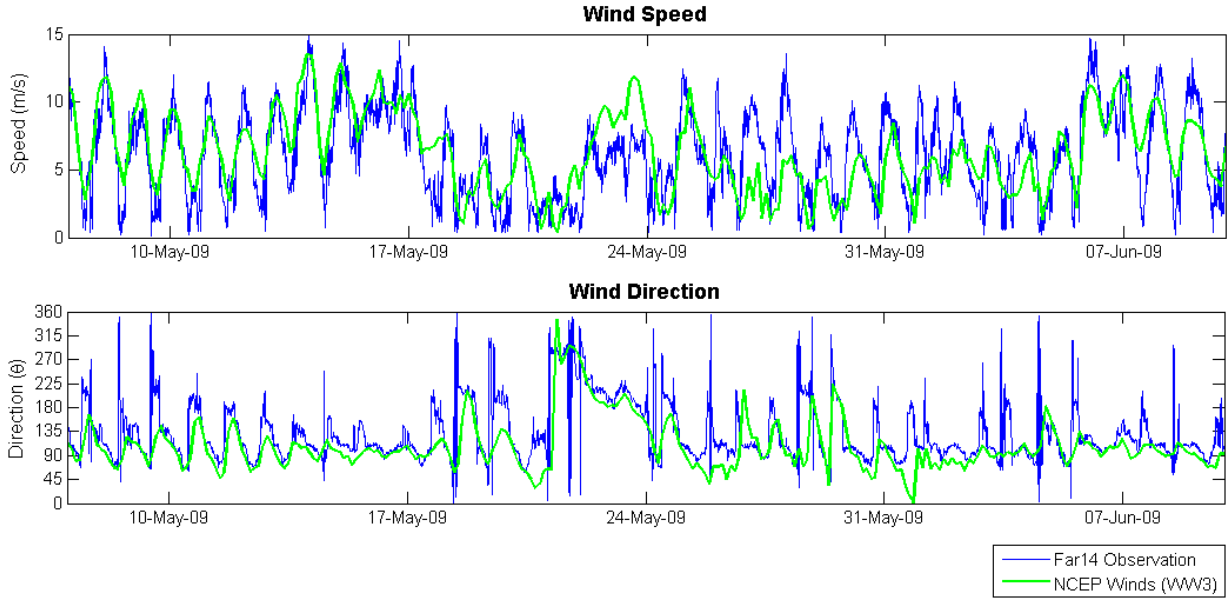

Figure 3-4 Comparison plot of NCEP winds against Far14 measurements. Period shown coincides with the period of ADCP deployment.

As indicated in the comparison plots, the Far14 measurements are well reflected in the NCEP winds. This suggests that there is little spatial variability in the winds over the model domain, with the wind speed and magnitudes showing a close correlation between the two datasets. For this reason, spatially variable wind forcing was not considered necessary given the low level of variability between the nearshore and offshore measurements and the likely localised extent of the sediment plumes. The winds were therefore taken from the Far14 dataset as it contained more frequent measurements (every 10 minutes as opposed to the three-hourly NCEP data) and moderately higher wind magnitudes on average, particularly for onshore winds.

3.4.1 Cyclones

Since the dredging is expected to occur during the cyclone season of November to April it was necessary to include cyclonic effects in the model. This was done through analysis of 20 years of data on historical cyclones that passed within close proximity of Dampier (i.e. those where the eye passed within 80km of the proposed study site). APASA's TCWIND model was employed to generate realistic cyclone winds for the hydrodynamic model. This model uses the commonly adopted numerical model defined by Holland (1980) for cyclone wind field generation. A simplified form of this model is provided in Equation 3.1 (Hearn and Holloway, 1990).

$$v(r) = \left\{(r_m / r)^b (P_n - P_c).* \exp\left[-(r_m / r)^b\right] / \rho_a + r^2 f^2 / 4\right\}^{0.5} - r|f|/2 \qquad \textbf{(3.1)}$$

Where: *v(r)* is the azimuthal wind speed

b = 1.5 + (980 - P_c)/120 - is a form factor,

P_c - the cyclone central pressure,

P_n - the ambient environmental pressure,

r - the distance from the centre of the cyclone,

ρ_a - the atmospheric density,

f - the Coriolis parameter, and

r_m - the radius to maximum wind intensity.

Three significant cyclones that were found to pass near the site were TC Orson (1989), TC Steve (2000) and TC Clare (2006), with their paths shown graphically in Figure 3-5. The necessary input parameters for these three cyclones were taken from the BOM cyclone database, which contains detailed information on Australian cyclones from the past 40 years.

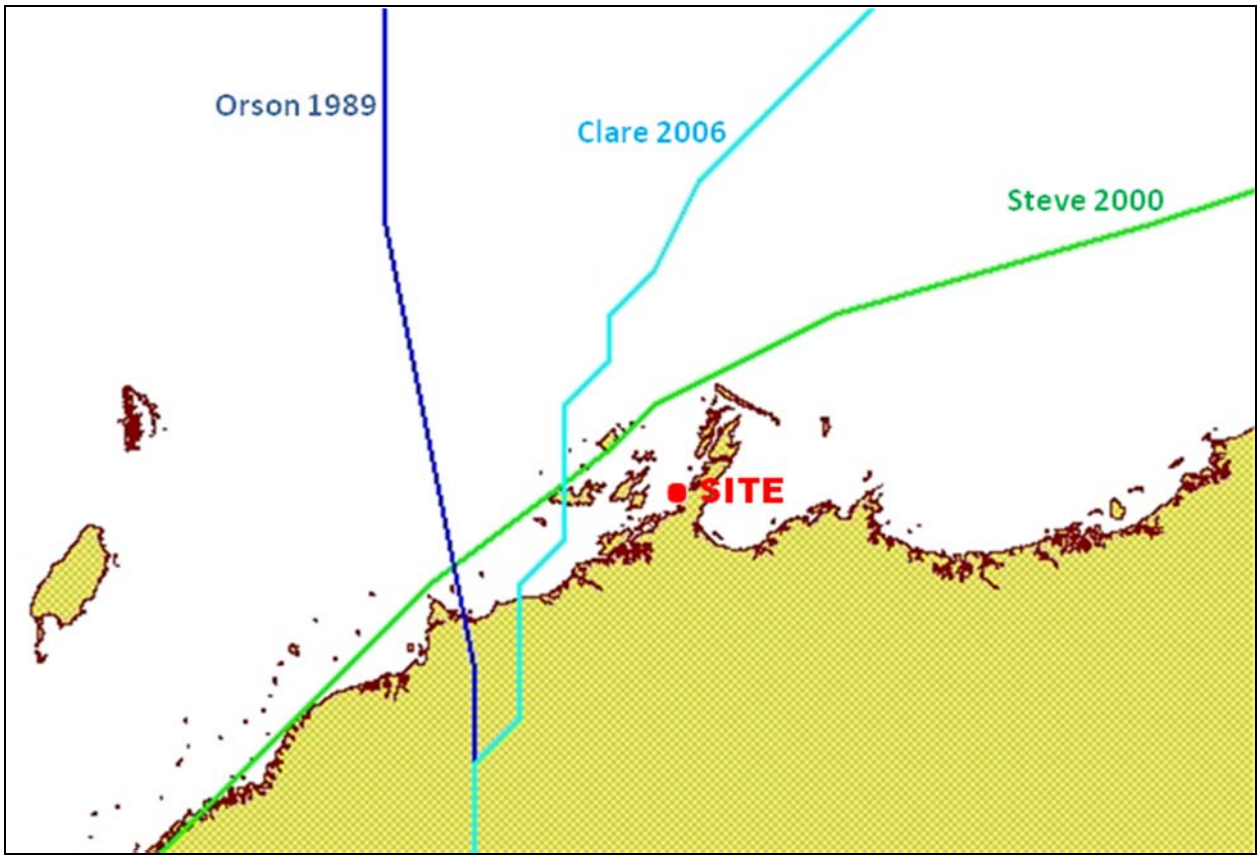

Figure 3-5 Cyclones paths of TC Clare (2006), TC Orson (1989) and TC Steve (2000), three significant cyclones to pass near Dampier.

As Figure 3-5 indicates, all of the selected cyclones pass on the western side of Mermaid Sound. This was an intentional element in the cyclone selection, as the clockwise rotation of cyclone winds would result in the winds channelling down Mermaid Sound. This would result in larger waves and currents than fetch limited winds from cyclones passing to the East, thus enabling more extreme conditions to be incorporated into the model. Details of these cyclones, including their maximum wind speed at the site as predicted by the model, are indicated in Table 3-1.

Table 3-1 Summary of cyclones Implemented into the energetic scenario model (BOM, 1992, BOM, 2000, BOM, 2006)

Cyclone (Year)	Minimum Central Pressure	Period of Occurrence	Predicted by TCWIND Wind Speed at Site	Recorded BOM Wind Speed Near Site
Clare (2006)	960 hPa	3 Jan - 10 Jan	39.1 m/s (140 km/h)	39.4 m/s (142 km/h)
Steve (2000)	970 hPa	27 Feb - 11 Mar	30.0 m/s (108 km/h)	27 m/s (98 km/h)
Orson (1989)	905 hPa	17 Apr - 24 Apr	43.8 m/s (158 km/h)	50.8 m/s Gusts (183 km/h)

The wind speed recorded by the BOM at stations near the DMSF site, shown in the above table, confirm that the TCWIND model is a relatively accurate predictor of wind speed at the site. Winds from the TCWIND model were only incorporated into the energetic model scenarios, with the details further discussed in Section 3.6.

3.5 Validation

The large tides that exist around Dampier and the Dampier Archipelago dominate the hydrodynamics that occur within the model domain. Thus, during ambient conditions, the barotropic component of the current speed is the main concern when ensuring the model provides a good approximation for the actual conditions within the Sound.

For this reason, extensive analysis was performed on the ability of the model to predict the tides at a number of sites within the model domain. The comparison between the model and observed conditions at three tidal stations, shown in Figure 3-6, is presented in Figure 3-7.

A quantitative analysis of the model skill at replicating the environmental conditions was conducted through the use of the Index of Agreement (IOA), presented in Wilmott (1981). This index, commonly used to assess model skill, is calculated according to equation 3.2.

$$\mathrm{IOA} = 1 - \frac{\sum |X_{\mathrm{model}} - X_{\mathrm{obs}}|^2}{\sum \left(|X_{\mathrm{model}} - \overline{X_{\mathrm{obs}}}| + |X_{\mathrm{obs}} - \overline{X_{\mathrm{obs}}}| \right)^2} \qquad \textbf{(3.2)}$$

In this equation, *X* represents the variable being compared and $\overline{X}$ the time mean of that variable. A perfect agreement can be said to exist between the model and field observations if the index gives a measure of one, and complete disagreement will produce an index measure of zero (Willmott, 1981). While it is difficult to find guidelines for what values of the IOA might represent a good agreement, Willmott et al (1985) suggests that values meaningfully larger than 0.5 represent good model performance (Willmott et al., 1985) . Clearly, the higher the IOA, the better the model performance.

For the Cape Legendre and Dampier tide prediction sites the IOA was 0.99 indicating an almost perfect agreement, with Hauy Islet producing only a slightly lower IOA of 0.97.

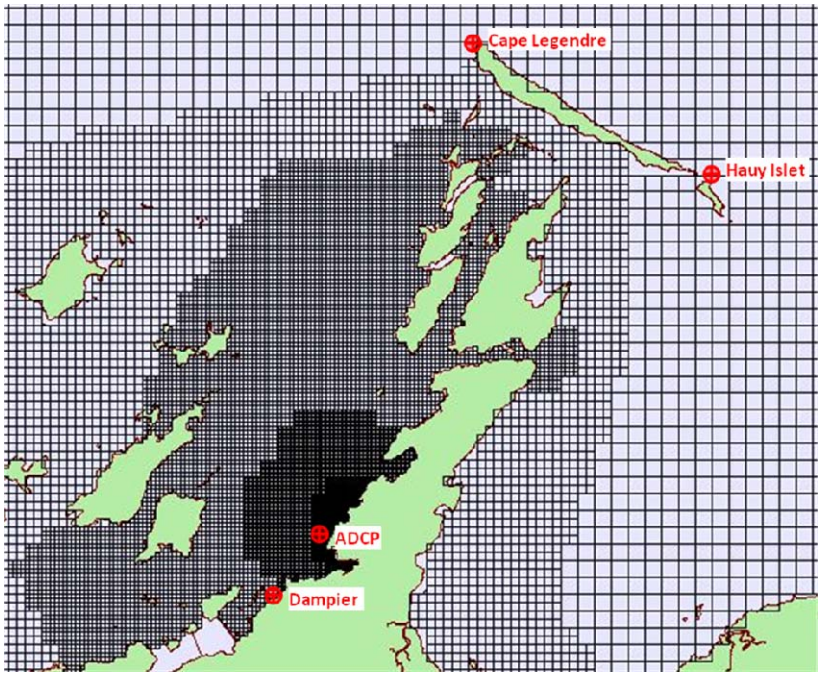

Figure 3-6 Locations of tide prediction stations (including the ADCP) on the model domain.

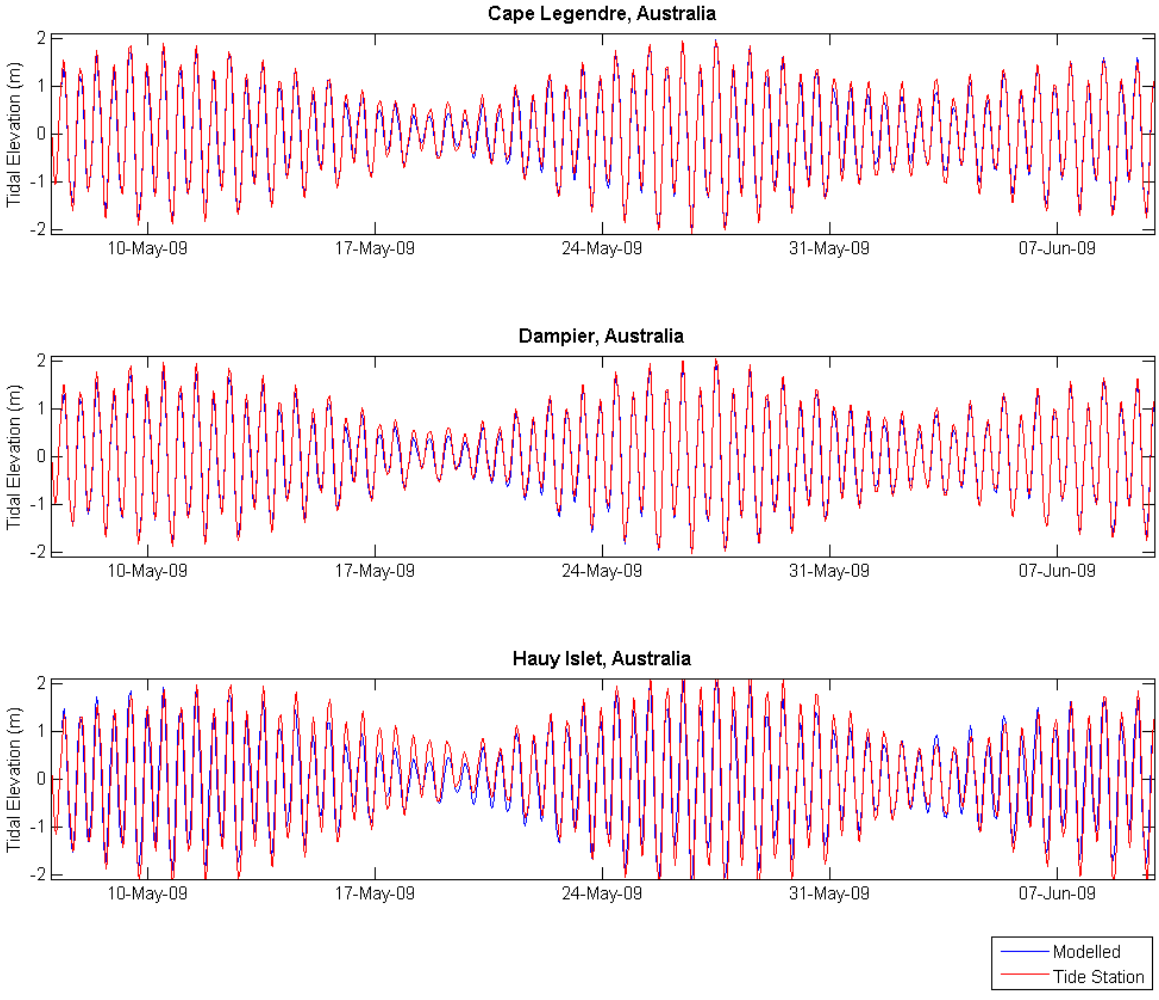

Figure 3-7 Model calibration against three tide prediction stations within the model domain.

In addition to this comparison, the ADCP recorded hourly water elevation readings over its entire period of record. A comparison of the water levels recorded by the ADCP and those estimated from the model at the ADCP deployment site is shown in Figure 3-8. The model reproduced the elevations measured at the ADCP site to a high degree of accuracy, with an IOA of 0.98 achieved in the comparison.

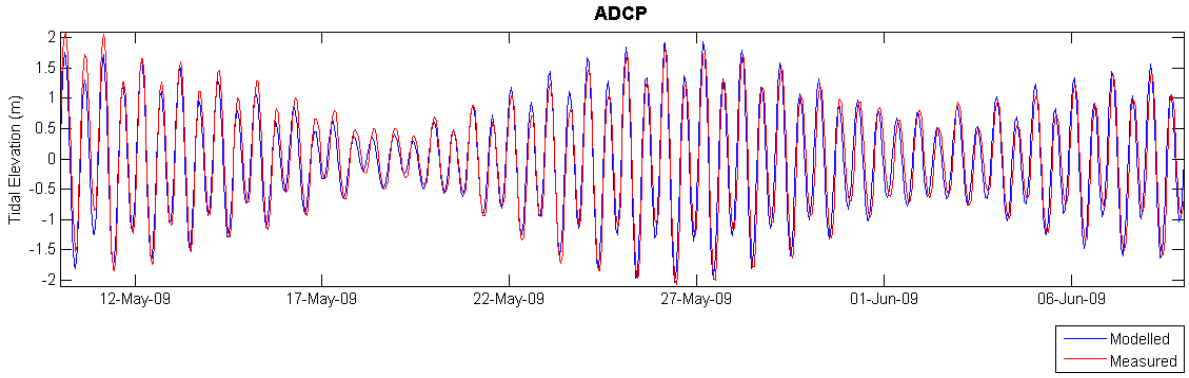

Figure 3-8 Model tide calibration against the ADCP measurements.

Following calibration of the model for water level prediction, the predicted currents were validated against the ADCP measurements. A variety of bottom friction and vertical viscosity parameters were tested before arriving at the final calibrated model, with the parameters employed in the final calibration consistent with those used in the Pluto Dredge Modelling work (APASA, 2006). The calibration plots generated during the final calibration are shown in Figure 3-9, Figure 3-10 and Figure 3-11 for the seabed, mid-depth and surface locations respectively. All comparison plots have been generated for the entire ADCP deployment period.

Quantitative assessment of these calibrations indicate that the IOA for current speed at the seabed, mid-depth and surface is 0.76, 0.79 and 0.78 respectively, indicating a relatively strong agreement between the model estimates and measures data. This is moderately increased for the N-S currently velocity component, where the IOA is 0.84, 0.86 and 0.83 for the respective depths. The E-W velocity component shows a slightly weaker calibration, as expected from the plots, with the IOA for the seabed, mid-depth and surface being 0.68, 0.75 and 0.75 respectively.

Figure 3-9 illustrates the better model prediction of the N-S velocity component than the E-W velocity components measurements. As the current speed and direction calibration indicate a relatively strong agreement, it is clear that moderately higher E-W velocity component magnitudes are the key factor for the slight discrepancy in this component. This is likely to be a result of variations in the bathymetry not being resolved in the models 100 m grid near the ADCP site, particularly applicable to the seabed calibration as the ADCP is located in a turning basin where the hydrodynamics are highly localised.

The calibration at mid-depth, indicated in Figure 3-10, shows that whilst certain spikes in current velocity are not being fully captured in the model, the N-S and E-W velocity components are better estimated than at the seabed. The smaller current magnitudes estimated from the model for the spring tide at the end of May are not consistent throughout the entire calibration period, with the model showing a much better prediction of current magnitudes during the later spring tide on the 8th of June. The dominant current direction is consistently preserved in the model.

The surface calibration indicates that the model is an accurate predictor of current speed and direction at this depth. Current magnitudes for both velocity components are well represented in the model, again with a better estimation achieved in the N-S velocity component. The model does show a portion of the currents directed W and NW that are not evident in the measurements. This is a result of strong offshore winds in the Far14 dataset that do not entirely reflect the winds at the BLB, which would be particularly hard to estimate given the protection from offshore winds provided by the berth.

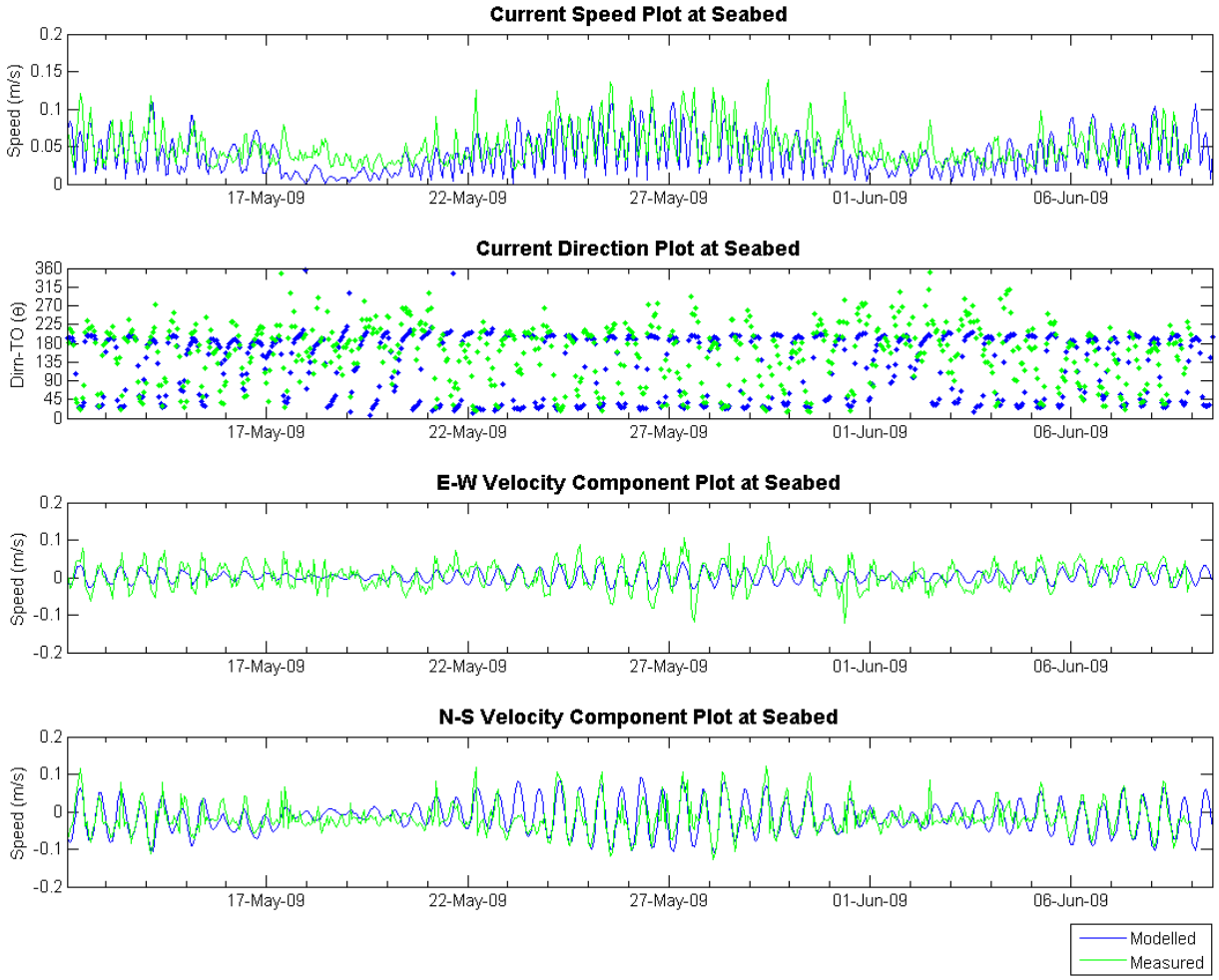

Figure 3-9 Model calibration of current velocity against the ADCP measurements at the seabed (approximately 2 m ASB) .

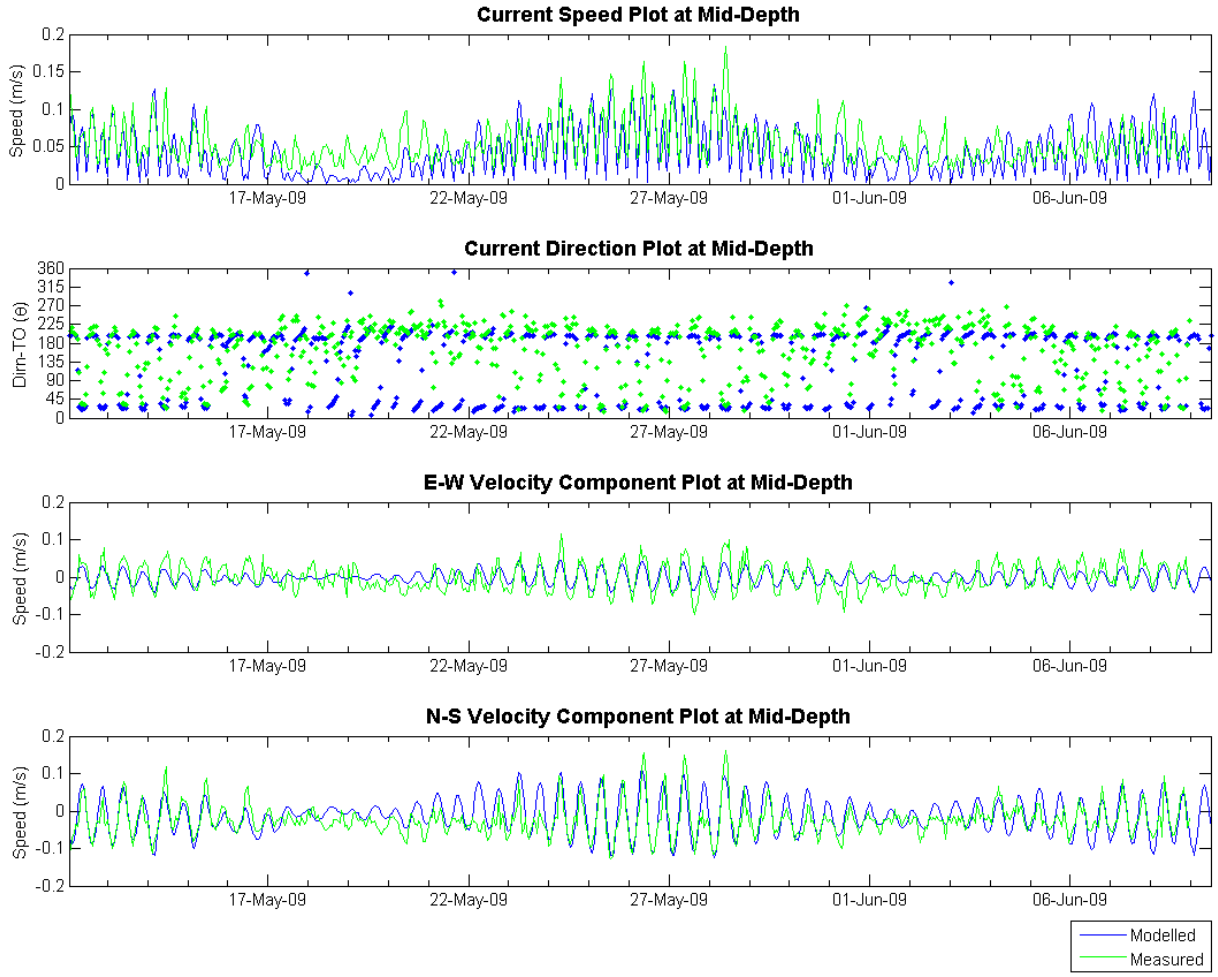

Figure 3-10 Model calibration of current velocity against the ADCP measurements at mid-depth (approximately 7 m ASB) .

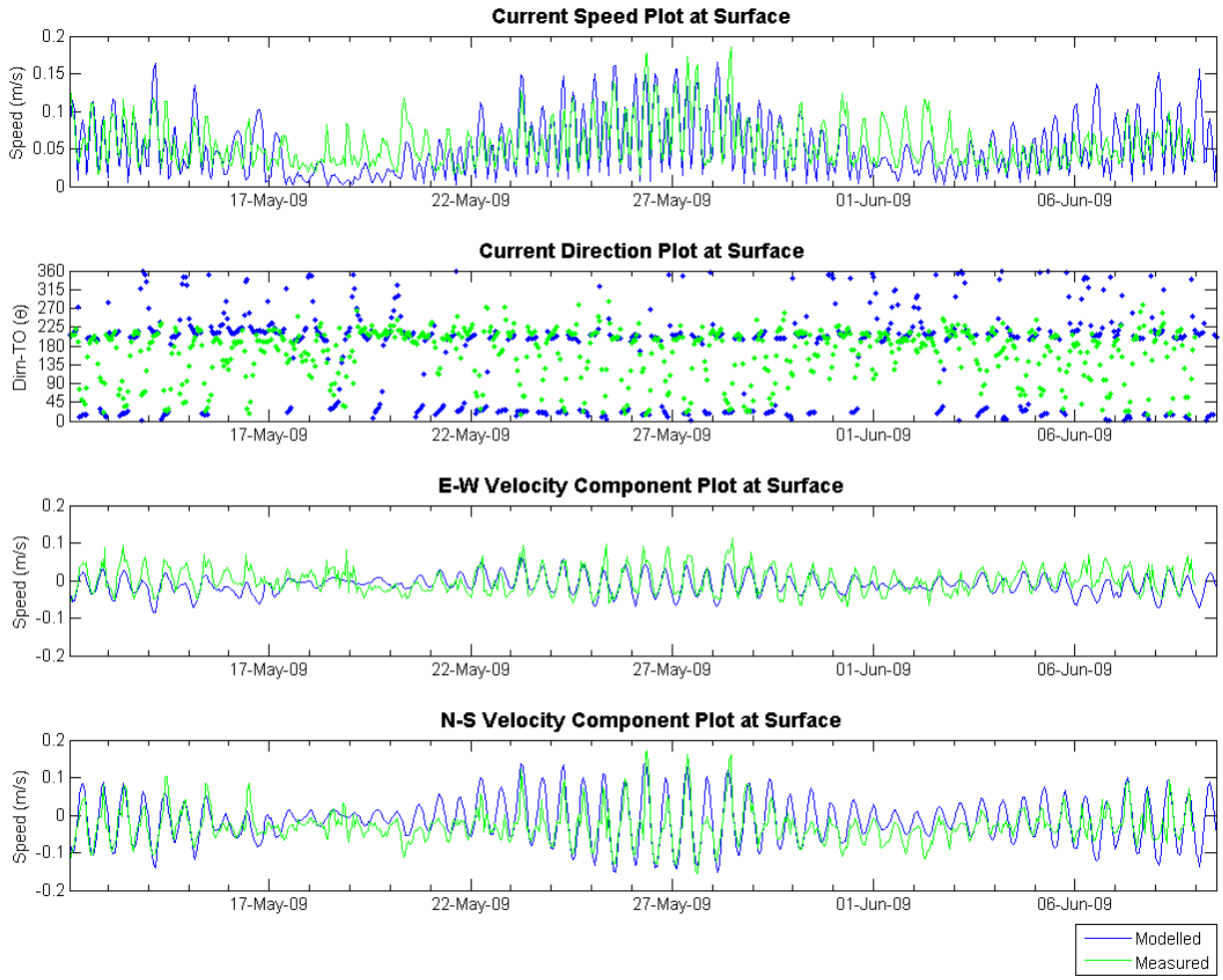

Figure 3-11 Model calibration of current velocity against the ADCP measurements at mid-depth (approximately 12 m ASB) .

3.6 Scenarios

The validated HYDROMAP model was run to create a 16 month hydrodynamic dataset consisting of two separate 8 month periods, representing ambient and energetic scenarios. These two scenarios were selected based on wave observations made within Mermaid Sound at the Navaid 9 buoy location and wind measurements made at the Far14 wind site. The 8 months from the predicted November 1st start to the following July were analysed for each year from 2006 to present and cross compared. The results of this analysis are presented graphically as rose plots for the wave and wind measurements in Figure 3-12.

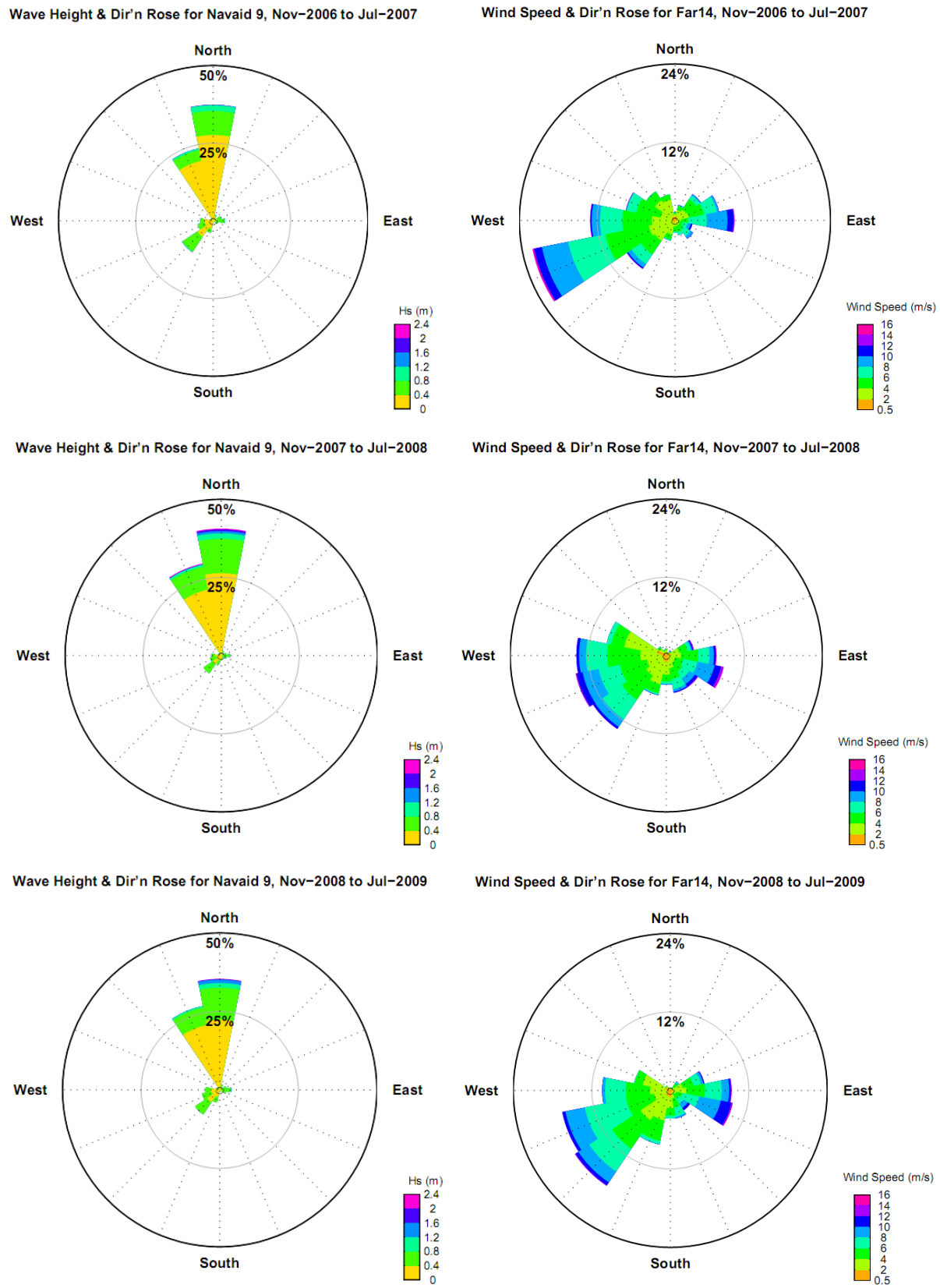

Figure 3-12 Directional wave height and wind speed roses for the Navaid 9 buoy (left) and Far14 (right) wind station respectively over three separate 8 month periods, dates as titled, from November to July. Data shown includes measurements from January 2005 to August 2009 for both datasets. The roses show the percentage occurrence of wind and wave direction (direction FROM) around the compass, with colour coding indicating the proportion in each speed class.

The period from November 06' to July 07' showed the calmest conditions of the three separate periods analysed, with wave height exceeding 1.2 m only 0.23 % of the time over this period. The November 07' to July 08' period showed the largest wave conditions, with waves over 1.2 m occurring approximately 2 % of the time. November 08' to July 09' also showed a stronger wave climate that the 06' to 07' period, with waves exceeding 1.2 m approximately 1.4 % of the time.

Similarly the records at Far14 station indicated particularly strong winds during the November 07' to July 08' period, with winds in excess of 10m/s (approx. 20 knots) occurring over 4.8 % of the time. November 06' to July 07' was again the calmest period, with winds exceeding the 10m/s threshold only 3.5 % of the time and November 08' to July 09' was characterized by moderate winds with the 10 m/s threshold exceeded 4.0 % of the time.

Based on these results, the average ambient scenario was selected as the period from November 08' to July 09', whilst the energetic scenario was selected as November 07' to July 08'. Wind forcing for the energetic scenario included cyclone winds, generated by the TCWIND model as mentioned earlier. The three cyclone events, described in Section 3.4.1, were included at the same periods within the year as their actual dates of occurrence. The result was a synthesized data set with a highly unlikely occurrence of tropical cyclones, in terms of both frequency and intensity.

The data for each of these simulations was archived as spatial 3D data on an hourly time-step for use as input into the sediment fate model.

4 WAVE MODELLING

4.1 Introduction

To represent the wave-induced component of re-suspension, a regional wave model has been established using the SWAN (acronym for Simulating WAves Nearshore) model. A SWAN model was developed to provide spatial wave conditions over a wide domain, spanning at least 37 km in all approaches to the project site. The large size of the wave model domain was a requirement to enable all sediments to be tracked over the long time span of the proposed dredging operation.

The model requirements included both a high spatial resolution close to the proposed dredge operation and to accommodate long run-times to cover the duration of the proposed dredge operation. The complex coastline around the project site and throughout the Dampier Archipelago, combined with the need to cover large areas at different resolutions made the selection of an unstructured mesh model applicable. Thus the regional wave model has been developed using the unstructured mesh version of SWAN.

The model has been run to create a hindcast database of spatial wave parameters that spans the two separate 8 month simulation periods and to provide a robust sample from which to analyse inter-annual variability. Model results have been validated against the available measured wave data at both the Navaid 9 station and against the recent ADCP measurements.

4.2 Model Description

The SWAN model is a spectral phase averaging wave model developed by the Delft University of Technology (Holthuijsen et al., 1997). SWAN is a numerical model for simulating realistic estimates of wave parameters in coastal areas for given wind, bottom and current conditions. The model is a third generation model based on the energy balance equation. In general, SWAN includes algorithms for the following wave propagation processes: propagation through geographic space, refraction due to bottom and current variations, shoaling due to bottom and current variations, blocking and reflections by opposing currents, transmission through or blockage by obstacles. The model also accounts for the dissipation effects due to whitecapping, bottom friction and wave breaking and non-linear wave-wave interactions. SWAN is fully spectral (in all directions and frequencies) and computes the evolution of wind waves in coastal regions with shallow water and ambient currents.

4.3 Computational Grid and Bathymetry

The computational grid for the SWAN model was setup using the unstructured mesh option. Unstructured meshes provide a much better representation of complex boundaries such as coastlines and areas around islands than do conventional regular grids. The biggest advantage of unstructured meshes is that they provide the opportunity to concentrate mesh resolution in areas of interest and regions of strong bathymetry variations, to a degree not possible using a regular or curvilinear grid. There is no need for nesting and an unstructured mesh will in general resolve the model area with superior accuracy and with significantly fewer grid points than with regular or curvilinear grids. Although the CPU cost per iteration is relatively higher than cases with structured grids, this effect is more than offset by the reduction in the number of grid points.

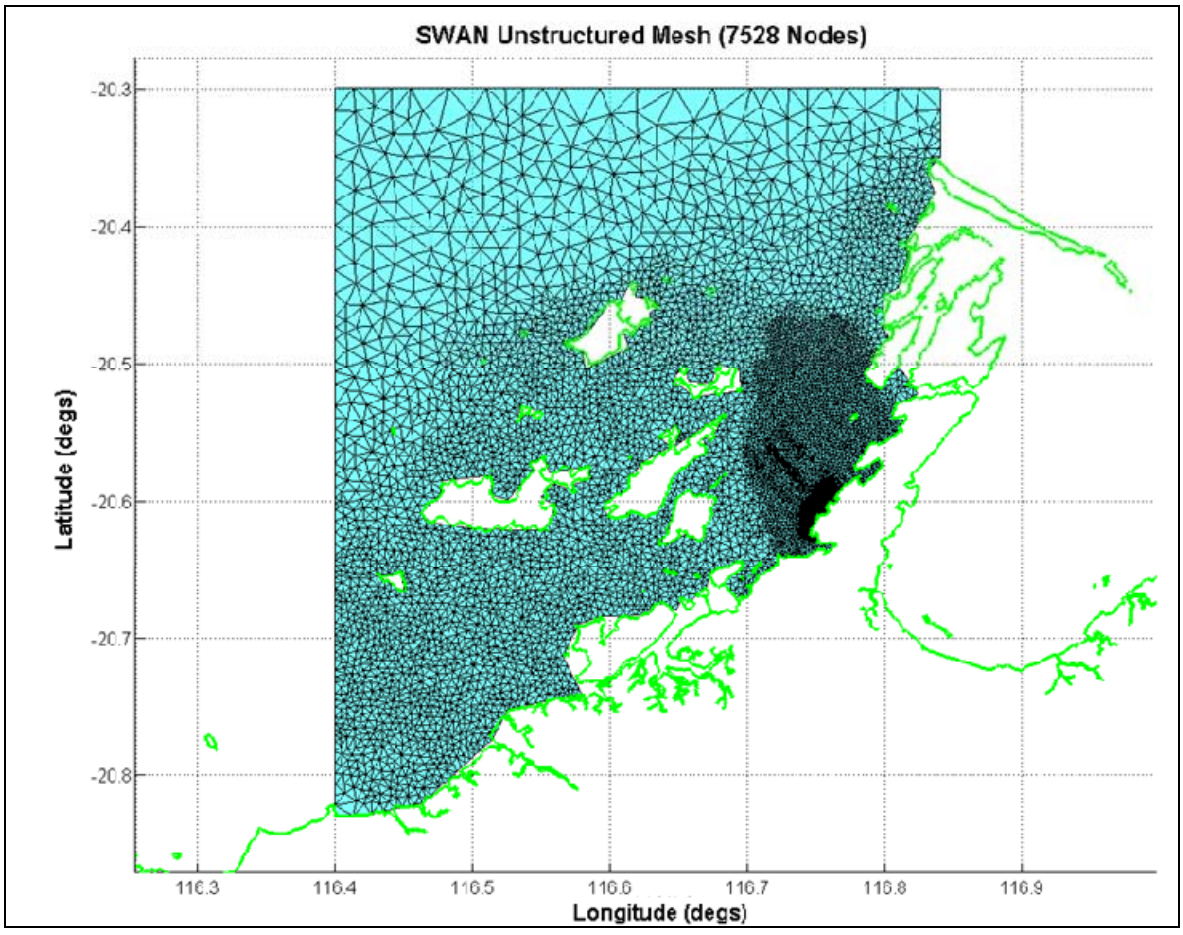

Figure 4-1 The computational mesh covering the domain for the SWAN model.

The final computational mesh is shown in Figure 4-1. The mesh contained 14,213 triangles with 7,528 vertices. The minimum triangle edge length in the mesh was 25 m and the maximum triangle edge length was 2.9 km.

The representation of the bathymetry over the mesh is shown in Figure 4-2. The same bathymetric dataset used in the HYDROMAP modelling has been used in the SWAN model

mesh. The mesh resolution has been adjusted for maximising computational efficiency, with the mesh has higher resolution in areas where the bathymetry or evolution of the waves change rapidly and lower resolution in areas where the physics or depth changes less.

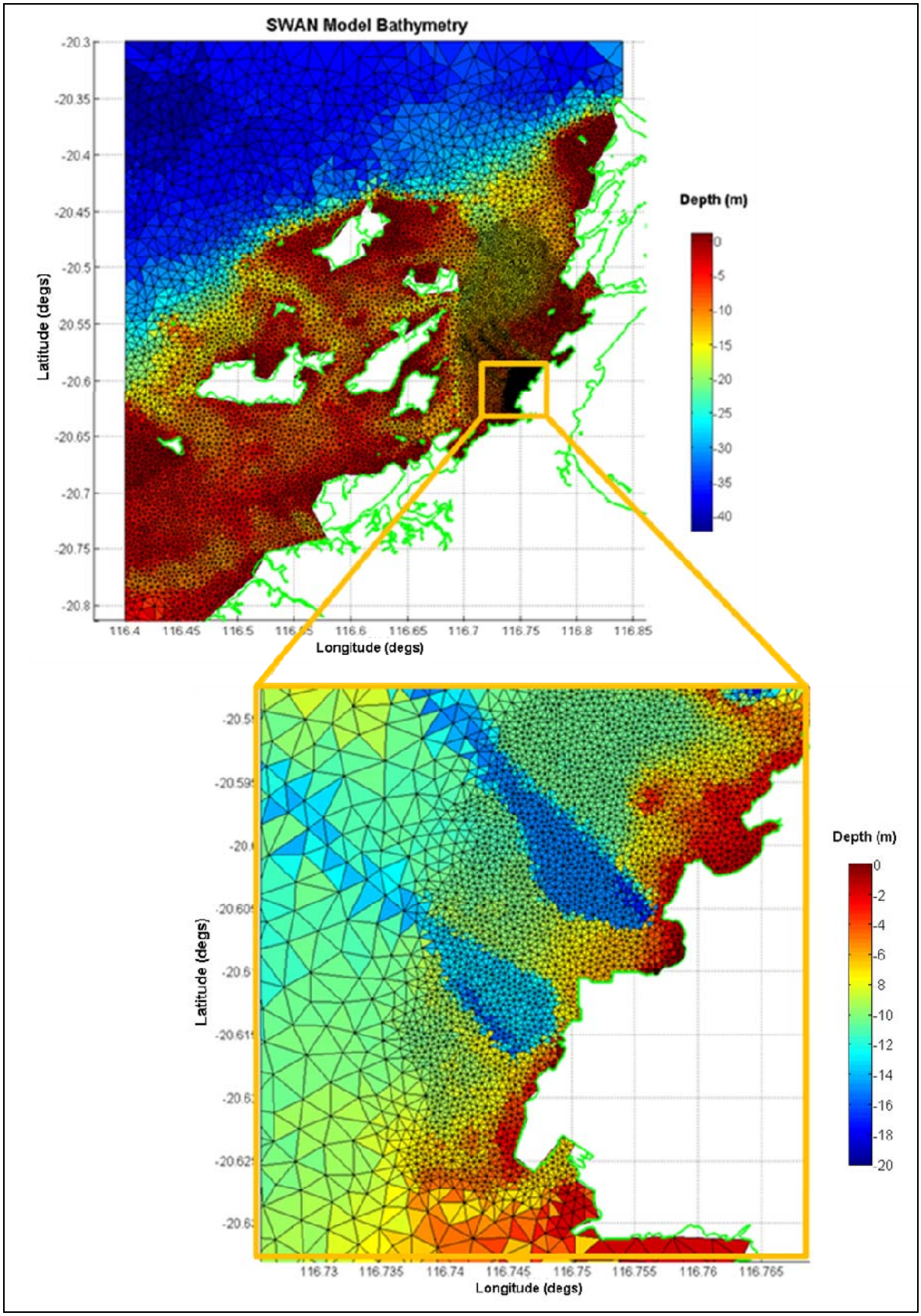

Figure 4-2 SWAN model Bathymetry over the computational mesh. The mesh spans the coast from Regnard Bay on the west to Dixon Island on the east and offshore to a depth of 42 m. Depths are shown with reference to MSL.

4.4 Model Forcing and Boundary Conditions

4.4.1 Water Levels and Currents

Water levels and currents were interpolated from the HYDROMAP output onto the SWAN unstructured mesh. The ambient current can affect the growth and decay of waves and in the case of a strong opposite current the wave steepness and wave height can increase significantly. In the case of Dampier, the local wind-generated currents are not generally strong enough to have a significant effect. However, during storms and periods of strong local winds, current-induced whitecapping and wave reflections may have an effect. Thus, currents were included in the SWAN modelling.

The water levels were included to capture the effect where elevated water levels allow larger waves to propagate to the coast, courtesy of a reduction in bottom friction and depth limited breaking.

4.4.2 Waves

SWAN requires the input of wave spectra along the open boundaries of the open ocean model domain. Typically, for use as boundary input into the SWAN model, hourly wave data is imported from the WaveWatch III (WW3) global wave model run by NOAA (Tolman, 2002).

In an effort to improve the model performance in this case, offshore wave measurements taken at the WEL NRA platform were also analysed for their suitability for use in the model. The location of the NRA platform with respect to the site is illustrated in Figure 2-1. Although NRA is a significance distance from the boundary of the model domain, it is located within close proximity to the nearest WW3 point at 116.25 ^{o}E, 20.00 ^{o}S. The key parameters that are used to force the model at the open boundary were plotted and compared for these two datasets. An example of this, over the ADCP deployment period, is illustrated in Figure 4-3.

The comparison clearly indicates that the WW3 data provides a good approximation of the actual wave conditions on the NWS as indicated in the NRA observations. Large wave conditions, however, are being under-predicted by the WW3 model making the NRA observations more conservative and therefore the preferred dataset to use in the model. Numerous gaps in the NRA dataset meant that a composite forcing file needed to be developed, using WW3 data where these gaps existed.

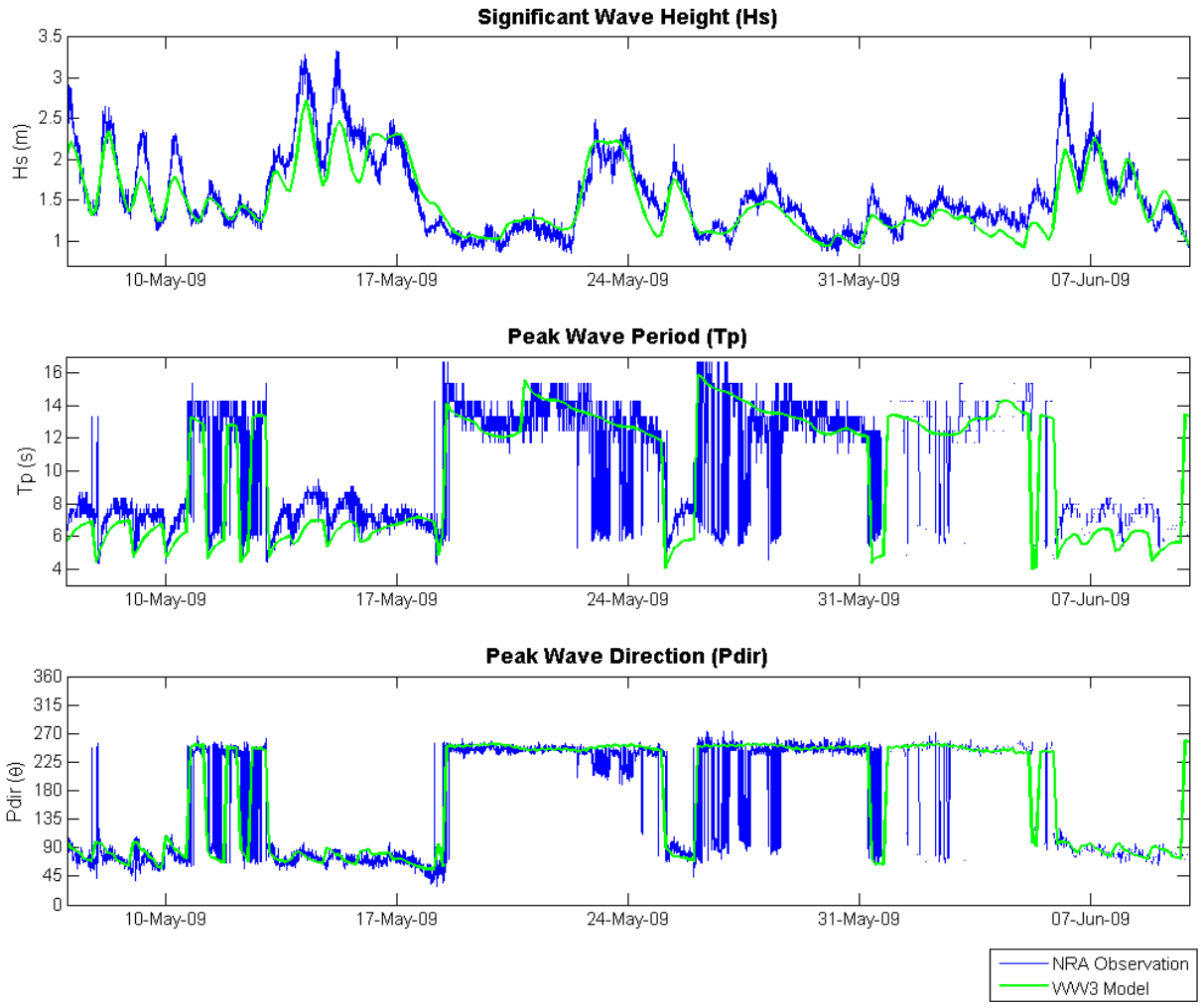

Figure 4-3 Comparison of WW3 global wave model output with the NRA observations.

4.4.3 Wind

The same wind dataset as used in the hydrodynamic modelling was adopted for the SWAN assessment. Again these single point-source winds were spatially implemented across the model domain as they represented a good approximation of the total area as described in Section 3.4.

4.5 Model Parameters

The physical processes selected for the simulations were: whitecapping, depth induced wave breaking, bottom friction and triad wave-wave interactions. The process of whitecapping in the SWAN model is represented by the pulse-based model of Hasselmann (1974), reformulated in terms of wave number as to be applicable in finite water depth (Hasselmann, 1974, Komen et al., 1984). For the depth induced wave breaking, the default SWAN parameterization was used with a 0.73 constant breaking factor (Eldeberky and Battjes, 1996).

Bottom friction was incorporated using the Madsen model (Madsen et al., 1988). This formulation is similar to that of Hasselmann et al. (1968), but in this case the bottom friction factor is a function of the bottom roughness length scale and the wave conditions. The bottom roughness length scale was set to 0.15 m. For modeling the triad wave-wave interaction SWAN uses the Lumped Triad Approximation Eldeberky (1996a), in each spectral direction. Quadruplet wave to wave interaction was set to default.

A non-stationary SWAN simulation was performed with a time step of 30 minutes and the convergence requirement set to 98.5 % of computational points. After an initial model spin-up, the convergence was generally obtained in the first few iterations, occasionally requiring up to 15 iterations when the sea state became particularly dynamic.

Model output was written on an hourly time-step for the entire computational grid, that was later post-processed to obtain wave parameters at the validation sites.

4.6 Model Validation

The wave model was validated against the ADCP measurements and Navaid 9 buoy records measured data available for the region. The large period of data available at Navaid 9 meant that a more complete model validation could be performed that enabled comparisons to be made during summer and winter conditions to ensure seasonal variability was being correctly predicted by the model. The months of January and July, for both the energetic and ambient scenarios, were selected as the representative summer and winter months respectively for the model validation. These comparison plots have been presented below in Figure 4-4 to Figure 4-7.

Figure 4-4 and Figure 4-5 clearly illustrates that the model is accurately predicting the wave height and direction recorded at the Navaid 9 location. As with the validation of the hydrodynamic model presented in Section 3.5, Willmott's IOA was again employed as a quantitative measure of the models performance. For January 08' and 09', the IOA for Hs was 0.92 and 0.87 respectively, indicating a particularly strong match between the model predictions and the measurements. The IOA was again strong for Tp and Direction, being 0.63 and 0.78 respectively for the ambient scenario (January 09') and 0.66 and 0.79 for the energetic scenario (January 08').

The comparisons during July also demonstrate that the model shows a high degree of skill at replicating the wave conditions, particularly Hs and Direction, at the Navaid 9 location. The IOA for Hs was 0.91 during July 08' and 0.90 for July 09'. This was only marginally lower for Direction at 0.80 and 0.75 for July 08' and 09' respectively. Tp again showed the lowest correlation at 0.62 and 0.65 for the July 08' and 09' periods respectively.

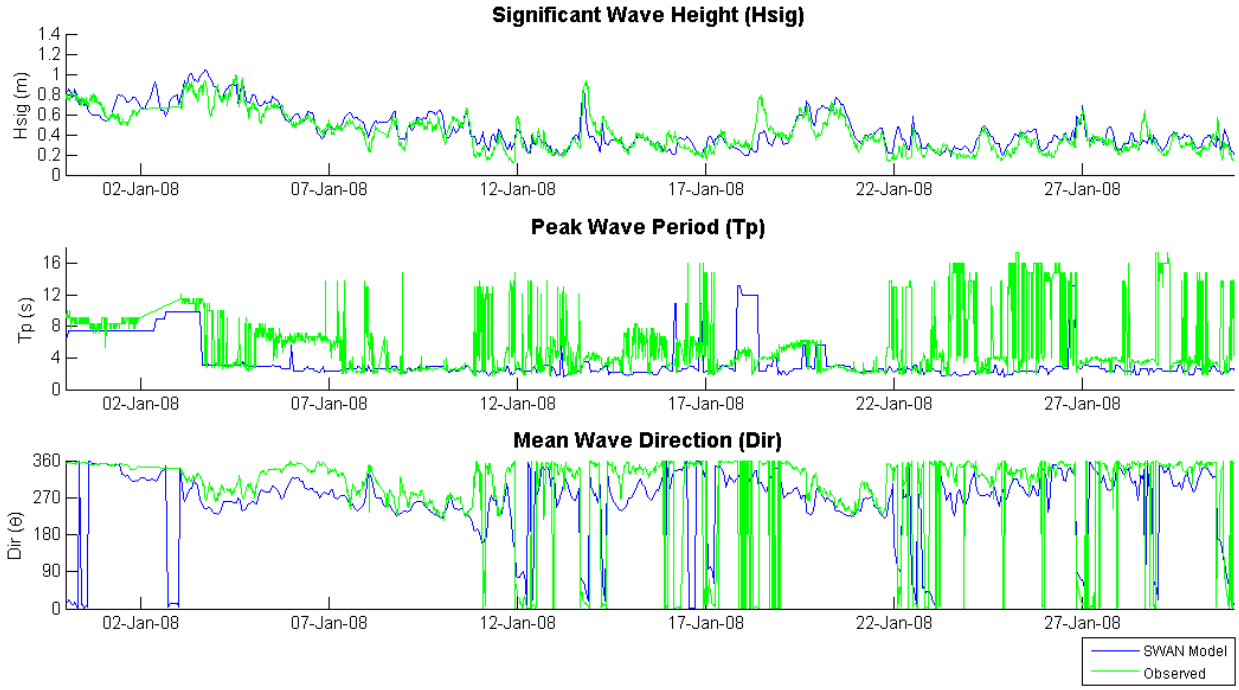

Figure 4-4 Comparison of key wave parameters from the SWAN model output with the Navaid 9 observations over January 2008.

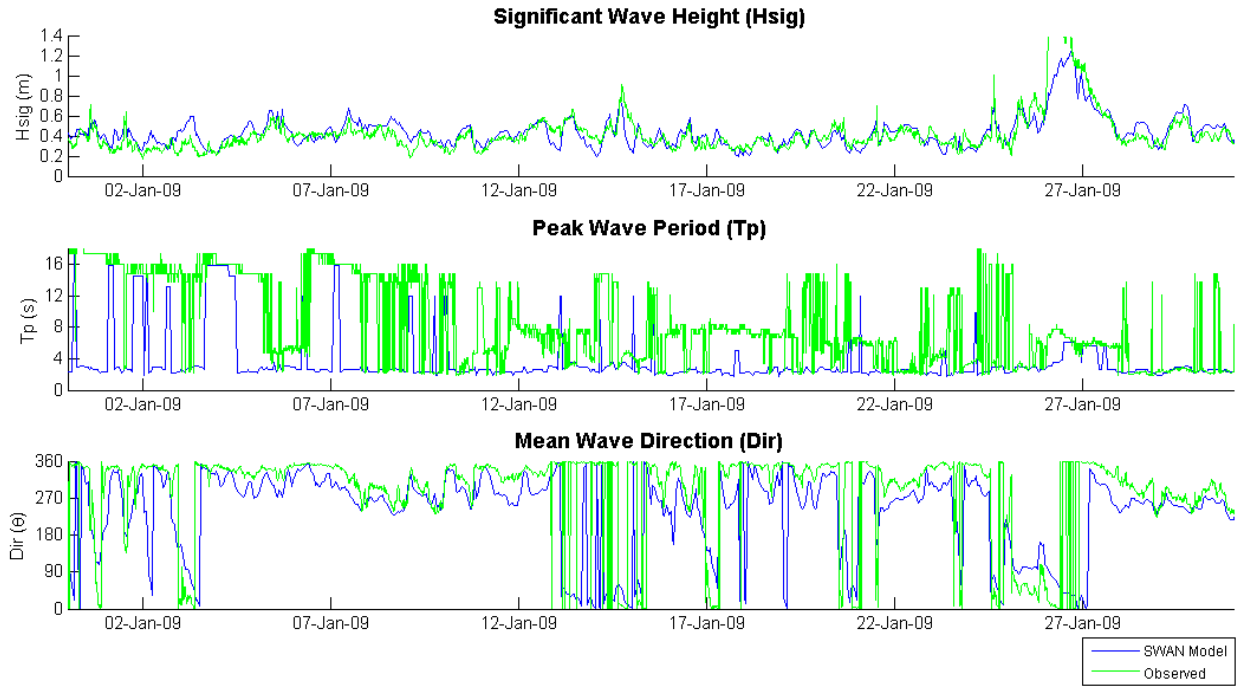

Figure 4-5 Comparison of key wave parameters from the SWAN model output with the Navaid 9 observations over January 2009.

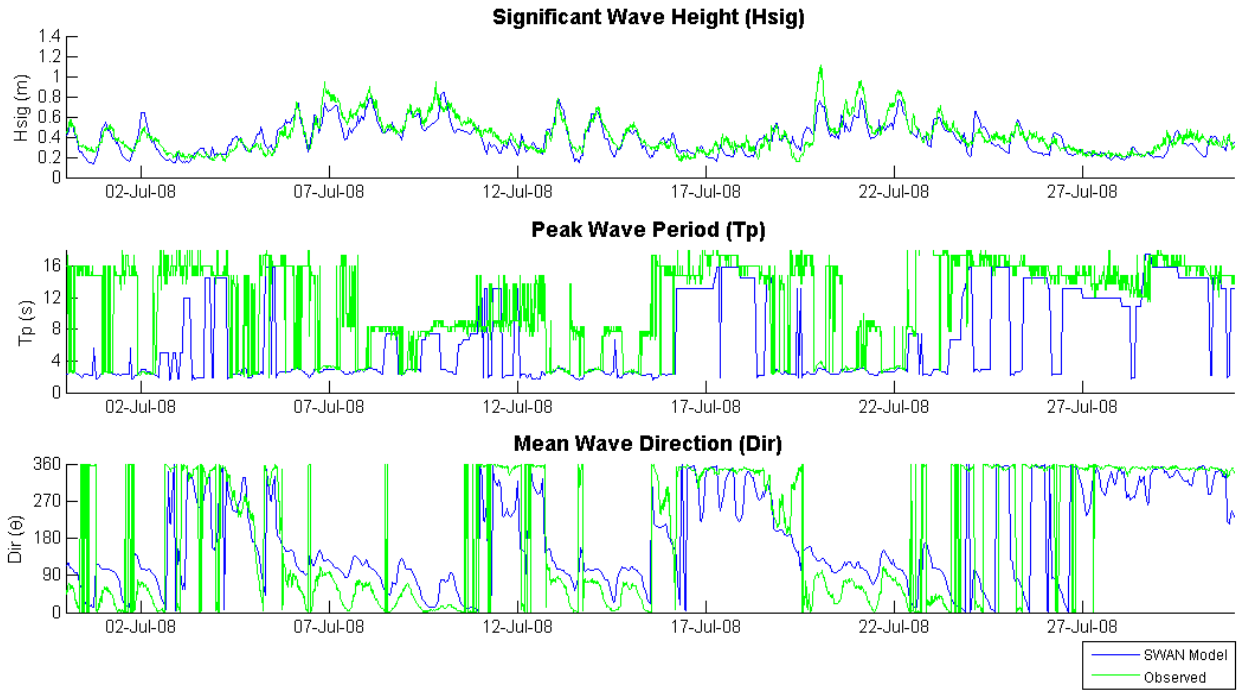

Figure 4-6 Comparison of key wave parameters from the SWAN model output with the Navaid 9 observations over July 2008.

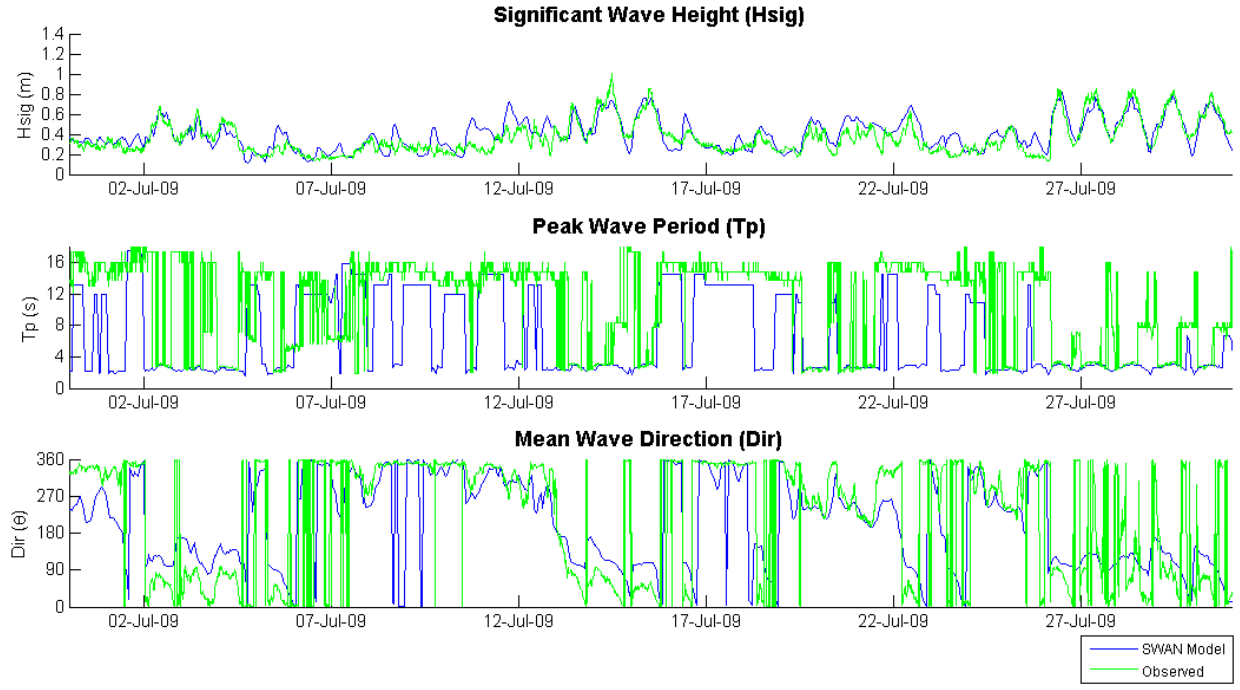

Figure 4-7 Comparison of key wave parameters from the SWAN model output with the Navaid 9 observations over July 2009.

The comparison of the model performance with the ADCP measurements is illustrated in Figure 4-8. Unfortunately, the Navaid 9 measurements during the ADCP deployment period contained a significant number of gaps so a cross comparison with these two measurements over this period was not possible.

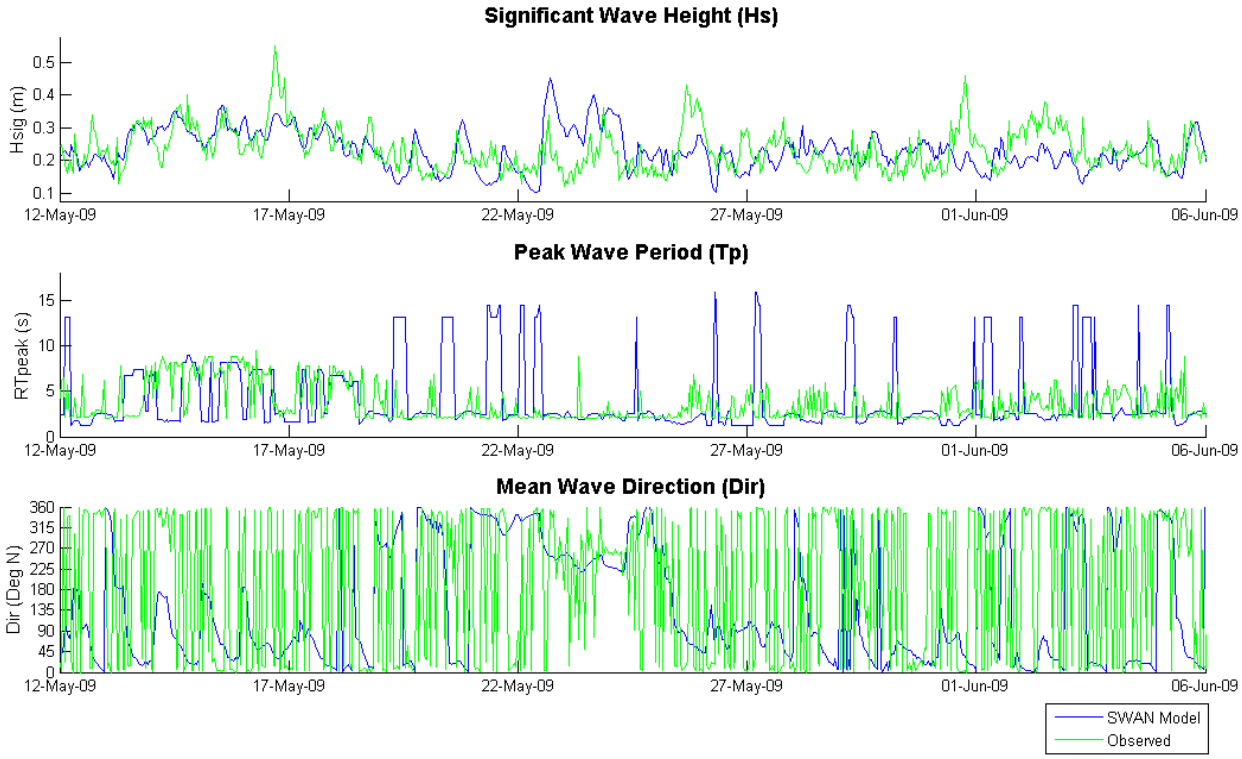

Figure 4-8 Comparison of key wave parameters from the SWAN model output with the ADCP observations over May and June 2009.

Figure 4-8 indicates a clear agreement between the measured and modelled data at the ADCP site. Although the model is able to capture most of the peak wave events, both in wave period and height, there are a number of events not replicated in the model. A quantitative assessment using the IOA yielded 0.62 for Hs, 0.65 for Tp and 0.67 for Dir over the period shown.

Given the high level of agreement observed between the model and the Navaid 9 measurements, the lower correlation observed at the ADCP site is likely to be a result of highly localised wave dynamics not being resolved within the model. The low wave energy at the ADCP site can also result in measurement errors in the ADCP records, particularly of direction and the separation of peak wave conditions from mean conditions. The proximity of the ADCP to the BLB, and its location in the turning basin, could also result in wave interactions that are not fully represented by the model. In summary, however, the model is a suitably accurate predictor of wave heights within Mermaid Sound and at the DMSF project site.

4.7 Scenarios

The SWAN wave model was run using over same time period and with the same wind forcing employed in the HYDROMAP modelling scenarios. As with the energetic simulation in HYDROMAP, cyclonic winds from the TCWIND model were included in the energetic scenario for the wave modelling.

Key parameters required for sediment fate prediction from the wave modelling include timeseries output of Hs, Tm01, Dir and Ubot. Each of these parameters were extracted from the model at each vertex location and saved for each timestep for input into the sediment fate model.

5 SEDIMENT FATE MODELLING

5.1 Introduction

The modelling of the dispersion of suspended sediment resulting from the dredging has been undertaken using an advanced fate model, SSFATE, operating within the ASA DREDGEMAP system. The model computes the differential total suspended sediment (TSS) concentration above background that directly results from the dredging operations, with full details of the model discussed in Section 5.2. Interpretation of the results in the context of the typical range of background values and of the likely effects is required.

For this study, the resulting TSS values throughout the dredging operations were assessed to determine the extent and behaviour of the plume.

5.2 Model

SSFATE (Suspended Sediment FATE) is a computer model originally developed jointly by the U.S. Army Corps of Engineers Engineer Research and Development Center and Applied Science Associates (ASA) to estimate suspended sediment concentrations generated in the water column and deposition patterns generated due to dredging operations in a current-dominated environment, such as a river (Johnson et al., 2000, Swanson et al., 2004, Swanson et al., 2000). ASA has significantly enhanced the capability of SSFATE to allow the prediction of sediment fate in marine and coastal environments, where wave forcing becomes important for reworking the distribution of sediments (Swanson et al., 2007).

SSFATE is formulated to simulate far-field effects (~25 m or larger scale) in which the mean transport and turbulence associated with ambient currents are dominant over the initial turbulence generated at the discharge point. A five class particle-based model predicts the transport and dispersion of the suspended material. The classes include the 0 to 130 micron range of sediment sizes that typically result in plumes. Heavier sediments tend to settle very rapidly and are not relevant over the larger time and space scales of interest here. Table 5-1 shows the material classes used in SSFATE.

Table 5-1 Material size classes used in SSFATE

Material Class	Size Range
Clay	*< 7 microns*
Fine Silt	*8 to 35 microns*
Coarse Silt	*36 to 74 microns*
Fine Sand	*75 to 130 microns*
Coarse Sand	*> 130 microns*

Particle advection is based on the simple relationship that a particle moves linearly with a local velocity, obtained from the hydrodynamic model, for a specified model time step. Particle diffusion is assumed to follow a random walk process. The Lagrangian approach of calculating transport through a grid-less space removes limitations of grid resolution, artefacts due to grid boundaries and also maintains a high degree of mass conservation.

Following release into the model space, the sediment cloud is transformed according to the following processes:

- Advection in the background three-dimensional current field.
- Diffusion by a random walk model with the mass diffusion rate specified ideally from measurements at the site. As particles represent an ensemble of real particles, each particle in the model has an associated Gaussian distribution, governed by particle age and the mass diffusion properties of the surrounding water.
- Settlement or sinking of the sediment due to buoyancy forces. Settlement rates are determined from the particle class sizes and include allowance for flocculation and other concentration dependent behaviour, following the model of Teeter (2001).
- Deposition of the sediment. Deposition is determined using a model that couples the deposition across particle classes (Teeter, 2001). The likelihood and rate of deposition depends on the shear stress at the bed. High shear inhibits deposition, and in some cases excludes it all together, with sediment remaining in suspension. The model allows for partial deposition of individual particles according to a practical deposition rate, thereby allowing the bulk sediment mass to be represented by fewer particles.
- Potential resuspension of material, governed by exceedance of required shear stress at the seabed due to the combined action of waves and currents. Different thresholds are applied for resuspension depending upon the duration of sedimentation, based on empirical studies that have demonstrated that newly settled sediments will have higher water content and are more easily resuspended by lower shear stresses (Swanson et al., 2007). The resuspension flux calculation also accounts for armouring of fine particles within the interstitial spaces of larger particles. Thus, the model can indicate whether deposits will stabilise or continue to erode over time given the shear forces that occur at the site. Resuspended material is released back into the water column to be affected by all of the processes defined above.

SSFATE formulations and proof of performance has been documented in a series of USACE Dredging Operations and Environmental Research (DOER) Program technical notes (Swanson et al., 2000, Johnson et al., 2000), and published in the peer-reviewed literature (Anderson et al., 2001, Swanson et al., 2004, Swanson J.C. et al., 2007). SSFATE has been applied and validated by APASA against observations of sedimentation and suspended sediments at multiple locations in Western Australia.

5.2.1 Model Domain and Bathymetry

The domain extents for the sediment fate model were selected through performing trial runs to determine appropriate extents based on the plume behaviour over the first three months of simulation. The final domain extents and model bathymetry are illustrated in Figure 5-1.

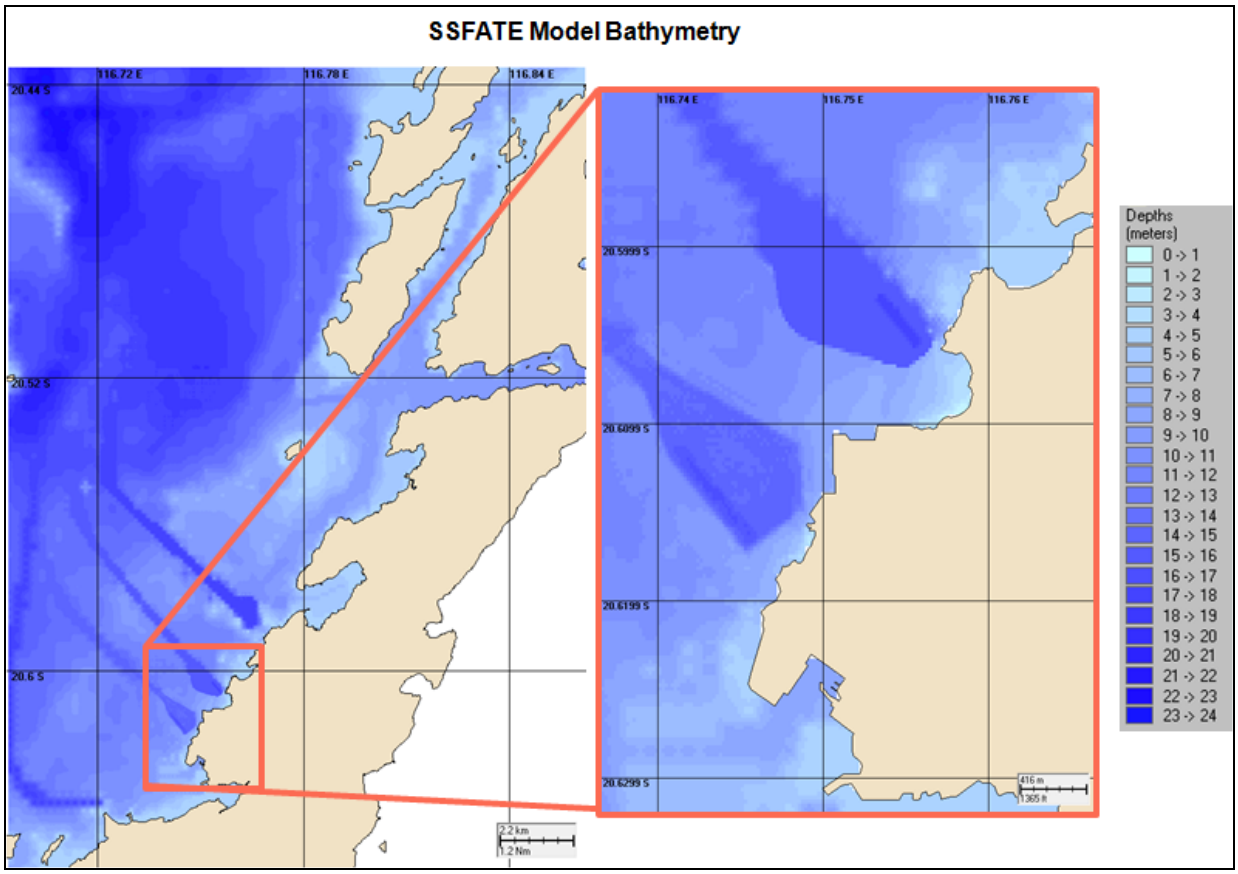

Figure 5-1 Bathymetry used in the sediment fate model grid. Left plot is the entire grid extent.

The final domain was based on a 50 m x 50 m computational grid and included most of Mermaid Sound. The minimum depth in the model was approximately 3.5 m (approximately 1.0 m below LAT) and maximum depth 23.4 m below MSL.

5.3 Specifications and assumptions of the main study

5.3.1 Dredging Methodology

The proposed dredging plan, as specified by the DPA and dredging consultant, involves a cutter suction dredging operation spanning four to six months. This operation involves cutter suction dredging of harder, consolidated material and discharging it via a floating pipe directly into the reclamation zone. The dredge cut sequence and calculated dredge volumes were provided by DPA's dredging consultant, with this information included in Appendix B.

In the model the dredge production rate and the location of the dredger were varied in time to provide a realistic representation of the movement of the sediment source. This took into account downtime as a result of daily maintenance, sea state conditions and other environmental factors, further discussed in Section 5.4.1. It is important to note that the modelling was based on an assumed dredging program and plant set and is therefore only representative of the most likely scenario.

5.3.2 Particle Size Distributions

Five material classes based on sediment grain sizes are used in SSFATE. The classes are biased towards the finer materials, as these are typically the most dispersive and are responsible for the greatest turbidity increases in the water.

Cutter suction dredgers produce mixed size fractions ranging from fine silts to small rock fragments. While the coarse material will settle rapidly, fine material is suspended by the rebounded energy of the discharge jet striking the seabed. An estimate of the appropriate size-composition of this suspended material to use in the model was determined from examining particle size distributions (PSD) obtained from geotechnical work performed on bores extracted directly from the dredging zone (Coffey, 2008). Details from each of the bores were consolidated and an estimate of the average PSD over the whole of the dredge area was determined. The resultant PSD employed in the SSFATE model is shown in Table 5-2, with the corresponding PSD used in the Pluto study also shown for comparison.

Table 5-2 Particle Size Distributions used for sediments suspended by the cutterhead

Material Class	Size Range (μm)	% of Total (DMSF)	% of Total (Pluto)
Clay	< 7	21	15
Fine Silt	7 to 35	6	8
Coarse Silt	35 to 75	5	12
Fine Sand	75 to 130	20	17
Coarse Sand	> 130	48	48

The Pluto distribution is shown to be similar to that produced from the geotechnical investigations for the DMSF project. This was expected since the Pluto site is directly adjacent to the current site, as indicated in Appendix A. The largest deviation in the PSD was for coarse silt material, which is balanced by an increase in the proportion of clay class particles. Overall, the amount of "fines", defined as material less than 75 microns, is approximately the same.

The proposed dredging method will produce two separate sources of sediment release, one from the cutter head and the other from the reclamation zone outfall. The location of the settling pond outflow has been specified by the dredge contractor and is shown in Appendix B. As the dredging is assumed to be segregated into operational and downtime periods, water and sediment are assumed to be intermittently flowing out of the settling pond, depending on when dredging is occurring.

As directed by the DPA, the concentration of sediments from the outfall is expected to be generally less than 170 mg/l. As a conservative estimate, it was assumed that the SSC of the outfall discharge would be consistently at 170 mg/l. We have assumed that only the fine sediments (silts and clays) are discharged at the outfall. The PSD for the outfall has therefore been redistributed to include only the fine sediments as a portion of the original sediment mass released at the cutterhead. The final PSD employed for the outfall is shown in Table 5-3.

Table 5-3 Particle Size Distributions used for Sediments Discharged at the Outfall

Material Class	Size Range (μm)	% of Total
Clay	< 7	65
Fine Silt	7 to 35	19
Coarse Silt	35 to 75	16
Fine Sand	75 to 130	0
Coarse Sand	> 130	0

5.3.3 Initial Vertical Distribution of Sediments

Typically in cutter suction dredging operations, material is observed to concentrate in the lower water column, with only small concentrations reaching the surface (Swanson et al., 2004). For this case in particular a vertical distribution closer to the seabed is expected due to the practice of pumping the dredge material away from the dredging site during dredging. Based on previous experience modelling cutter suction dredging operations a vertical distribution of sediments that is close to the seabed was assumed as shown in Table 5-4.

Table 5-4: Initial vertical distribution of sediments in the water column setup by loss from the cutterhead.

Elevation above seabed (m)	% of sediments
10	5
7	15
3	20
2	40
1	20

Although the vertical distribution was biased towards the seabed, reflecting the discharge height, a proportion was released towards the surface to account for billowing of the plume. The 5 and 15 % release rates at 10 and 7 m respectively was a conservative estimate, as particles suspended to this level in the water column would undergo a significant amount more dispersion as a result of being in a stronger current field.

The vertical distribution of sediments released from the outfall were biased near the surface, as this is where the sediments would be released. Based on past studies on outfall discharge, and using the local water depth at the outfall of 6 m, an appropriate initial vertical distribution of sediments was determined with this shown in Table 5-5.

Table 5-5 Initial vertical distribution of sediments in the water column setup by outfall

Elevation above seabed (m)	***% of sediments***
6	30
5	25
4	25
2	10
1	10

The volume of material resuspended during the dredging operation is proportional to the production rate. Published resuspension rates for cutterhead dredges range from less than 0.1 % to over 5 % of the production rate, however, data from the most comprehensive studies show resuspension rates for cutterhead dredges are generally less than 0.5 % (USACE, 2008). Using this as a basis for reference, a resuspension rate of 0.5 % was selected as a suitable yet conservative estimate for the current study.

5.3.4 Mixing Coefficients

The addition of energy to a shallow coastal environment through tides and waves, results in dissipation through bottom friction and turbulent mixing of the water column. The diffusion ([m^2/s]) is the model parameter which describes the degree of turbulent mixing. The vertical diffusion profile is particularly important as it is the only parameter within the model which determines upward transport of dredged material. The amount of turbulence affects the vertical concentration profile of suspended sediment in the water column. Obviously the more sediment that stays higher in the water column, the higher probability there is that it will be advected further by currents.

There is no literature on vertical turbulence estimates within Dampier. Katsumata (2006) estimates that the energy dissipation due to tides on the North West Shelf results in a vertical diffusivity of the order 10^{-4}-10^{-3} m^2s^{-1} (Katsumata K., 2006). Results of that study were quantified using a large scale numerical model and are not based on any field data, other than to compare tidal magnitudes. However, this work did provide a range of vertical diffusion values to base the sediment transport model upon. The only field study which model results could be based upon was from measurements of suspended sediment after a dredging operation in Dampier by Stoddart and Anstee (2004). Measurements concluded that suspended sediment concentrations were well mixed in the near and far field of the dredging operation (Stoddart and Anstee, 2005).

Through analysing results from prior test simulations within Mermaid Sound during the Pluto Dredging Study, a suitable horizontal dispersion coefficient of 0.5 m^2/s was adopted with a vertical diffusion coefficient of 10^{-3} m^2/s (APASA, 2006).

5.4 Dredge Simulation Scenarios

The dredge modelling was performed for both the ambient and energetic scenarios detailed in Section 3.6. Variations in environmental forcing and the application of cyclones in the energetic scenario resulted in varying levels of downtime and hence dredging completion dates, discussed below.

5.4.1 Downtime for Dredging Operations

There were a number of conditions that would result in downtime for the dredge operations. This included an inherent 7 hour downtime for daily maintenance, expected to occur during daylight hours, sea state downtime and coral spawning closure. Each of these were implemented into the dredging schedule using their actual, or expected, period of occurrence in the year, to accurately simulate the entire dredging operation.

Two separate coral spawning periods are expected to occur over the course of the dredging operations. These events are predicted to occur 7-9 days after the full moon in December and March. As a conservative estimate it was assumed that dredging would cease 5 days after the

full moon and recommence in 7 days time. The dates, as input into the dredge model, are indicated in Table 5-6.

Table 5-6: Coral spawning closure dates for the two spawning events in December and March

Spawning Event	**Full Moon Date**	**Predicted Spawning Start**	**Predicted Spawning End**	**Dredging Operations Stop**	**Dredging Operations Recommence**
December 2010	Tues 21st Dec 2010	Tues 28th Dec 2010	Thur 30th Dec 2010	Sun 26th Dec 2010	Sun 2nd Jan 2011
March 2011	Sun 20th Mar 2011	Sun 27th Mar 2011	Tues 29th Mar 2011	Fri 25th Mar 2011	Fri 1st Apr 2011

It was assumed that the limiting wave conditions would be approximated by Hs over 0.7 m and Tp over 8 seconds, as suggested by the dredging consultant (Haydn Pike, pers. comm). The approximate downtime as a result of these limiting wave conditions was determined through examining the wave model output at the dredge site for both the ambient and energetic scenario's. For the ambient scenario, the specified wave conditions restraints results in a sea-state downtime of approximately 10.5 %, with this increasing to 19.1 % for the energetic scenario.

In addition to this, the energetic scenario included downtime as a result of cyclone closure. The cyclone closure dates for the historical cyclones included in the energetic scenario were taken as two days before and three after the cyclone passed near Dampier (which typically coincided with the date of landfall for the cyclones). A summary of these dates is provided in Table 5-7. Again these closure dates were implemented using their actual period of occurrence in the year.

Table 5-7: Cyclone closure dates for the three cyclones included in the energetic scenario

Cyclone (Year)	**Dates Cyclone was within 80 km of Dampier**	**Approximate Closure Dates**	**Total Closure Period**
Clare (2006)	9th to 10th January	7th Jan to 13th January	6 days
Steve (2000)	6th to 7th March	4th to 10th March	6 days
Orson (1989)	23rd April	21th to 26th April	5 days

Overall the dredging operation for ambient scenario was approximately 159 days, with an estimated date of completion on the 8th of April 2011. This was extended in the energetic scenario to 173 days, where the estimated completion date was the 20th of April 2011. Both of these completion dates agree with the expected duration of a 4-6 month operation.

5.5 Thresholds

The objective in setting thresholds is to set a levels of SSC, sedimentation or other parameter which can act as a signal that potential impacts may occur. The exceedance of that threshold may then trigger a series of predetermined management responses. The underlying basis for the threshold is that a tangible risk of impact is evident once the threshold has been exceeded.

For this study, as directed by the DPA, the thresholds employed during the Pluto Dredge Modelling Study were used. Subsequent field monitoring programs during and after the Pluto dredging operations have since confirmed that these thresholds are conservative and substantially underestimate the levels of suspended sediment and sedimentation required to cause detectable morality (Mscience, 2009a). Full documentation of these thresholds and the methodology used in their determination can be found in SKM (2007).

5.5.1 TSS

In summary the suspended sediment thresholds are defined by TSS limits for three distinct zones, as illustrated in Figure 5-2 . Table 5-8 indicates the maximum allowable concentrations of suspended sediments over a specified duration for the three given zones.

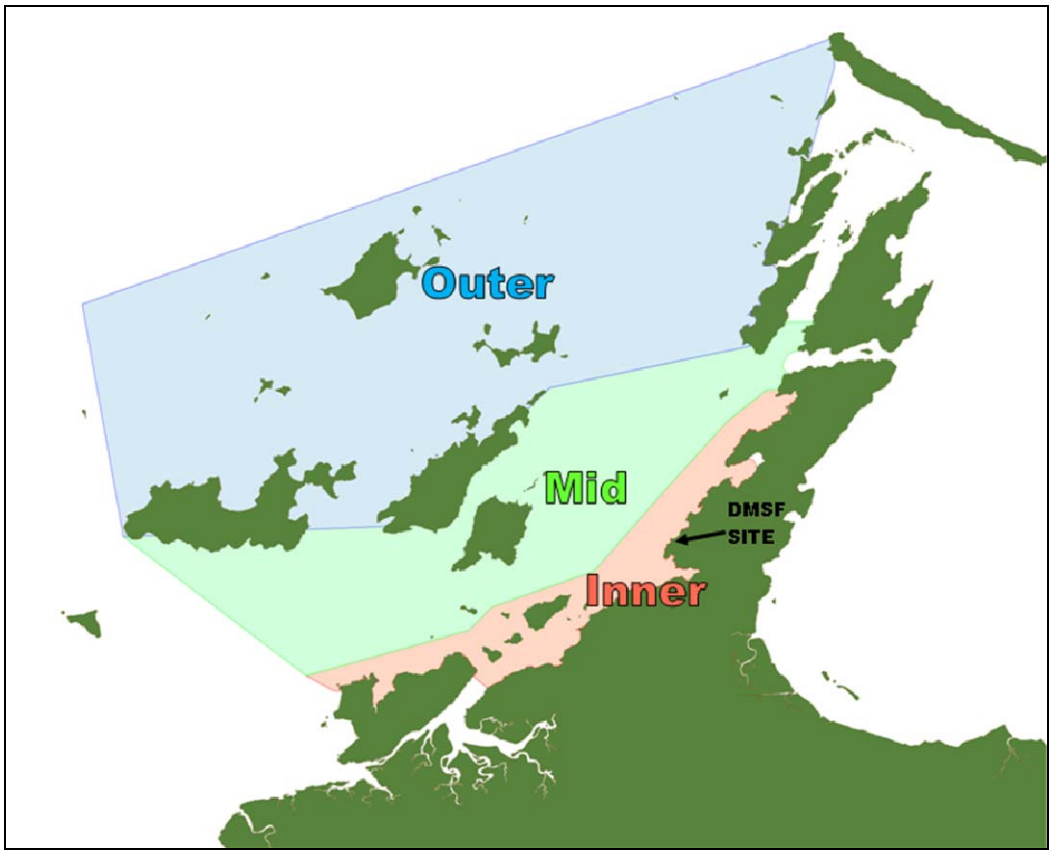

Figure 5-2 Map of ecological management zones defining separate threshold limits.

Table 5-8: Suggested allowable frequency of intensity-duration events per month for model interrogation (SKM, 2007)

	Inner	Mid	Outer
Threshold Concentration	35 mg/l	10 mg/l	10 mg/l
Max # of 1 hr events per month	16	10	4
Max # of 2 hr events per month	8	2	2
Max # of 3 hr events per month	5	1	2
Max # of 4 hr events per month	2	1	1
Max # of 5 hr events per month	1	1	1
Max # of 6 hr events per month	0	0	0

An allowance for background concentrations was included in the threshold analysis as the values in Table 5-8 relate to total in water concentrations of suspended sediments. Based on a recent turbidity monitoring program at the project site an appropriate level of background SSC was selected as 5.25 mg/l for the entire domain (Mscience, 2009b). This was based on the 80th percentile of a number of turbidity measurements made near site and further reaches of Mermaid Sound. The 80th percentile was selected as a more conservative value to use than the mean.

For ease of comparison the same thresholds were applied to the energetic scenario. It should be noted, however, that these thresholds relate to ambient conditions. Exceedances due to cyclone events should be considered in the knowledge that natural resuspension rates would almost certainly lead to an exceedance of the SSC thresholds.

5.5.2 Sedimentation

Sedimentation thresholds were defined using three different intensity-duration brackets as defined in Table 5-9. An allowance for background sedimentation rates was set based on those values used during the Pluto project. This was 2.3 mg/cm^2/day for the inner zone and 1.0 mg/cm^2/day for the mid and outer zones.

Table 5-9: Acute, Medium and Chronic Term Thresholds for model interrogation (SKM, 2007)

	Inner Zone	**Mid - Outer Zone**
Acute (for any day)	Flag if > 33 mg/cm^2/day	Flag if > 6.6 mg/cm^2/day
Medium Term (for any 5 days in a 15 day period*)	Flag if > 60 mg/cm^2/day	Flag if > 12 mg/cm^2/day
Chronic Term (for any 15 days in a 30 day period*)	Flag if > 36 mg/cm^2/day	Flag if > 9 mg/cm^2/day

*Days do not need to be consecutive.

These thresholds were applied to the energetic scenario in the same manner as the ambient case.

5.6 Dredge Model Results

5.6.1 TSS Concentrations

Model results of suspended sediment (SSC) concentrations were analysed for each scenario over the entire six month dredging operation. The maximum suspended sediment concentration throughout the water column was used in this analysis as it provided a conservative estimate of the likely suspended sediment concentrations anywhere in the water column. The maximum value typically occurred near the seabed due to the gradual settlement of the suspended sediment.

The results are presented as contour plots as this type of analysis provides insight into the footprint of the area affected by sediment plumes as well as indicating regions likely to experience the highest SSC.

Please note that all values presented here represent SSC solely as a result of the dredge operations, and therefore represent concentrations above background levels. Background SSC concentrations have **NOT** been included in these data presentations, however, are included in the threshold analysis.

A few snapshots from the model have been presented in Figure 5-3 and Figure 5-4 that represent the strongest plumes generated during the summer (December to February) and autumn (March to May) period of the dredging operations for each scenario.

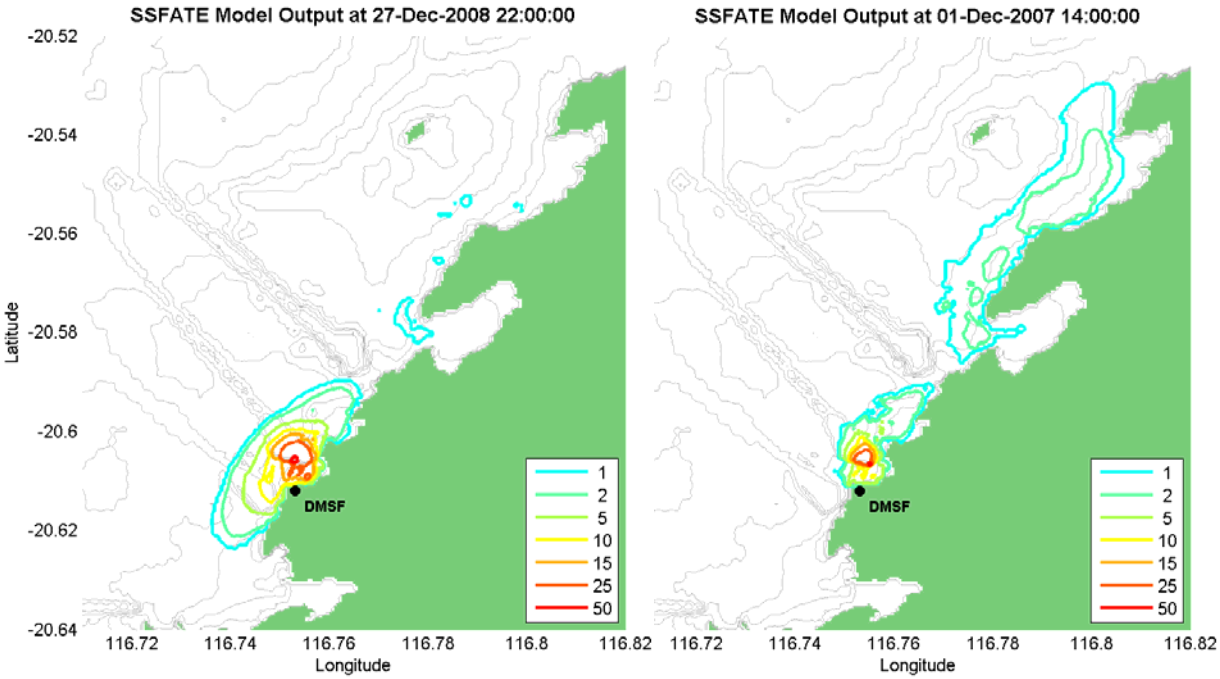

Figure 5-3 Snapshot of strongest plume generated during Summer for the ambient (left) and energetic (right) modelled scenarios. Bathymetry contours are shown in grey.

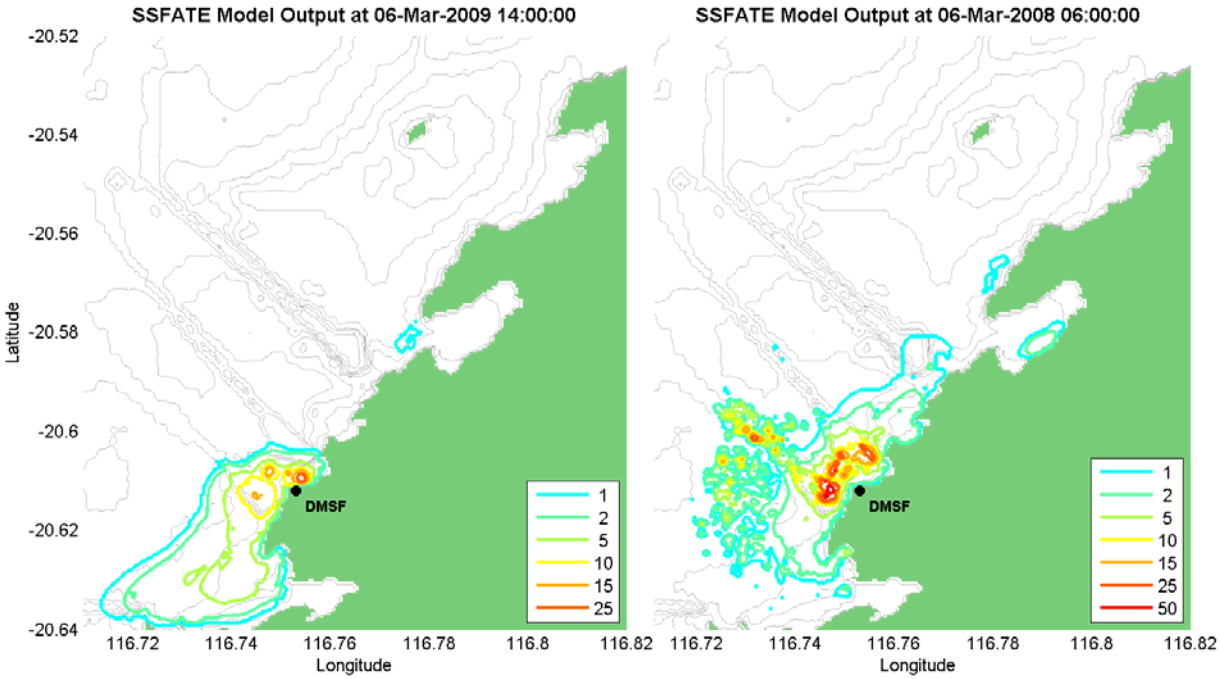

Figure 5-4 Snapshot of strongest plume generated during Autumn for the ambient (left) and energetic (right) modelled scenarios. Bathymetry contours are shown in grey.

These images show that the plume is concentrated at the dredge and outfall zone. The two scenarios were forced with completely different time-based forcing, meaning a direct comparison of these images is not possible. Figure 5-4, however, clearly indicates the larger

portion of high concentrations offshore generated by the Cyclone Steve event included in this run.

In addition to these model snapshots, the 80th and 95th percentile values of SSC were also determined. These provide a representation of the relative frequency of occurrence of the plume throughout the area of interest. Results from the ambient and energetic scenarios for the selected percentiles are presented in Figure 5-5 and Figure 5-6.

Results for both the ambient and energetic simulations indicate that the sediment plume generated from the dredging activities and outfall discharge would be dominantly transported north-east. Although the results varied between the two scenario's, as indicated in the 95th percentile plots, both simulations indicated that the plume would extend only as far as 4 to 5 km from the dredge zone with concentrations in excess of 5 mg/l above background. Plume movement southwards towards King Bay was more common during the ambient run, whilst the occurrence of concentrations exceeding 5 mg/l further than 2km of the coast only occurred in the energetic scenario.

The area affected by higher TSS concentrations (in excess of 20 mg/l) were generally restricted to the immediate region surrounding the dredge zone and only apparent 2 to 5 % of the time during the dredging operations. The highest sustained plume concentrations were within 200 m of the outfall discharge point along the northern reclamation wall.

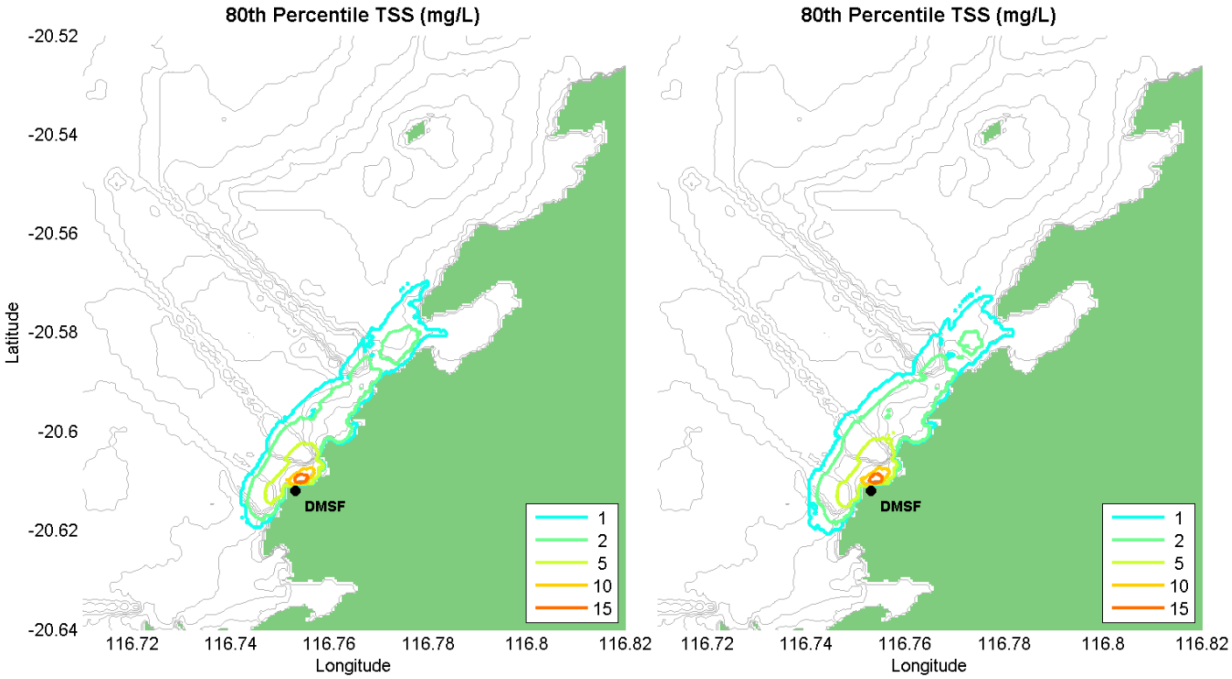

Figure 5-5 Estimate of the 80th percentile of the maximum water column TSS (mg/l) for the ambient (left) and energetic (right) modelled scenarios. Bathymetry contours are shown in grey.

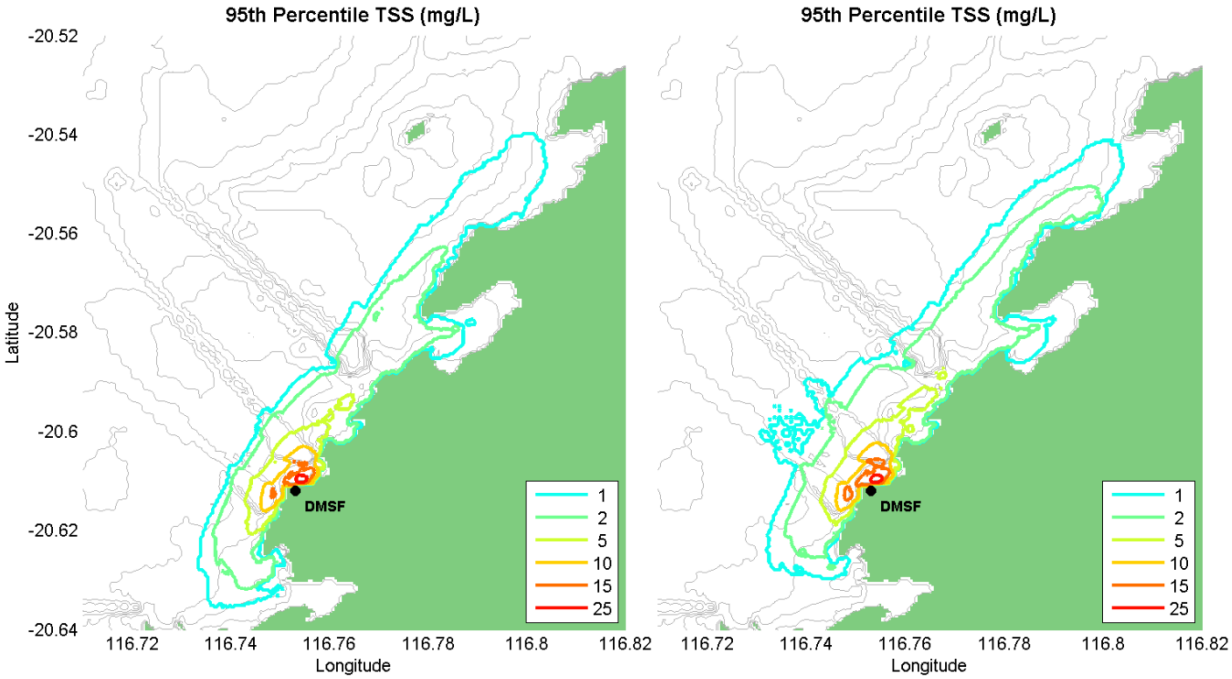

Figure 5-6 Estimate of the 95th percentile of the maximum water column TSS (mg/l) for the ambient (left) and energetic (right) modelled scenarios. Bathymetry contours are shown in grey.

Threshold Exceedance

The spatial comparison against the thresholds defined in Section 5.5 are illustrated in Figure 5-7. The results were analysed in terms of the total occurrences of suspended sediment events in excess of the defined intensity-duration-frequency thresholds specified in Table 5-8, including and allowance for background concentration.

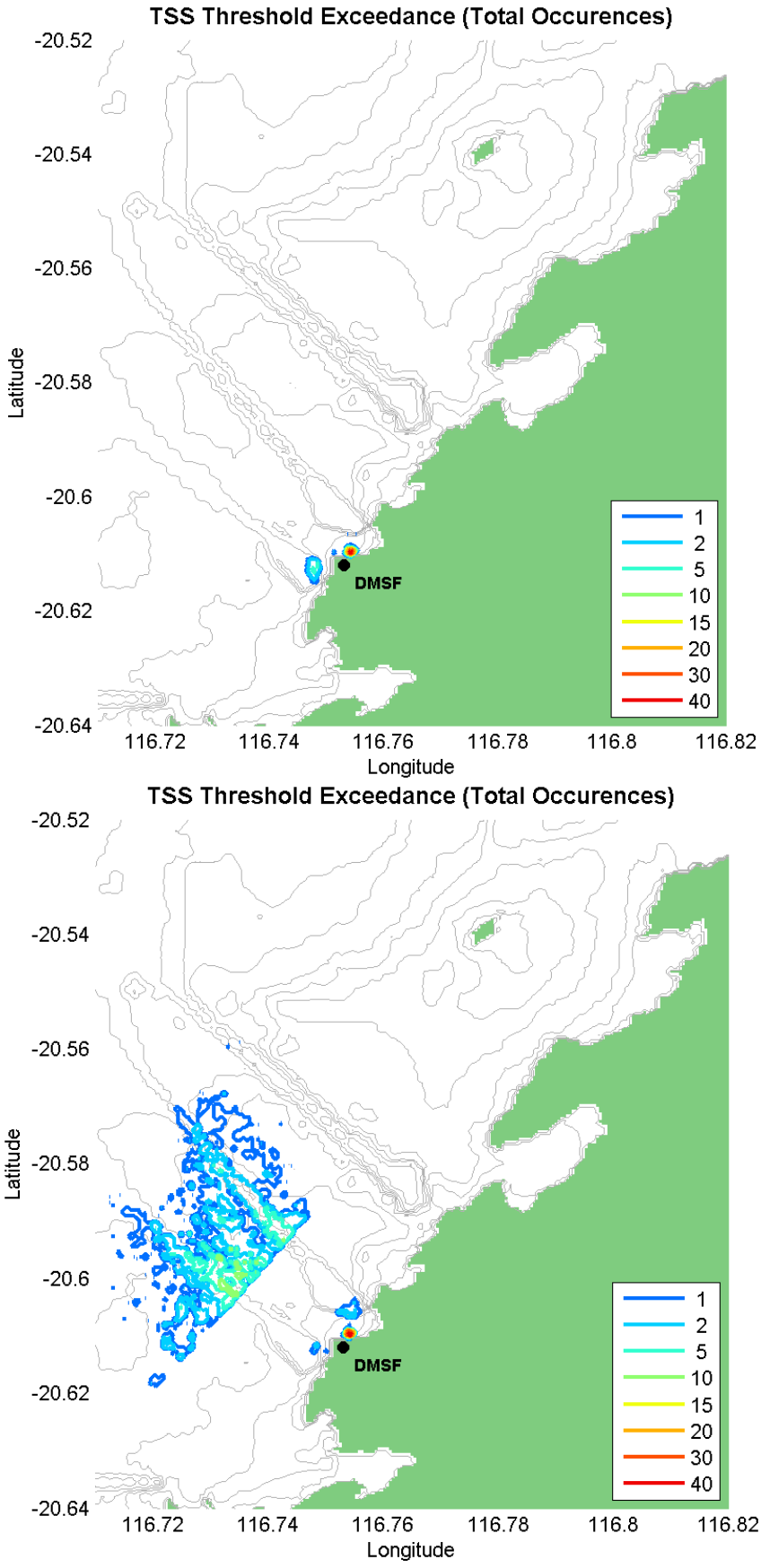

Figure 5-7 TSS threshold exceedance based on total number of events above allowable frequency of intensity-duration thresholds over the entire dredge period for the ambient (top) and energetic (bottom) modelled scenarios. Bathymetry contours are shown in grey.

As with the percentile analysis of TSS, the threshold analysis clearly illustrates a sustained exceedance in the immediate waters (within 100 m) of the outfall discharge point. The continual discharge from this point source during dredging results in all durations shown in Table 5-8 being exceeded at least once. Examination of the 95 th percentile plots, in Figure 5-6, suggests that these exceedances are only moderately above the 35 mg/l threshold with the addition of the background SSC.

The energetic scenario again shows that threshold exceedances in excess of 10 occurrences over the entire dredging period are localised to the outfall discharge point. The offshore movement of the plume to the mid threshold zone, as a result of the cyclone events included in the energetic scenario, generated a series of occurrences in this zone. It should be noted that since dredging operations are to cease two days before and after cyclone events that these exceedances all occur due to the resuspension of deposited sediment. As natural SSC during cyclonic events are likely to be high, the additional elevation may not be of undue concern.

5.6.2 Bottom Deposition

To assess the impact on sediment distribution throughout Mermaid Sound, bottom deposition was output from the model. Hourly output of bottom deposition was generated over the model domain, for the duration of the dredging operation. As with the TSS analysis, contour plots were prepared for the 80th, 95th and 98th percentile values of daily sedimentation rates for each of the simulation scenarios and cross-compared. These contour plots for the respective percentiles are presented in Figure 5-8 and Figure 5-9.

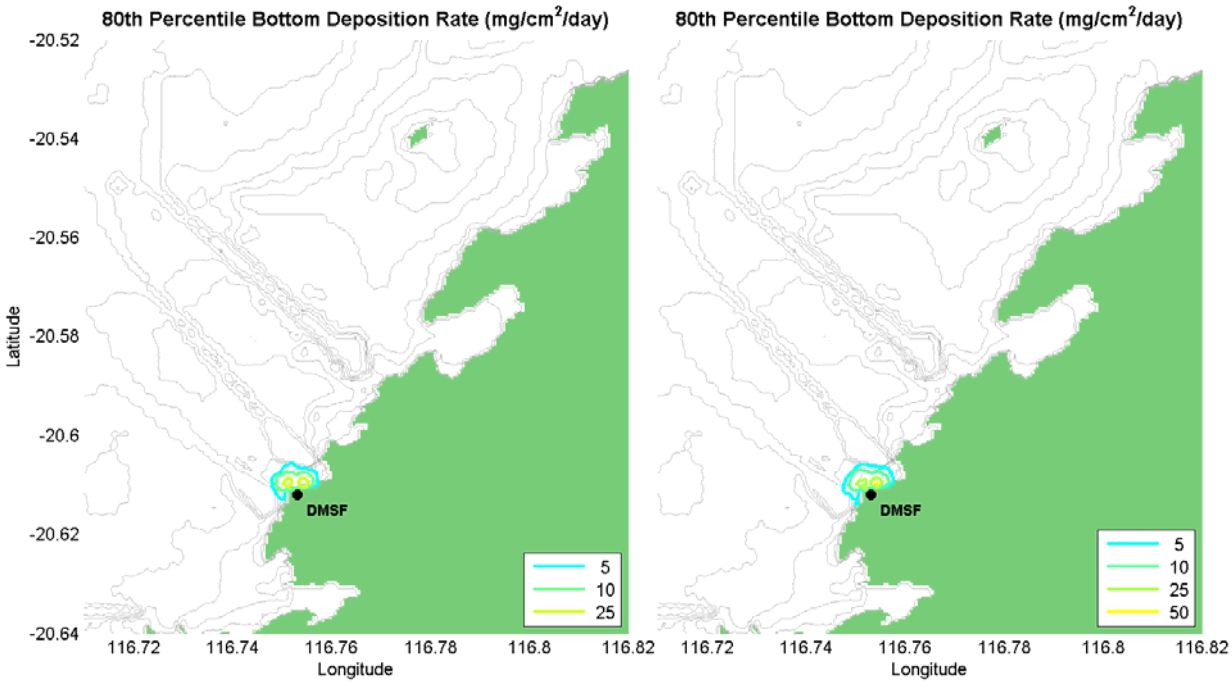

Figure 5-8 Estimate of the 80th percentile of the sedimentation rate (mg/cm^2/day) for the ambient (left) and energetic (right) modelled scenarios. Bathymetry contours are shown in grey.

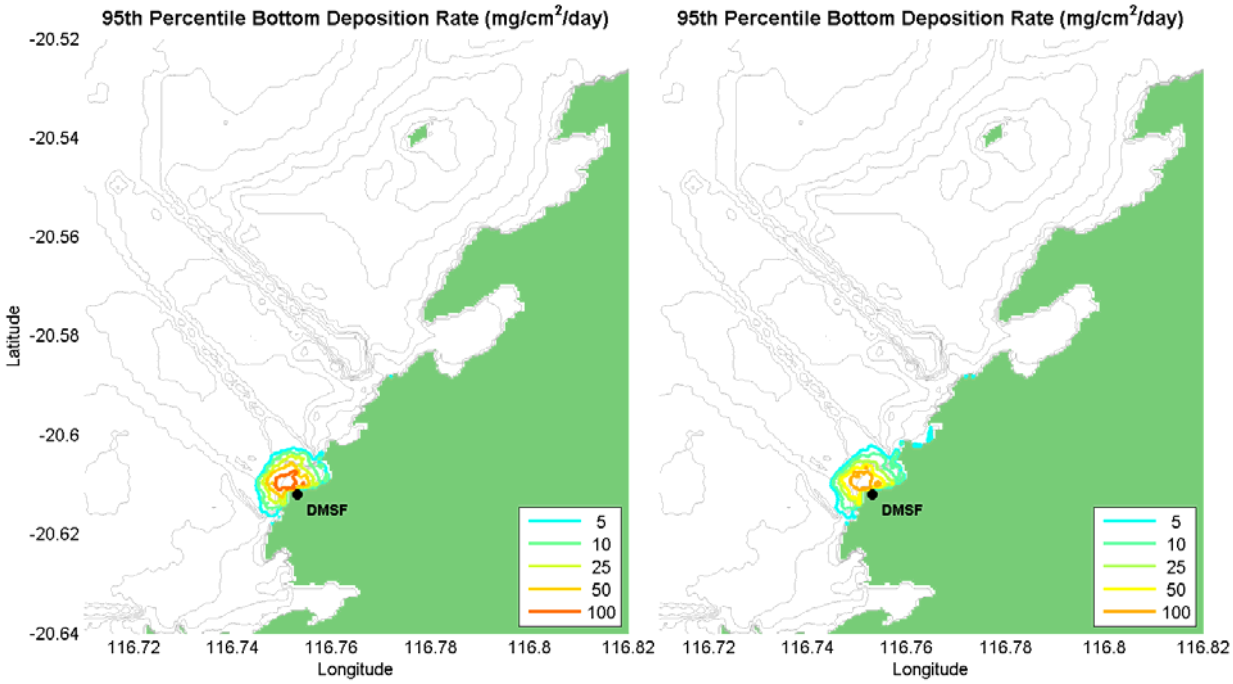

Figure 5-9 Estimate of the 95th percentile of the sedimentation rate (mg/cm^2/day) for the ambient (left) and energetic (right) modelled scenarios. Bathymetry contours are shown in grey.

As these figures indicate, most of the bottom deposition of materials is predicted to occur within close proximity to the dredge areas as the generally coarse material (74 µm and greater) settles within minutes of being suspended by the cutterhead. Only marginal differences in the sedimentation rate footprint are observed between the ambient and energetic simulations, with slightly lower and more dispersed sedimentation rates evident in the energetic scenario as a result of the increased intensity of the environmental forcing.

Threshold Exceedance

Exceedance of the sedimentation thresholds for both the ambient and energetic modelled scenarios is presented in Figure 5-10 to Figure 5-12 for the acute, medium and chronic term thresholds respectively. The images show the total number of days where the given thresholds were exceeded over the entire model duration.

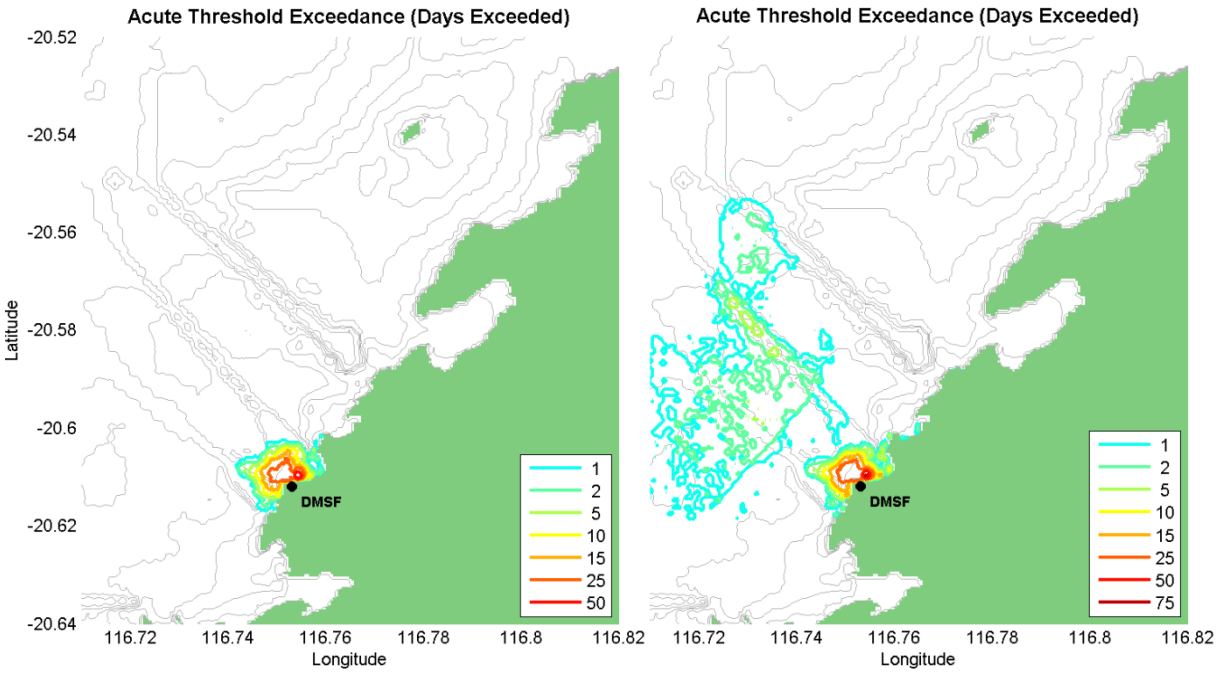

Figure 5-10 Acute sedimentation rate threshold exceedance based on total number of days exceeded over the entire dredge period for the ambient (left) and energetic (right) modelled scenarios. Bathymetry contours are shown in grey.

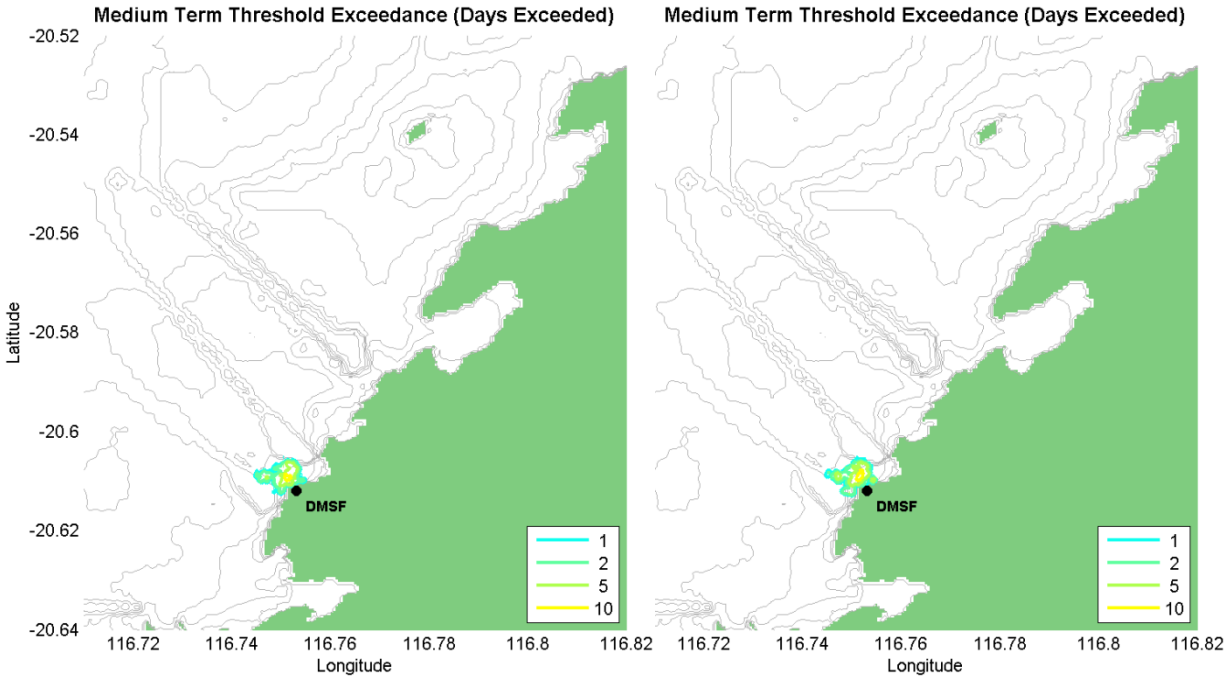

Figure 5-11 Medium term sedimentation rate threshold exceedance based on total number of days exceeded over the entire dredge period for the ambient (left) and energetic (right) modelled scenarios. Bathymetry contours are shown in grey.

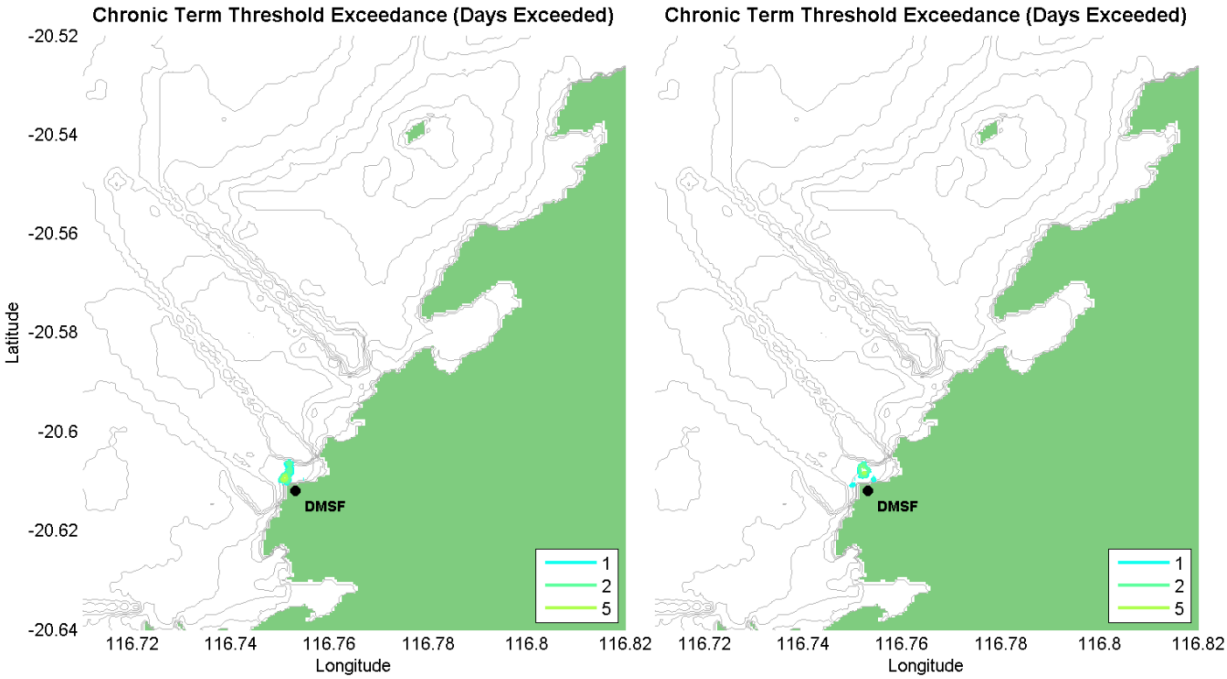

Figure 5-12 Chronic term sedimentation rate threshold exceedance based on total number of days exceeded over the entire dredge period for the ambient (left) and energetic (right) modelled scenarios. Bathymetry contours are shown in grey.

Zones where the model predicted sedimentation rates would exceed the given threshold allowances were mostly concentrated around the dredge and outfall sites. Acute threshold exceedances were the most common, with over 62 days, out of the 159 days of dredging predicted during the ambient scenario, showing sedimentation rates in excess of the set thresholds. This was moderately increased for the energetic case to 75 days (out of the 173 day estimated dredging duration), with some of these extending offshore from the key areas of operation as a result of resettlement of resuspended materials following cyclones.

Medium and chronic term threshold exceedances were even more localised to the dredge zone, with chronic threshold exceedance only occurring 6 days over the entire simulation. The medium term exceedance was estimated to occur a total of 13 days over the duration of the dredge works, however, only within the designated dredge footprint.

In summary, all of the sedimentation rate threshold exceedances for the ambient scenario, and most of those in the energetic scenario, occurred either in the dredge zone or within 200 m of its extents.

5.6.3 Sedimentation in Pluto Turning Basin

An assessment of the overall level of sedimentation within the Pluto turning basin resulting from the DMSF dredging was made to address concerns raised by WEL. The turning basin is directly adjacent to the dredge zone, as depicted in Appendix A, and has been dredged to approximately 12.5 m below MSL. As this is 2-3 m below the 11m dredge depth for the DMSF outer dredge area, it is a proposed that a tapered slope of 1:2 will be constructed between the two dredge zones.

To assess the total level of sedimentation expected to occur within the Pluto turning basin, the bottom thickness, as determined from the SSFATE model, was output and analysed. To account for the increased porosity of the settled "wet" sediments after suspension from the cutter-head, it was assumed that the settled sediments would have the same properties as a loosely packed, well sorted natural sand bed where porosity is typically 0.46 (Soulsby, 1997).

The bottom thickness was initially analysed spatially for both the ambient and energetic modelled scenarios. The total accumulated level of sedimentation two months after the end of the dredging operations is illustrated in Figure 5-13 for both the ambient and energetic scenarios.

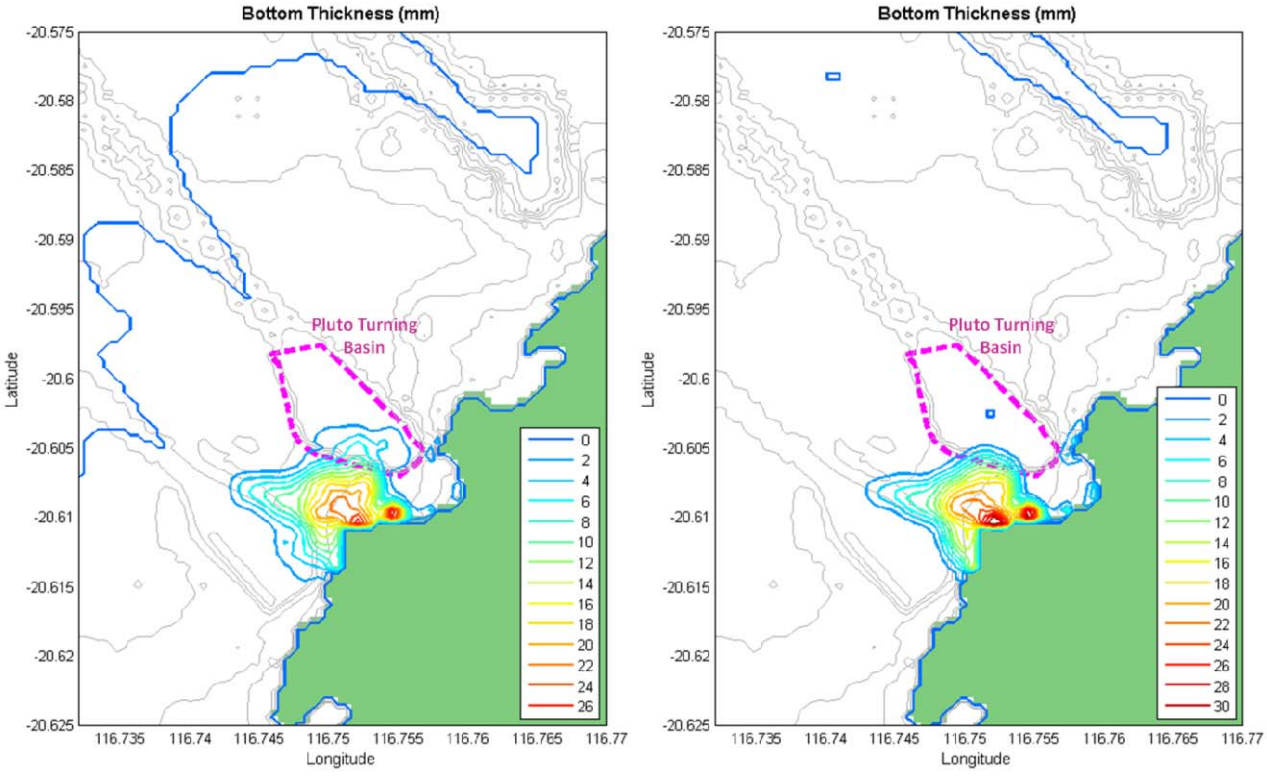

Figure 5-13 Total bottom thickness increase (mm) as a result of dredging operations for the DMSF project for the ambient (left) and energetic (right) modelled scenarios. Pluto turning basin extents are indicated. Bathymetry contours are shown in grey.

As the plots indicate, most of the deposition resulting from the dredging operations and outfall discharge occurs within the immediate vicinity of the DMSF project zone. Accumulated settled

sediments in excess of 14 mm are contained within the extents of the proposed dredge zone and immediately adjacent to the outfall discharge point. A quantitative assessment of the sedimentation within the Pluto turning basin indicated that the maximum level of deposition within the turning basin was expected to be 10.8 mm during the ambient scenario and reduced to 10.1 mm for the energetic, where stronger environmental forcing increased dispersion of sediments. These maximum values occur in the southwest portion of the dredge zone only. The ambient scenario produced and average bottom thickness of 1.6 mm across the turning basin zone, reduced in the energetic scenario to 0.6 mm.

6 OIL SPILL MODELLING

6.1 Background

Spill modelling was carried out using ASA's three-dimensional oil spill model, SIMAP (Spill Impact Mapping and Assessment Program). SIMAP is designed to simulate the fate and effects of spilled hydrocarbons for both the surface slick and the three-dimensional plume that is generated in the water column from sub-surface releases (French, 1998, French et al., 1999, Spaulding et al., 1994).

The SIMAP physical fates model calculates the transport, spreading, entrainment, evaporation and decay of surface slicks and the entrained and dissolved oil released from the slicks. Input specifications for oil-types include the density, viscosity, pour point, distillation curve (volume lost versus temperature) and the aromatic/aliphatic component ratios within given boiling point ranges. These algorithms are used to proportion the distribution of the oil (as mass and concentrations) over time into the following components:

- Surface bound oil;
- Entrained oil (non-dissolved oil droplets that are physically entrained by wave action);
- Dissolved hydrocarbons (principally the aromatic hydrocarbons);
- Evaporated hydrocarbons;
- Sedimented hydrocarbons; and
- Decayed hydrocarbons.

The SIMAP trajectory model separately calculates the transport of the material that is on the water surface (as surface slicks), in the water column (as either entrained whole oil droplets or dissolved hydrocarbon), has stranded on shorelines, or that has precipitated out of the water column onto the seabed. The model calculates the transport of surface slicks as a combination of the forces exerted by surface currents and forces exerted by wind acting on the oil. Transport of entrained oil (i.e. oil that is below the water surface) is calculated using the surface currents only.

For seabed releases, a blowout module is used to calculate the rising of oil droplets and the dissolution of soluble components into the water column, based on the depth and general pressure of the release accounting for the size of oil parcels that are produced. Higher rates of dissolution are produced for high pressure releases (e.g. where a high gas pressure is forcing the release) as these produce smaller parcels with a larger surface area/volume ratio. Droplet sizes are important for controlling the rise rate of the oil and the response to breaking waves (which force the sinking of slick oil into the water column). Release rates and other parameters are based on empirical measurements (Spaulding et al., 2000).

6.2 Stochastic Modelling

SIMAP can be used to predict the fate of a single spill under defined conditions, or of multiple spills that occur under a random selection of prevailing conditions (referred to as stochastic modelling). The stochastic model performs a large number of simulations for a given spill site, randomly varying the spill time, so that the transport and weathering of each slick are subject to a different set of prevailing wind and current conditions. By sampling the environmental data archive at random, the data sets will be representative of the distribution of the prevailing conditions. During each simulation, the model records the grid cells that were contacted by oil particles, as well as the amount of time that had elapsed prior to the contact or exposure.

Once the stochastic modelling is complete, the results are compiled from each of the sample trajectories to provide a statistical weighting to the likelihood of exposure. Results can be summarised as:

1. the probability that a grid cell may be exposed to oil slicks;
2. the minimum time before exposure could occur; and
3. Concentrations that could be involved

The first estimate is calculated from the frequency of exposures during all simulations, while the latter estimate is the worst-case for any of the sample trajectories (French et al., 1999). The stochastic modelling approach provides an objective measure of the possible outcomes of a spill, as well as the means of quantifying the likelihood of a given outcome. The most commonly occurring conditions would be selected most often while conditions that are more unusual can also be represented.

6.3 Scenarios

Quantitative spill modelling was used to examine two, hypothetical, hydrocarbon spill scenarios. The details of these scenarios, as provided by Response Resource Management Pty Ltd are (Priestly, 2009):

1. A spill of 50,000 litres of 380 CST HFO which leaks over a period of 30 to 45 minutes originating 60 metres off the face of the new DMSF wharf. The spill could occur at any stage of tide.
2. A spill of 2,500 litres of tropical automotive diesel fuel TADF, occurring instantaneously from alongside the wharf at any stage of tide

Each of these scenarios was examined individually under both summer and winter forcing conditions, resulting in a total of four spill scenarios being modelled. Each stochastic simulation included 100 runs using random selection of prevailing conditions for each season.

6.3.1 Nature of the hydrocarbons investigated

Heavy fuel oil (API 12.3; specific gravity 975 kg m^{-3}) is manufactured by adding low-volatile solvents to residual oils from refining processes to achieve a desired gravity, viscosity and pour point. Volatile and semi-volatile components contribute a small proportion to heavy fuel oil and the product has very high viscosity (3,200 centipoise @ 25° C); therefore, when exposed to the atmosphere, the volatile components are lost, resulting in an oil blend that is resistant to evaporation. Weathering simulations for heavy fuel oil, shown in Figure 6-1, indicated that due to evaporation and decay the hydrocarbon mass would reduce by about 10 % over a period of 5 days. Note that heavy fuel oil takes up water as a water-in-oil emulsion in a process that increases the volume of slicks and dramatically increases the viscosity.

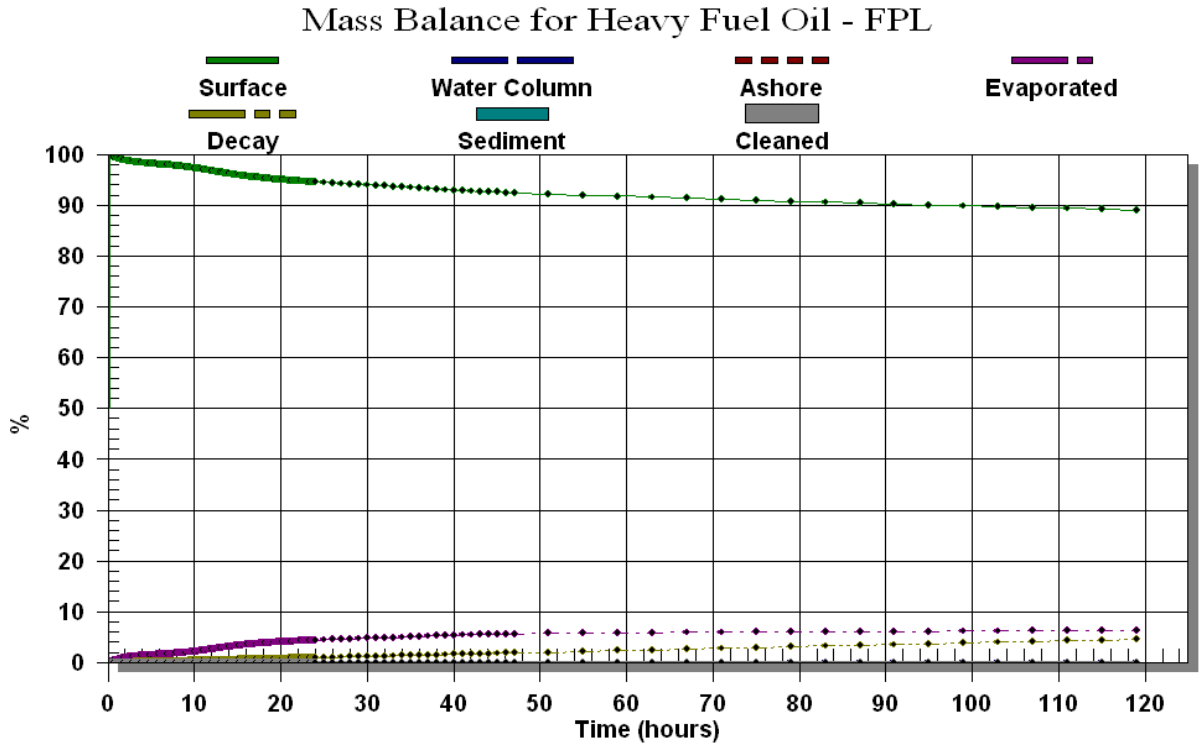

Figure 6-1 Predictions for the weathering of heavy fuel oil released onto the water surface.

Marine diesel (API 37.6; specific gravity 829 kg m^{-3}) is a mixture of volatile and persistent hydrocarbons. Weathering analysis presented in Figure 6-2 indicates that approximately 40 % by mass is predicted to evaporate over the first day or two of exposure to the atmosphere for diesel spilled onto the water surface under calm sea conditions, and the remainder persisting for an extended period. Note that the heavier components of diesel may physically entrain into the upper water column as oil droplets in the presence of waves, but can refloat to the surface if wave energies abate.

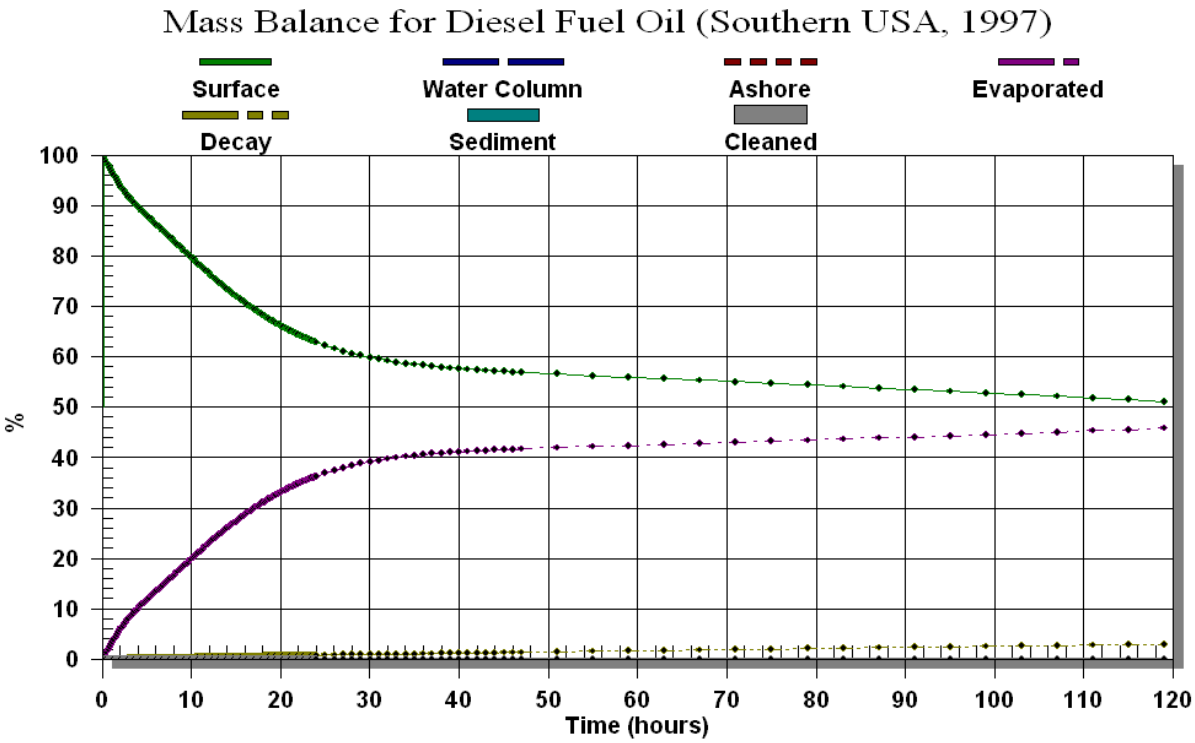

Figure 6-2 Predictions for the weathering of diesel released onto the water surface.

6.3.2 Thresholds used

The SIMAP model is able to track oil to concentrations that are lower than biologically significant levels and threshold concentrations are specified to control the recording of "exposure" to surrounding locations. An oil slick is unlikely to cause impacts due to smothering once it has thinned to 0.001 mm (French et al., 1999, NOAA, 1997).

Thresholds for registering contact by surface slicks for surface waters were assessed at a number of concentrations, to provide guidance on the spatial area that could potentially be affected at different thickness. Based on the relationship between slick thickness and appearance (Bonn Agreement, 2004, NOAA, 1997) as indicated in Figure 6-3, three thresholds were applied:

- 10 g/m^2 (0.0100 mm), appearing as yellow-brown "true" oil colour
- 1 g/m^2 (0.0010 mm), appearing as rainbow sheen
- g/m^2 (0.0001 mm), appearing as silver sheen

These thickness thresholds also provide some guidance to the potential for environmental harm. For example, estimates for the minimal thickness of oil that will result in harm to seabirds through ingestion from preening of contaminated feathers, or the loss of thermal protection of their feathers, has been estimated by different researchers at 0.0100 mm to

0.0250 mm (10 - 25 g/m^2) (French, 1996, Kroops et al., 2004). Hence, any oil layer thickness in excess of this order of magnitude is likely to be harmful to birds that contact the slick.

Contact of oil on shorelines was only registered in the model when the predicted thickness of stranded oil exceeded a threshold of 10 g/m^2 (0.01 mm). This is equivalent to the lowest thickness where the oil will appear as an oily brown film (Figure 6-3), and hence generate the potential for smothering or, at least, staining of the shoreline. For entrained oil, a particularly conservative threshold concentration of 1.0 ppb was specified. This was based on reviews by French (2000) which indicated concentrations of the order of 10 ppb (an order of magnitude higher than the current thresholds) would be the no-effect concentration for relatively sensitive marine species, given relatively long exposure (> 24 hrs) to the most toxic soluble compounds.

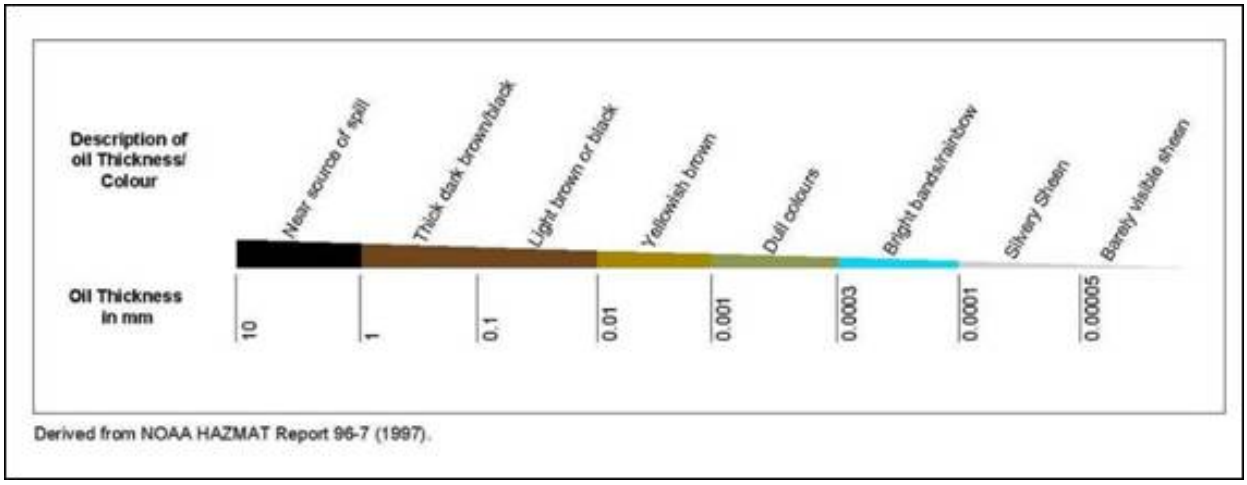

Figure 6-3 Surface oil colour description as a function of surface oil layer thickness (NOAA, 1997)

6.4 Oil Spill Modelling Results

6.4.1 Heavy fuel oil spill

The persistence of this oil type allows for slicks to potentially drift further before coming ashore, thus increasing potential risks to more distant shorelines, or to repeatedly expose local shorelines over a longer duration if oil is trapped within the local circulation. Due to the high viscosity and density, heavy fuel oil tends to stick to substrates and accumulate on shorelines at a greater thickness, with deleterious impacts through smothering or toxicity through direct contact. The high viscosity of the floating emulsion presents a high risk to seabirds, through oiling of their feathers.

The high viscosity tends to limit the penetration of fine-grained sediments, but allows penetration and sticking to creviced and bouldered rocky shorelines (Fingas, 2000, Fingas and Brown, 2000). If left in place, heavy fuel oil tends to reduce to a tar-like substance that is very slow to weather biologically. Weathered heavy fuel oil will also have a closer density to seawater and will trap suspended sediments so that slicks may sink to the seabed in some circumstances (Brown et al., 1998).

Stochastic modelling indicated that, in accord with the prevailing winds, slicks would most probably drift north-north-east against the Burrup Peninsula toward Angel and Dolphin Islands during summer (Figure 6-4) and drift west toward East and West Lewis Islands during winter (Figure 6-5). The watersbetween the release site, the east side of West Intercourse , East Lewis and West Lewis Islands and the south sides of Angel and Dolphin Islands would have higher than 0 % probability of exposure to surface oil during both modelled seasons. The above area also delineates the area covered by visible yellowish-brown oil film, with probabilities in excess of 40 % of the 10 g/m^2 threshold being exceeded restricted to 5-6 km northeast of the release site during summer. Similarly during winter this threshold exceedance of greater than 40 % probability would occur only in within regions of less than 3-4 km directly offshore from the release site. Rainbow and silvery sheens would spread well beyond this zone, mostly in north to north-western and south-western directions during summer, and north-north-east to south-west during winter, as indicated in Figure 6-4 and Figure 6-5.

There is a 100 % estimated probability that some heavy oil will contact the shore somewhere within Mermaid Sound (Figure 6-6). This was found to be the case during both seasonal simulations. During summer, there is the highest frequency of onshore winds from the west and southwest, hence there was the highest estimated likelihood that slicks would drift eastward onto the coast. Consistent with this, the western shoreline of the Burrup Peninsula to the north of the release site would have the highest probability of oil exposure (up to 83 %,top panel in Figure 6-6). During winter, easterlies prevail and result in high probabilities of oil exposure (up to 57 %) to the eastern shoreline of East Lewis Island (bottom panel in Figure 6-6).

Surface oil may contact the shore of the Burrup Peninsula within one hour, while it would reach West Intercourse, East Lewis and Dolphin Islands within the first 5 hours, and West Lewis and Angel Islands within the first 7-8 hours, after the spill during both summer and winter. The eastern shoreline of East Lewis Island as well as West Intercourse Island was also predicted to be at risk of exposure by slicks during both modelled seasons.

Simulations indicated that there would be no build up of entrained oil underneath slicks.

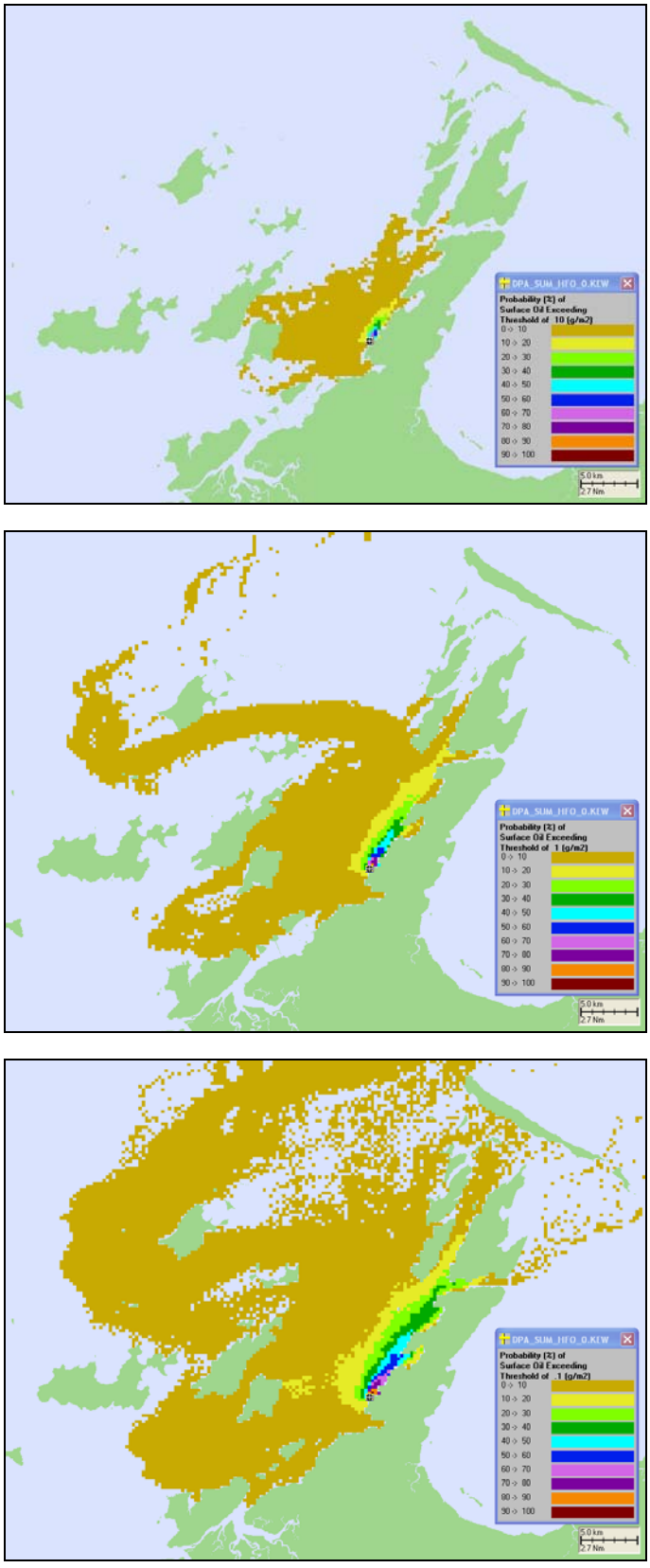

Figure 6-4 Probability of surface oil exposure (>10.0 g/m^2 in top, >1.0 g/m^2 in middle, and >0.1 g/m^2 in bottom image) from a spill of 50,000 litres of heavy fuel oil during summer. Results summarised from 100 independent simulations.

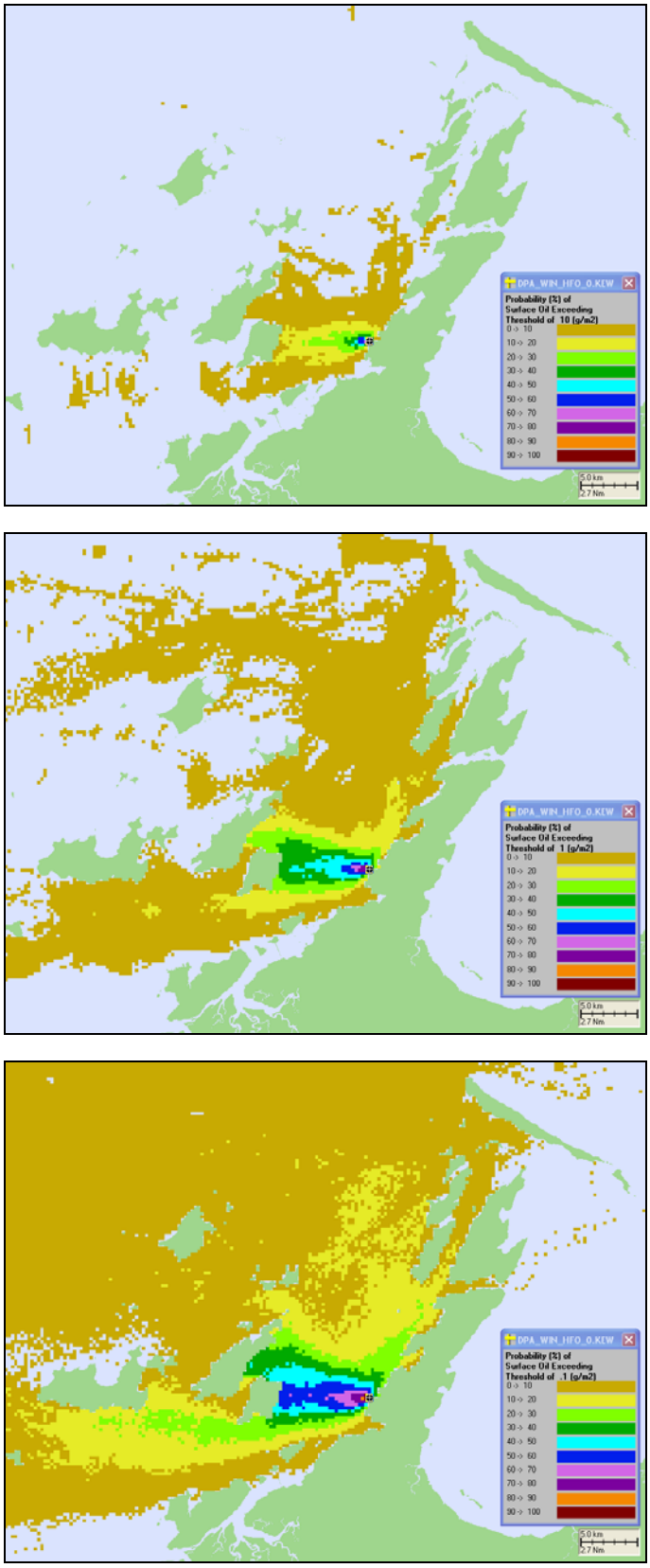

Figure 6-5 Probability of surface oil exposure (>10.0 g/m^2 in top, >1.0 g/m^2 in middle, and >0.1 g/m^2 in bottom image) from a spill of 50,000 litres of heavy fuel oil during winter. Results summarised from 100 independent simulations.

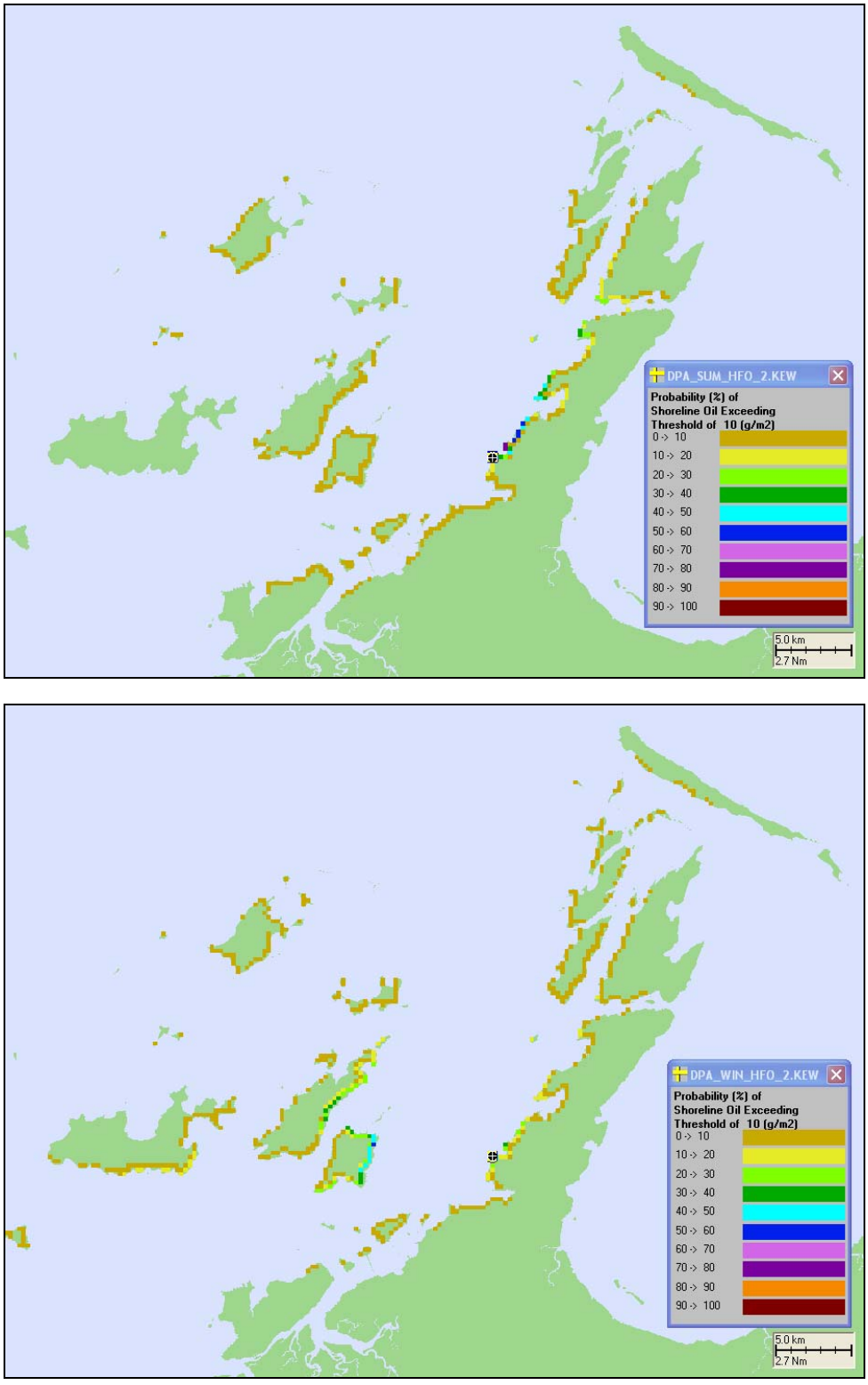

Figure 6-6 Probability of shoreline exposure above 10 g/m^2 (thickness of 10 µm) as a result of a 50,000 litres spill of heavy fuel oil under summer (top) and winter (bottom) conditions. Results summarised from 100 independent simulations.

6.4.2 Diesel spill

For the modelled spill of diesel oil, the discharge was assumed to be onto the surface waters and simulations indicate that spreading and evaporation will be the primary weathering mechanisms, although some entrainment will occur where there is breaking wind waves.

There were no slicks predicted to exceed the 10 g/m^2 threshold for the modelled seasons as the release is instantaneous and diesel weathers relatively fast. Waters within the central part of Mermaid Sound near the release site were, however, predicted to be potentially in range of slicks thicker than 1.0 g/m^2 (rainbow sheen) with probability of exposure lower than 40 % even for the most exposed areas. The results are shown for both summer and winter in Figure 6-7 and Figure 6-8 respectively. When taking a lower threshold into consideration, slicks of oil thicker than 0.1 g/m^2 (silvery sheen) would have higher (up to 70 %) probabilities of surface oil exposure and would cover a larger area to the north and south-west compared to the higher threshold of 1.0 g/m^2.

Tidal motions acting north-south along Mermaid Sound were predicted to transport slicks of diesel parallel with the Burrup Peninsula over subsequent tides. Easterly (during summer) or westerly drift (during winter) onto or off the Burrup Peninsula respectively, was a function of the prevailing winds. Slicks would have a high (up to 70 %) probability of shoreline contact with the Burrup Peninsula during summer months (top panel in Figure 6-9) when there is a high frequency of winds from the westerly, south westerly and southerly sectors. Minimum drift times were expected to be within one hour, while any site on the peninsula predicted to be oiled would receive diesel within 10 hours of the spill.

During winter, when easterly winds are more frequent, the Burrup Peninsula near the release site (probability of up to 60 %) as well as East Lewis Island (probability of up to 30 %) would have the highest probability of exposure from slicks (bottom panel in Figure 6-9). It would take less than an hour for diesel to oil the Burrup Peninsula and about 5 hours to reach East Lewis Island during winter months.

The highest probability of entrained diesel above 1 ppb is predicted to be lower than 40 %, relevant only for the waters in close vicinity of the release site and in Withnell Bay during summer (Figure 6-10, top panel). During winter, predicted probability of entrained diesel above 1 ppb did not exceed 20 % for the cases considered (Figure 6-10, bottom panel).

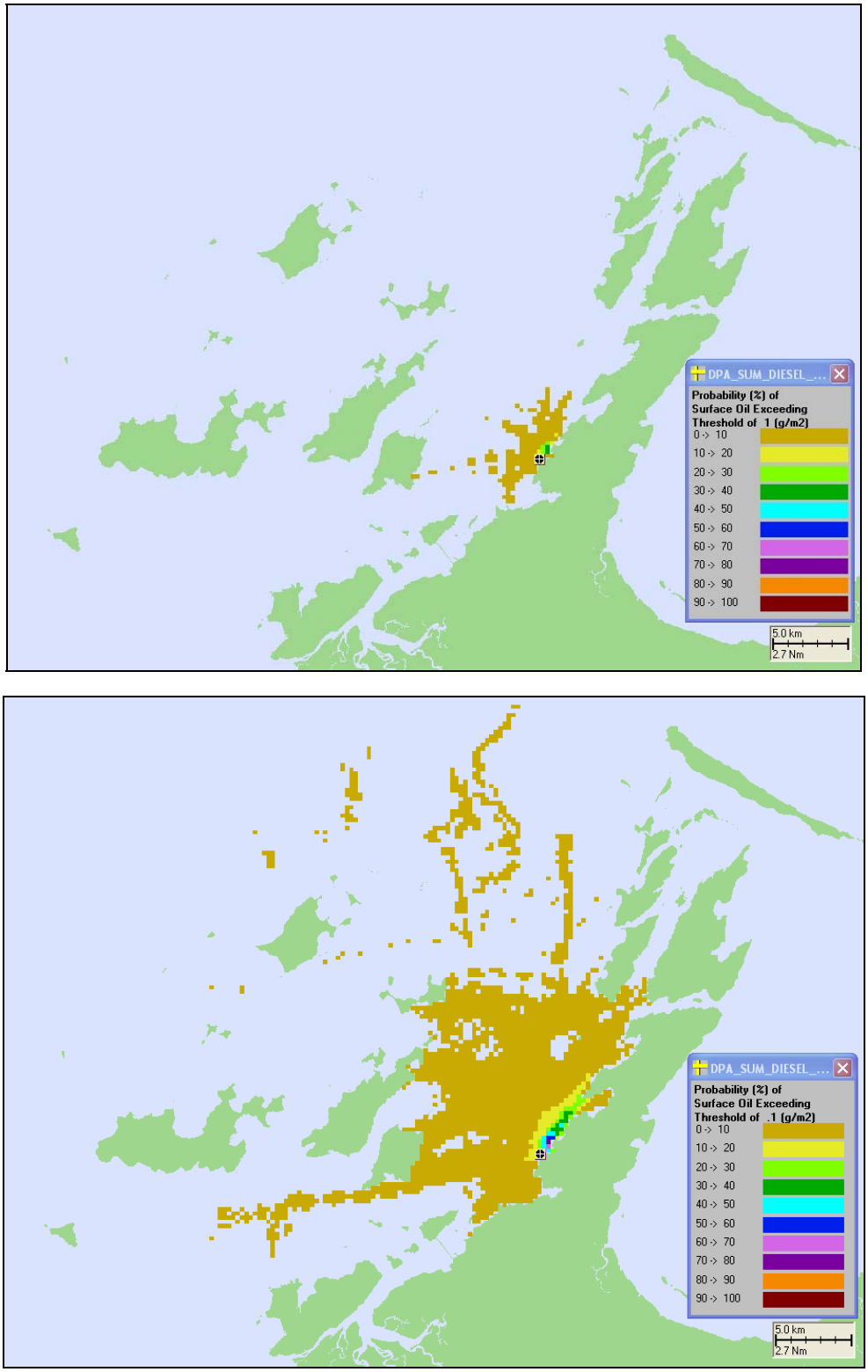

Figure 6-7 Probability of surface oil exposure (>1.0 g/m^2 in top and >0.1 g/m^2 in bottom image) from 2500 litres diesel oil spill during summer. Results summarised from 100 independent simulations.

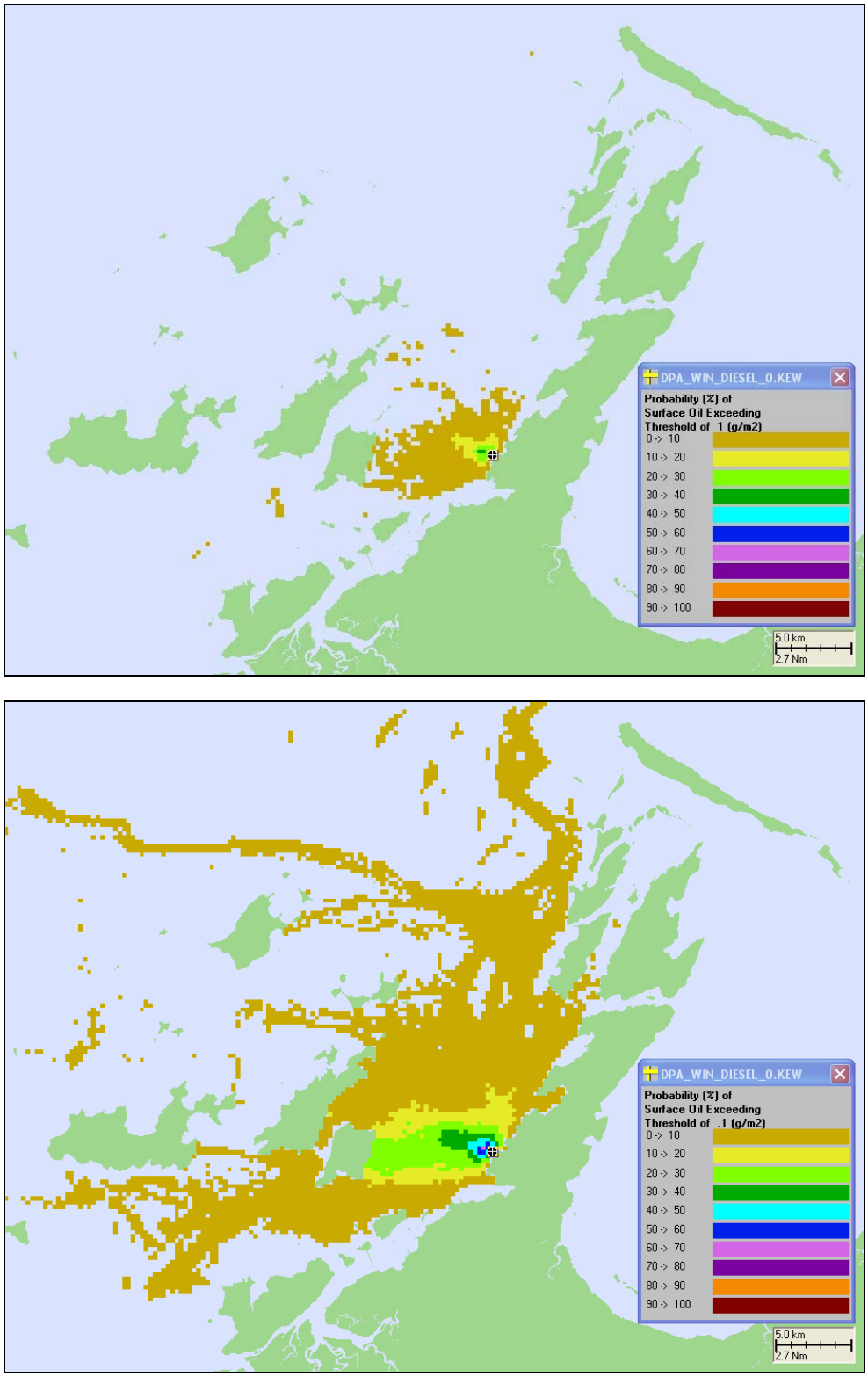

Figure 6-8 Probability of surface oil exposure (>1.0 g/m^2 in top and >0.1 g/m^2 in bottom image) from 2500 litres diesel oil spill during winter. Results summarised from 100 independent simulations.

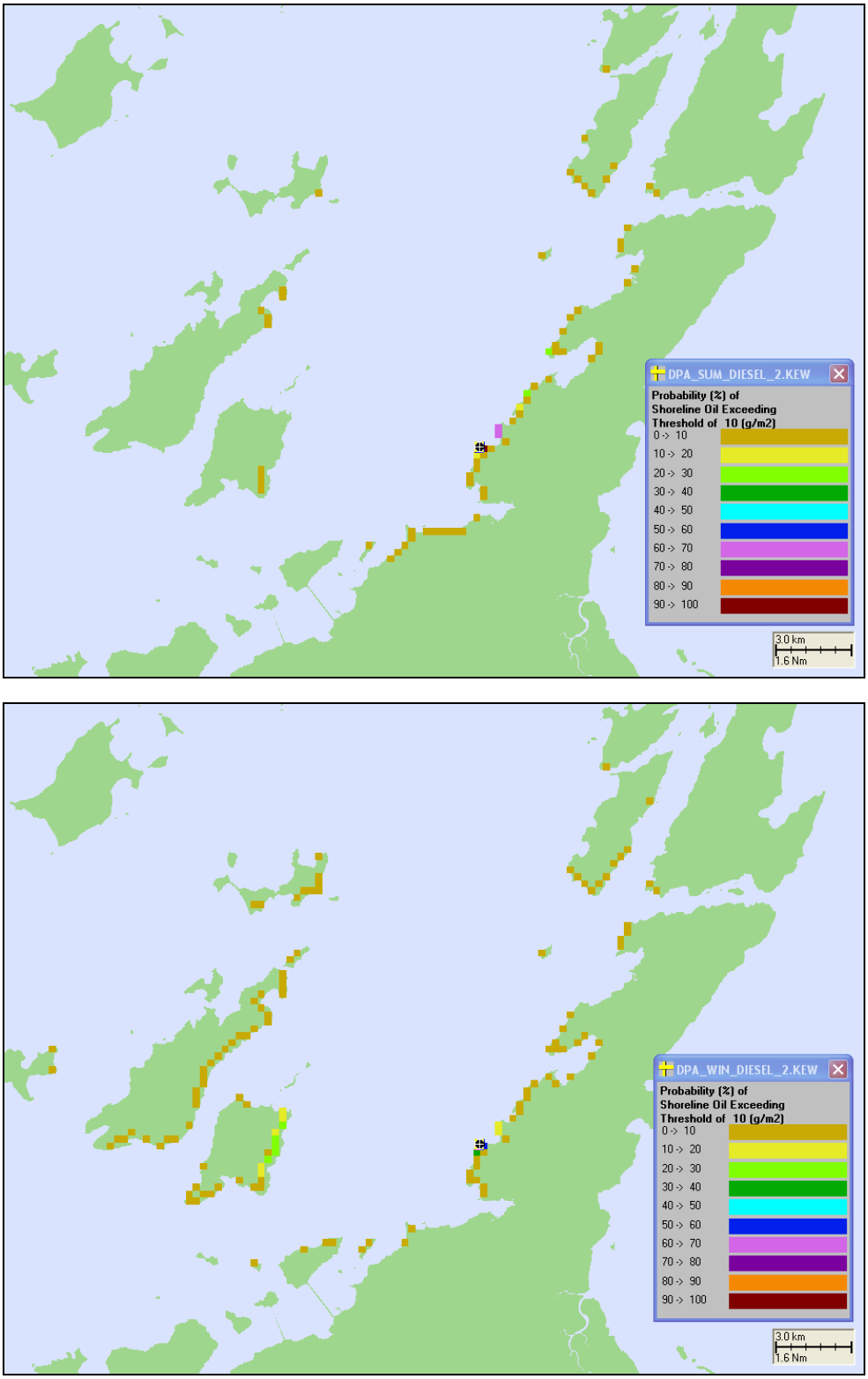

Figure 6-9 Probability of shoreline exposure above 10 g/m^2 (thickness of 10 µm) as a result of a 2500 litres spill of diesel oil under summer (top) and winter (bottom) conditions. Results summarised from 100 independent simulations.

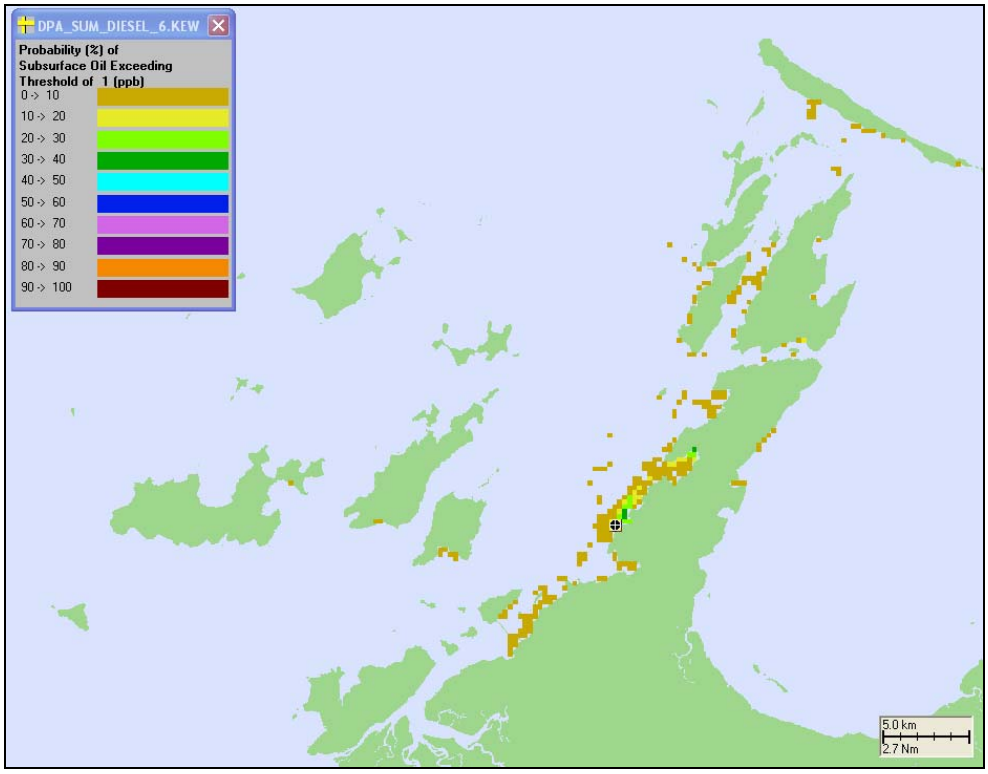

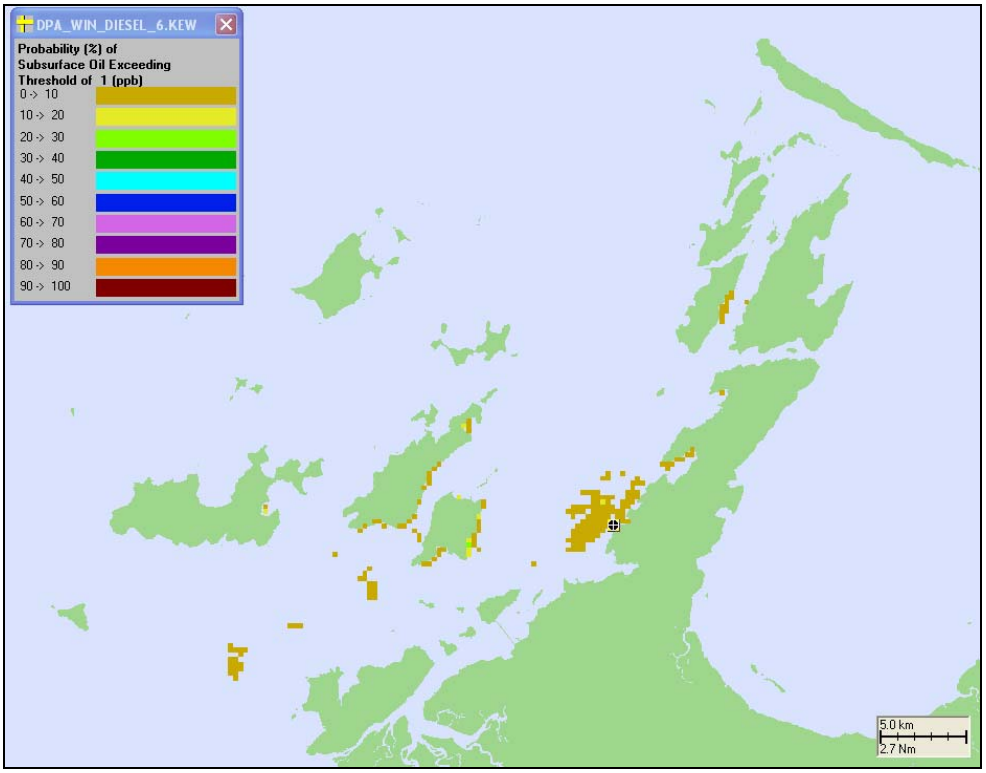

Figure 6-10 Probability of entrained oil above 1 ppb as a result of a 2500 litres spill of diesel oil under summer (top) and winter (bottom) conditions. Results summarised from 100 independent simulations.

7 ASSESSMENT OF CHANGES TO BEACH DYNAMICS

7.1 Description and Assessment Methodology

As part of the scope of this study, and to directly address a particular concern of the DEC, an assessment of the changes that the proposed port expansion may have on the beach dynamics to the immediate north of the site was conducted. This involved an examination of the changes to the current, wave and tide conditions at the beach caused by the new coastline and adjusted bathymetry as a result of the dredging.

To do this, two scenarios were developed that represented the proposed construction layout and existing layout respectively. Currents and waves were modelled for these two scenarios, forced with the same environmental conditions over the same hindcast modelling period. The modelling period used for comparison was from September 2008 to August 2009 and is expected to depict the potential change over a typical year.

7.2 Computational Grids and Bathymetry

The model domains employed for the SWAN wave model for the existing and after construction scenarios are shown in Figure 7-1. Bathymetry information for the dredge zone and the reclamation zone extents were taken from drawing 42906759-037-B in Appendix A.

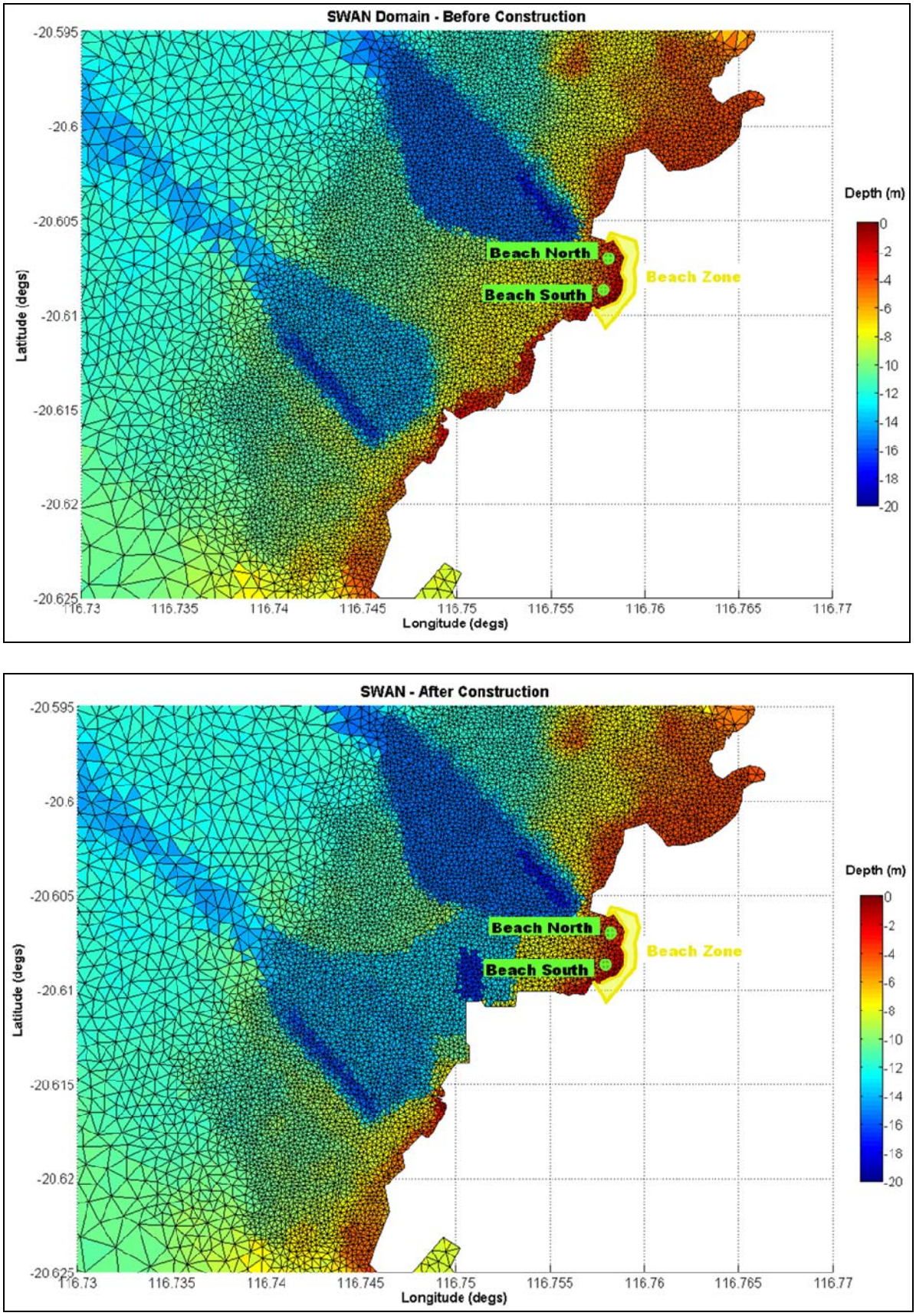

Figure 7-1 SWAN Domain and Bathymetry in the Nearshore Zone Before (top) and After (bottom) Construction.

The HYDROMAP circulation model grid was similarly adjusted with the same coastline and bathymetry information employed in the wave models, illustrated in Figure 7-1, for the existing and after construction scenarios respectively.

7.3 Results

The tide, current and wave conditions predicted by the model were examined separately to gauge the relative change in each as a result of the altered bathymetry and coastline. Two sites, named Beach North and Beach South, were selected as comparison points, with their locations illustrated in Figure 7-1. Details of these sites are provided in Table 7-1.

Table 7-1 Details of the Control Sites for the Beach Dynamics Assessment

Output Site	Location	Depth (below MSL)	Distance to Shoreline (at MSL)
Beach North	116.758 E, 20.607 S	3.8 m	60 m
Beach South	116.757 E, 20.609 S	4.7 m	65 m

The sites are situated in the north and south segments of the shallow, nearshore beach zone, where adjustments to the wave climate and currents would have the most impact on sediment resuspension and displacement. Although the model output at these two sites was analysed over the entire modelling period, only the results for the winter month of July are shown, as this was the period where the greatest change between before and after conditions was predicted.

7.3.1 Tides

Variations to the tides at the beach as a result of the modified bathymetry and coastline were expected to be minimal, if not negligible. For completeness, however, a comparison was made comparing the tidal elevations at the two reference points for the beach, with these shown in Figure 7-2 for the winter comparison period.

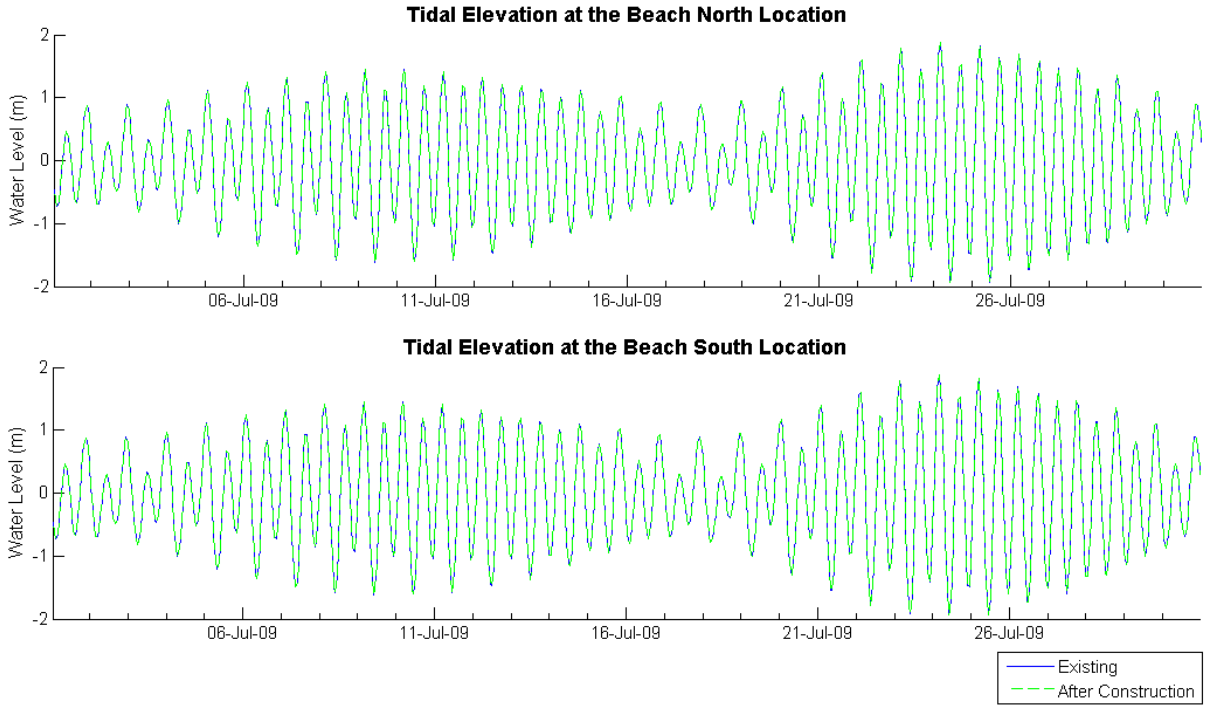

Figure 7-2 Tide Comparison at the Beach North (top) and South (bottom) Locations from the Existing and After Construction Models over July.

As expected the tidal elevation showed no difference between the existing and after construction simulations, with an IOA of 1 calculated between the two scenarios over the entire model duration.

7.3.2 Currents

The introduction of a new dredge region and adjustment to the coastline in the immediate approaches to the beach was expected to have a noticeable effect on the currents. The depth averaged currents were used in the analysis, as the shallow depths of the output locations meant that depth variations in current speed and direction were likely to be minimal. Comparison plots of the E-W and N-S current components are presented in Figure 7-3 and Figure 7-4 respectively.

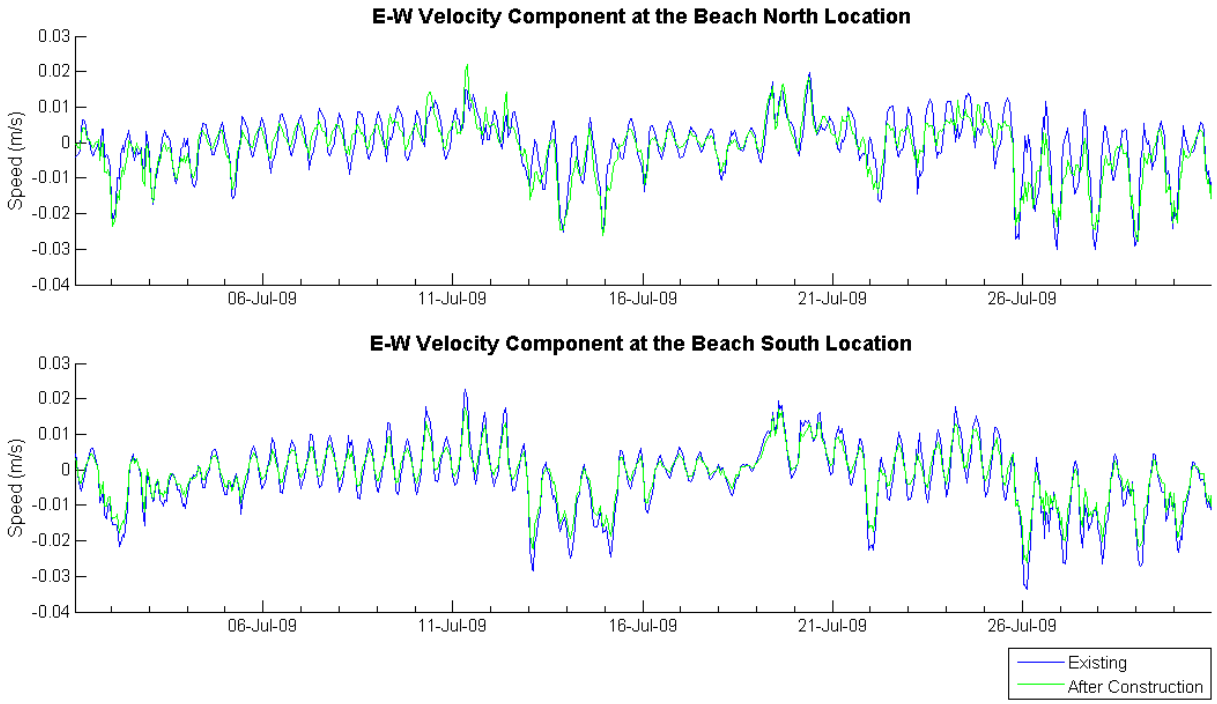

Figure 7-3 E-W Current Velocity Component Comparison at the Beach North (top) and South (bottom) Locations from the Existing and After Construction Models over July.

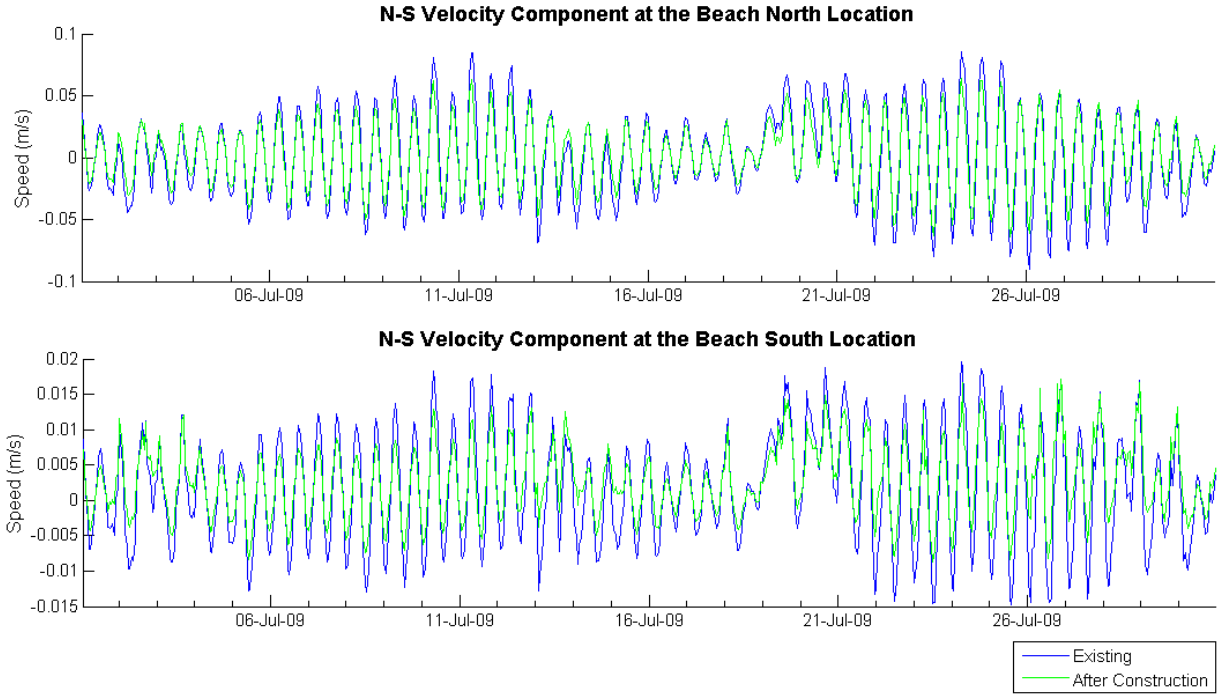

Figure 7-4 N-S Current Velocity Component Comparison at the Beach North (top) and South (bottom) Locations from the Existing and After Construction Models over July.

As the comparison plots depict, the Beach North and Beach South locations shared similar magnitudes for the E-W current velocity component. During the representative winter month the E-W current velocity IOA was 0.93 for the beach north location and 0.97 for the beach south location, indicating a strong correlation between the two scenarios.

During the winter month the N-S current velocity IOA was 0.97 for the beach north location and 0.92 for the beach south location. Both sites, particularly the Beach South location, experience a reduction in the magnitude of the currents as a result of the proposed development. This is a direct result of the obstruction to nearshore currents caused by the reclamation zone, with the effect more noticeable at the Beach South site due to its closer proximity to the development.

To further analyse the results, current speed and direction roses were produced and compared for each of the sites to better measure the degree of change in the dominant current speed and direction that was expected to occur as a result of the port expansion. Again these were produced for the representative winter month for both the Beach North and South locations. The current roses are illustrated in Figure 7-5 and Figure 7-6 for the Beach North and South sites respectively.

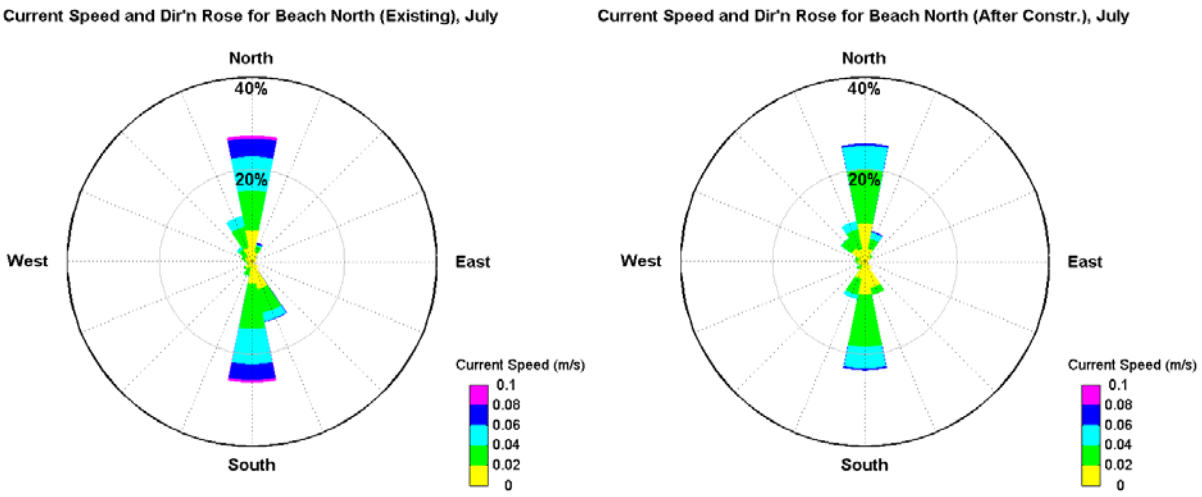

Figure 7-5 Current Speed and Direction Roses at the Beach North location for the existing and after construction scenarios during the representative summer and winter months (as titled).

Figure 7-5 clearly illustrates the reduced current magnitude and slight change in directionality, as a result of the port expansion. The representative winter month of July saw the percentage of currents exceeding 0.05 m/s fall from 9.1 % to 3.8 % for northward currents and 7.1 % to 2.7 % for the southward currents. Although the current direction is shown to be altered as a result of the modified coast and bathymetry, with northward currents offset towards the west and southward currents to the east in both the months shown, this change is only moderate with the dominant currents still acting in a north-south direction.

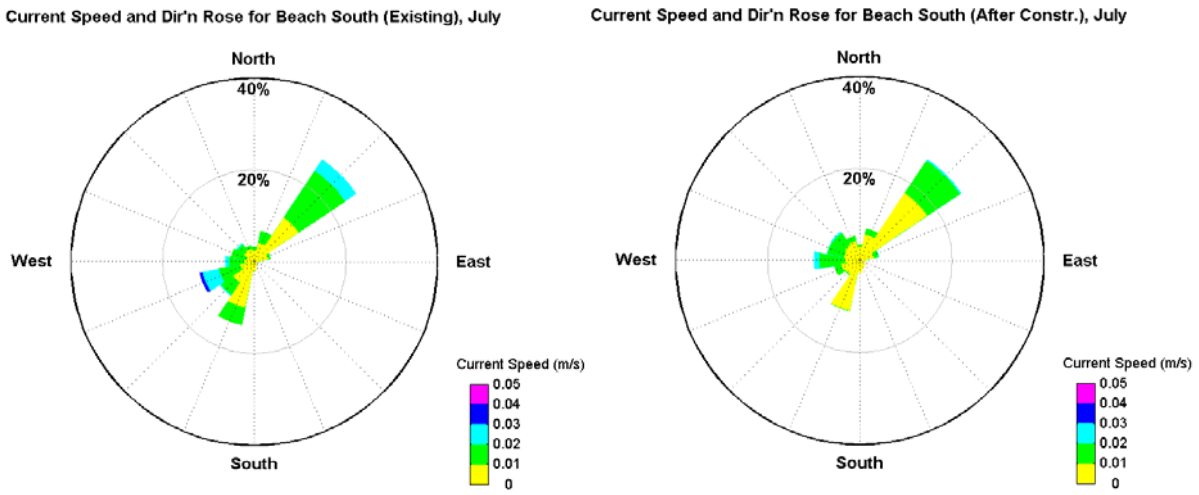

Figure 7-6 Current Speed and Direction Roses at the Beach South location for the existing and after construction scenarios during the representative summer and winter months (as titled).

The Beach South location, shown in Figure 7-6, again illustrates a slight change in current magnitude and direction as a result of the port expansion. During July, currents in excess of 0.02 m/s directed northeast (from NNE to ENE) were reduced from 2.9 % to 0.6 % and currents directed southwest (from SSW to WSW) were reduced from 4.5 % to 0 % as a results of the port expansion. As with the Beach North Site, the dominant current direction at the Beach South location remains unaffected as a result of the proposed port expansion.

7.3.3 Waves

Adjustments to the wave climate at the site were analysed through investigating changes to the dominant wave characteristics, namely significant wave height (Hs), swell height (Hswell), peak wave period (Tp), mean wave direction (Dir) and the maximum bottom orbital velocity (Ubot). Hs, Tp and Ubot all directly influence particle re-suspension rates, and are therefore expected to have the greatest impact on erosion and deposition characteristics in the nearshore zone.

Plots of the comparisons made between the existing and after construction predictions from the model are presented in Figure 7-7 for the representative winter month.

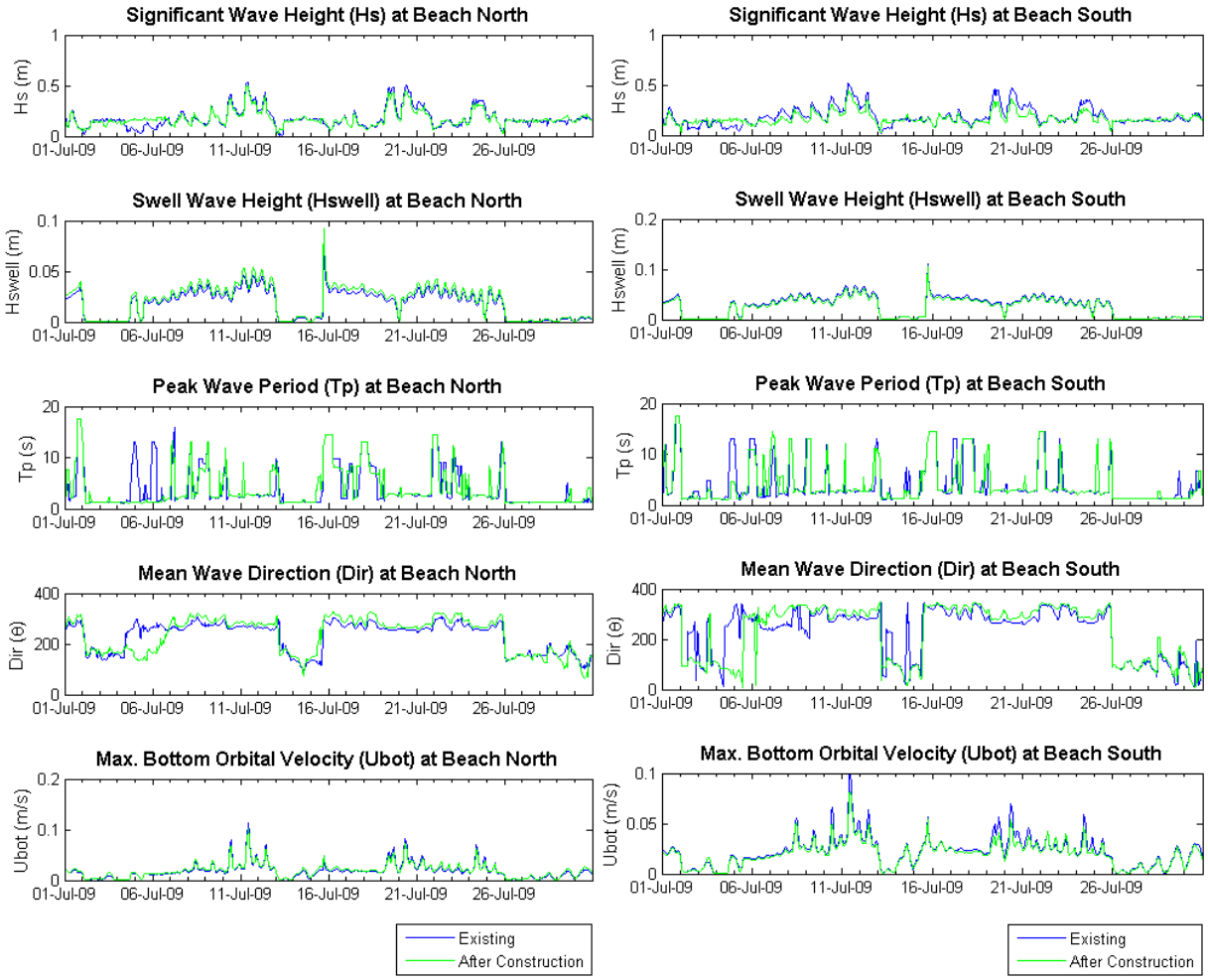

Figure 7-7 Comparison of Key Wave Parameters at the Beach North (left) and South (right) Locations from the Existing and After Construction Models over July.

For the representative winter month of July, the modified coastline and bathymetry was found to have only a minor impact on the wave conditions experienced at the two locations selected. The IOA for Hs was consistently high with 0.96 and 0.90 for the Beach North and South locations respectively. Although the correlation for Tp was moderately low at 0.90 and 0.92 for the North and South sites, the Ubot correlation was again high at 0.98 for each location. Hswell increased marginally at the Beach North site for the after construction scenario, however, Hs and Tp remained relatively unchanged in magnitude.

The Hs estimated at the Beach South location was reduced in the after construction scenario over most of the modelling period. Most of this loss in wave energy at the beach is a result of the wave shadow produced by the modified coast. To further examine the extent of this wave shadow, spatial plots of the 95th Percentile of Hs (i.e. wave height exceeded by the largest 5% of waves over a given period) were produced and analysed. These were again produced for the representative winter month pre and post construction with the results illustrated in Figure 7-8.

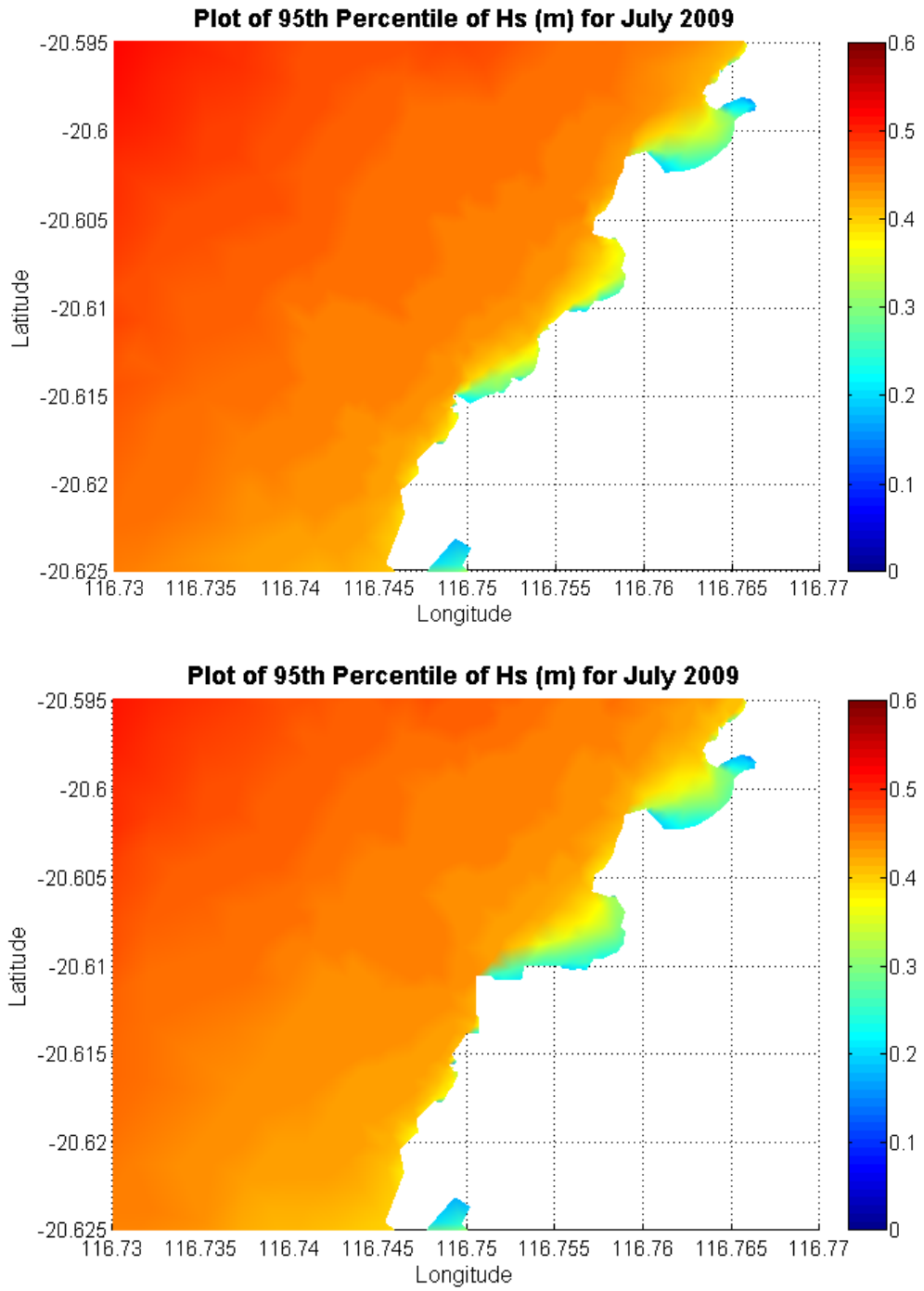

Figure 7-8 Spatial Plot of 95th Percentile of Hs for the Existing (top) and After Construction (bottom) scenarios over July.

Figure 7-8 clearly illustrates the wave shadow generated by the proposed reclamation zone on the beach. Analyzing the percentile plots over the entire model run shows that a larger wave shadow is generated during the winter month, which is a direct result of the larger portion of waves incident from the west and southwest directions during this period. Although the shadow is larger during this month, it is still highly localised, with impacts to the wave climate only occurring in regions less than 1.5 km from the northern reclamation wall. The existing shadow generated by the rocky shoals on the south side of the beach means that alteration to

the wave climate at the beach are only moderate, and focused towards the southern extents nearest the development.

7.4 Assessment and Recommendations

The results from this assessment of the changes to the current, wave and tide conditions clearly indicates that the proposed development will have only a minor effect on the current and wave conditions at the beach, with its effect on tides negligible. The reclamation zone construction and dredging is expected to marginally alter the current and wave energy at the beach zone, with an expected reduction in the overall magnitude of these at the southern extents of the beach. This effect on the beach dynamics is highly localised with impacts north of the beach expected to be negligible.

This analysis is limited in its ability to provide a quantitative assessment of the developments impact on deposition and erosion of beach material. However, as any long term change to the beach due to the post-construction modifications is expected to be very small, we recommend that a monitoring program be put in place to measure long term change. Such a program would need to include establishment of baseline conditions, and may typically be undertaken using aerial imagery, ground survey or a combination of both.

8 CONCLUSIONS

Asia-Pacific ASA (APASA) has completed a marine modelling study to assess suspended sediment plumes, potential coastal impacts and oil spill risks associated with developing infrastructure for the expansion of its existing cargo wharf and port facilities in Dampier, Western Australia. The current (HYDROMAP) and wave (SWAN) models that were developed demonstrated a high level of agreement with field observations.

The sediment fate modelling component has assessed total suspended solids (TSS) concentrations and sedimentation against the thresholds employed for the Pluto Dredging Project. These thresholds were considered appropriate for the current study following monitoring work during and after the Pluto dredging operations that suggested they represented substantially conservative levels for coral mortality.

The results from the sediment fate modelling demonstrated that:

- The suspended sediment plume is predicted to be relatively close to the Dampier coast, with concentrations above 20 mg/l restricted to the immediate region surrounding the dredge zone.
- Both scenarios indicated that the plume would extend only as far as 4 to 5 km from the dredge zone with concentrations in excess of 5 mg/l above background.
- The highest sustained plume concentrations were within 200 m of the outfall discharge point along the northern reclamation wall, with concentrations in excess of 25 mg/l observed here 6-7 % of the time during both scenarios.
- Exceedance of the nearshore TSS threshold of 35 mg/l occurred only within the immediate vicinity of the outfall discharge site, and to a lesser degree within the dredge zone and adjacent BLB turning basin.
- Exceedance of acute sedimentation are predicted to occur within the dredge zone and to a lesser extent within approximately 100 m of its perimeter, with the most severe acute exceedances occurred within 200 m of the outfall discharge zone.
- Medium and chronic term thresholds exceedance was restricted to the extents of the dredge zone and predicted to be exceeded less than 15 days over the entire dredge operation.
- Areas more than 5 km from the DMSF development site are predicted to remain below the designated TSS and sedimentation thresholds for the entire dredging operation under ambient conditions. Exceedance of the nearshore TSS threshold of 35 mg/l was predicted to occur primarily within the immediate vicinity of the outfall discharge site, and to a lesser degree within the dredge zone and adjacent BLB turning basin.
- Offshore exceedances were predicted during the energetic scenario as a result of resuspension during cyclone events, however, these are not expected to be significantly in excess of background rates.

- Exceedance of acute sedimentation thresholds are predicted to occur within the dredge zone and to a lesser extent within approximately 100 m of its perimeter.
- The most severe acute exceedances are predicted to occur within 200 m of the outfall discharge zone, where more than 50 days of exceedance was predicted during the dredging operations.
- Exceedance of the medium and chronic term thresholds are expected to be restricted to the extents of the dredge zone and predicted to be exceeded less than 15 days over the entire dredge operation.
- Areas more than 5 km from the DMSF development site are predicted to remain below the designated TSS and sedimentation thresholds for the entire dredging operation under ambient conditions.
- Predicted sedimentation within the Pluto turning basin indicated an average increase of 0.6 to 1.6 mm over the entire turning basin, with a maximum increase of 11 mm along the south-western extent.

In addition to the dredge dispersion modelling, oil spill modelling was conducted to assess the exposure risk of an accidental hydrocarbon release at the port. This included simulations of a summer and winter simulation of both a 50,000 litre heavy fuel oil spill off the face of the wharf and 2,500 litre diesel fuel spill from alongside the wharf. The results from the oil spill modelling show that:

- Weathering analysis of heavy fuel oil indicated only a 10 % reduction in its mass would occur over a period of 5 days, whilst 40 % of the diesel fuels mass will evaporate over the first two days of exposure.
- The heavy fuel oil would likely drift north-east against the Burrup Peninsula toward Angel Sound during summer and west toward East and West Lewis Islands during winter.
- Probabilities of surface oil thicknesses harmful to seabirds in excess of 40 % were restricted to 5-6 km in a northeast direction from the spill site during summer and 3-4 km directly offshore during winter.
- The model predicts that the heavy oil will contact the shoreline somewhere within Mermaid Sound, with an 83 % probability that this will occur to the immediate north of the release site during summer and 57% probability of contact to the eastern shoreline of East Lewis Island during winter.
- Simulations indicated there would be no build up of entrained heavy fuel oil underneath slicks.
- There were no slicks predicted to reach levels detrimental to seabirds for the diesel fuel spill, with exceedances of lower thresholds only moderate even in exposed areas.

- Prevailing winds during summer again moved the diesel slicks northeast along the Burrup Peninsula, with winter characterised by offshore movement as with the heavy fuel oil scenarios.
- During winter, shoreline exposure to the Burrup Peninsula near the release site has a probability of 60 %,with a 30 % probability of shoreline exposure for East Lewis Island.
- The highest probability of entrained diesel concentrations being above 1 ppb is predicted to be lower than 40 %, relevant only for the waters in close vicinity of the release site and in Withnell Bay during summer.
- During winter, the predicted probability of entrained diesel concentrations above 1 ppb was below 20 %.

An assessment of the alterations to the existing beach dynamics to the north of the site was conducted to assess the ongoing impact of the proposed development structures on the beach morphology. The results indicated that:

- The proposed development will have only a minor effect on the current and wave conditions at the beach to the immediate north of the DMSF site, with its effect on tides negligible.
- The reclamation zone construction and dredging is expected to marginally alter the current and wave energy at the beach zone, with an expected reduction in the overall magnitude at the southern extents of the beach.
- This effect on the beach dynamics is highly localised with impacts north of the beach expected to be negligible.

REFERENCES

ANDERSON, E., B. JOHNSON, T. ISAJI & E. HOWLETT. 2001. *RE: SSFATE (Suspended Sediment FATE), a model of sediment movement from dredging operations.* Type to PRESENTED AT WODCON XVI WORLD DREDGING CONGRESS.

APASA 2006. Pluto LNG Sediment Dispersion Study-Dredging Operations Associated with Construction of a Navigation Channel, Installation of a Subsea Gas Export Trunkline and Disposal of Spoil. Report prepared for SKM.

BOM 1992. Report on Cyclone *Orson* April 1989. *In:* BUREAU OF METEOROLOGY (ed.). Department of the Arts, Sport, the Environment and Territories.

BOM. 2000. *Tropical Cyclone Steve* [Online]. Perth Bureau of Meteorology. Available: http://www.bom.gov.au/info/cyclone/steve/index.shtml [Accessed 17 June 2009 2009].

BOM. 2006. *Tropical Cyclone Clare* [Online]. Perth Bureau of Meteorology. Available: http://www.bom.gov.au/weather/wa/cyclone/clare/index.shtml [Accessed 17 June 2009 2009].

BONN AGREEMENT 2004. Bonn Agreement Aerial Surveillance Handbook Bonn Agreement.

BROWN, H. M., OWENS, E. H. & GREEN, M. Year. Submerged and sunken oil: Behavior, response options, feasibility and expectations. *In:* Proceedings of the 21st Arctic and Marine Oil Spill Program Technical Seminar (AMOP) Technical Seminar, 1998 Alberta, Canada.

COFFEY 2008. Factual Report, Nearshore Geotechnical Investigation, Dampier Cargo Berth Expansion Project. Prepared for Dampier Port Authority, October 2008

DAVIES, A. M. Year. The numerical solutions of the three-dimensional hydrodynamical equations using a B-spline representation of the vertical current profile. *In:* NIHOUL, J. C. J., ed. 8th liege colloquium on Ocean hydrodynamics, 1977a. Elsevier 49-68.

ELDEBERKY, Y. & BATTJES, J. A. 1996. Spectral modelling of wave breaking: Application to Boussinesq equations. *J. Geophys. Res.,* 101**,** 1253-1264.

FINGAS, M. F. 2000. *The Basics of Oil Spill Cleanup*. *CRC Press***,** 256.

FINGAS, M. F. & BROWN, C. E. Year. *Review of Oil Spill Remote Sensing*. *In:* Proceedings of Spillcon 2000, 2000 Darwin, Australia.

FRENCH, D. Year. Modeling the impacts of the North Cape Oil Spill. *In:* Twenty-first Arctic and Marine Oil Spill Program (AMOP), Technical Seminar, 1998 Alberta, Canada. 387-430.

FRENCH, D., REED, M., JAYKO, K., FENG, S., RINES, H., PAVIGNANO, S., ISAJI, T., PUCKETT, S., KELLER, A., FRENCH III, F. W., GIFFORD, D., MCCUE, J., BROWN, G., MACDONALD, E., QUIRK, J., NATZKE, S., BISHOP, R., WELSH, M., PHILLIPS, M., INGRAM, B.S., 1996. The CERCLA type A natural resource damage assessment model for coastal and marine environments (NRDAM/CME). *Technical Documentation, Vol. I - Model Description. Final Report, .* Office of Environmental Policy and Compliance, U.S. Dept. of the Interior, Washington, DC.

FRENCH, D., SCHUTTENBERG, H. & ISAJI, T. Year. Probabilities of oil exceeding thresholds of concern: examples from an evaluation for Florida Power and Light. *In:* Proceedings of the 22nd Arctic and Marine Oil Spill Program (AMOP) Technical Seminar, June 1999, 1999. Environment Canada, pp. 243-270.

GORDON, R. 1982. *Wind driven circulation in Narragansett Bay, Ph. D. Thesis.* University of Rhode Island, Department of Ocean Engineering, Kingston, RI, 161 pp.

HASSELMANN, K. 1974. On the spectral dissipation of ocean waves due to whitecapping. *Bound.-layer Meteor.,* 6**,** 107-127.

HEARN, C. & HOLLOWAY, P. 1990. A Three-Dimensional Barotropic Model of the Response of the Australian North West Shelf to Tropical Cyclones. *Journal of Physical Oceanography,* 20**,** 60-80.

HOLTHUIJSEN, L. H., BOOIJ, N., RIS, R., ANDORKA GAL, J. H. & DE JONG, J. C. M. Year. A verification of the third-generation wave model "SWAN" along the southern North Sea coast. *In:* Proceedings 3rd International Symposium on Ocean Wave Measurement and Analysis, 1997 WAVES '97, ASCE. 49-63.

ISAJI, T., HOWLETT, E., DALTON, C. & ANDERSON, E. Year. Stepwise-Continuous-Variable-Rectangular Grid. *In:* 24th Arctic and Marine Oilspill Program Technical Seminar, Zigic et al., 2003, 2001. 597-610.

ISAJI, T. & SPAULDING, M. 1984. Notes and Correspondence. A Model of the Tidally Induced Residual Circulation in the Gulf of Maine and Georges Bank. *Journal of Phys. Ocean.***,** 1119-1126.

JOHNSON, B. H., ANDERSON, E., ISAJI, T. & CLARKE, D. G. 2000. Description of the SSFATE numerical modeling system. DOER Technical Notes Collection (TN DOER-E10). *U.S. Army Engineer Research and Development Center, Vicksburg, MS. .*

KATSUMATA K. 2006. Tidal stirring and mixing on the Australian North West Shelf. *Marine and Freshwater Research,* 57**,** 243-254.

KOMEN, G. J., HASSELMANN, S. & HASSELMANN, K. 1984. On the existence of a fully developed wind-sea spectrum. *J. Phys. Oceanogr.,* 14**,** 1271-1285.

KROOPS, W., JAK, R. G. & VAN DER VEEN. Year. Use of dispersants in oil spill response to minimize environmental damage to birds and aquatic organisms. *In:* Interspill 2004, Presentation no. 429, 2004. D.P.C.

MADSEN, O. S., POON, Y.-K. & GRABER, H. C. Year. Spectral wave attenuation by bottom friction: Theory. *In:* 21 th Int. Conf. Coastal Engineering, ASCE, 1988. 492-504.

MSCIENCE 2009a. Dampier Marine Services Facility: Water Quality Impacts For The Pluto Program in an Area of Intensive Dredging, (REP No. MSA142R2). Perth, WA.

MSCIENCE 2009b. Dampier Port Wharf Construction: Water Quality Descriptors (REP No. MSA142R1) Perth, WA.

NOAA 1997. *Aerial Observations of Oil at Sea (96-97* HAZMAT *Report)*. National Oceanic and Atmospheric Administration, Seattle, Washington.

OWEN, A. 1980. A three-dimensional model of the Bristol Channel. *J. Phys. Oceanography,* 10**,** 1290-1302.

PRIESTLY, C. 2009. Dampier Marine Services Facility (DMSF) Oil Spill Risk Assessment. RESPONSE RESOURCE MANAGEMENT PTY LTD

SKM 2007. Pluto LNG Project: Revised Simulation and Impact Assessment of Disposal into Spoil Ground 2B. Perth, WA: Sinclair Knight Merz Pty Ltd.

SOULSBY, R. 1997. *Dynamics of Marine Sands: A manual for Practical Applications*, HR Wallingford.

SPAULDING, M. L., BISHNOI, P. R., ANDERSON, E. & ISAJI, T. Year. An integrated model for prediction of oil transport from a deep water blowout. *In:* submitted to the Arctic and Marine Oil Spill Program (AMOP) Technical Seminar, 2000 Alberta, Canada.

SPAULDING, M. L., KOLLURU, V. S., ANDERSON, E. & HOWLETT, E. 1994. Application of three-dimensional oil spill model (WOSM/OILMAP) to hindcast the Braer Spill. *Spill Science & Technology Bulletin,* 1**,** 23.

STODDART, J. A. & ANSTEE, S. 2005. Water quality, plume modelling and tracking before and during dredging in Mermaid Sound, Dampier, Western Australia. *Corals of the Dampier Harbour: Their Survival and Reproduction During the Dredging Programs of 2004, Mscience Pty Ltd.* Perth WA.

SWANSON, J., ISAJI, T., CLARKE, D. & DICKERSON, C. Year. Simulations of dredging and dredged material disposal operations in Chesapeake Bay, Maryland and Saint Andrew Bay, Florida. *In: Proceedings* of the 36th TAMU Dredging Seminar, WEDA XXIV, 2004 Orlando, Fl.

SWANSON J.C., ISAJI T. & GALAGAN C. Year. Modeling the Ultimate Transport and Fate of Dredge-Induced Suspended Sediment Transport and Deposition. *In:* Proceedings of Wodcon 2007, 2007 Lake Buena Vista, Florida.

SWANSON, J. C., ISAJI, T. & GALAGAN, C. Year. Modeling the Ultimate Transport and Fate of Dredge-Induced Suspended Sediment Transport and Deposition. *In:* Proceedings of Wodcon 2007, 2007 Lake Buena Vista, Florida.

SWANSON, J. C., ISAJI, T., WARD, M., JOHNSON, B. H., TEETER, A. & CLARKE, D. G. 2000. Demonstration of the SSFATE numerical modeling system. *DOER Technical Notes Collection (TN DOER-E12).* U.S. Army Engineer Research and Development Center, Vicksburg, MS.

TEETER, A. M. 2001. *Clay-silt sediment modelling using multiple grain classes. Part I:Settling and deposition, Coastal and Estuarine Fine Sediment Processes*, WH McAnally and AJ Mehta (Eds), Elsevier Science BV.

TOLMAN, H. L. 2002. Testing of WAVEWATCH III Version 2.22 in NCEP's NWW3 Ocean Wave Model Suite, Technical Note No. 214.

USACE 2008. *Dredging Operations and Environmental Research Program - The Four Rs of Environmental Dredging: Resuspension, Release, Residual, and Risk,* Washington, DC, US Army Corps of Engineers.

WILLMOTT, C., ACKLESON, S., DAVIS, R., FEDDEMA, J., KLINK, K., LEGATES, D., O'DONNELL, J. & ROWE, C. 1985. Statistics for the evaluation and comparison of models. *Journal of Geophysical Research,* 90**,** 8995 - 9005.

WILLMOTT, C. J. 1981. On the Validation of Models. *J. Phys. Oceanogr.,* 2**,** 184-194.

ZIGIC, S., ZAPATA, M., ISAJI, T., KING, B. & LEMCKERT, C. Year. MODELLING OF MORETON BAY USING AN OCEAN/COASTAL CIRCULATION MODEL. *In:* Proceedings from the Coasts & Ports Australasian Conference, 2003.

APPENDIX A

Proposed Development and Harbour Layout

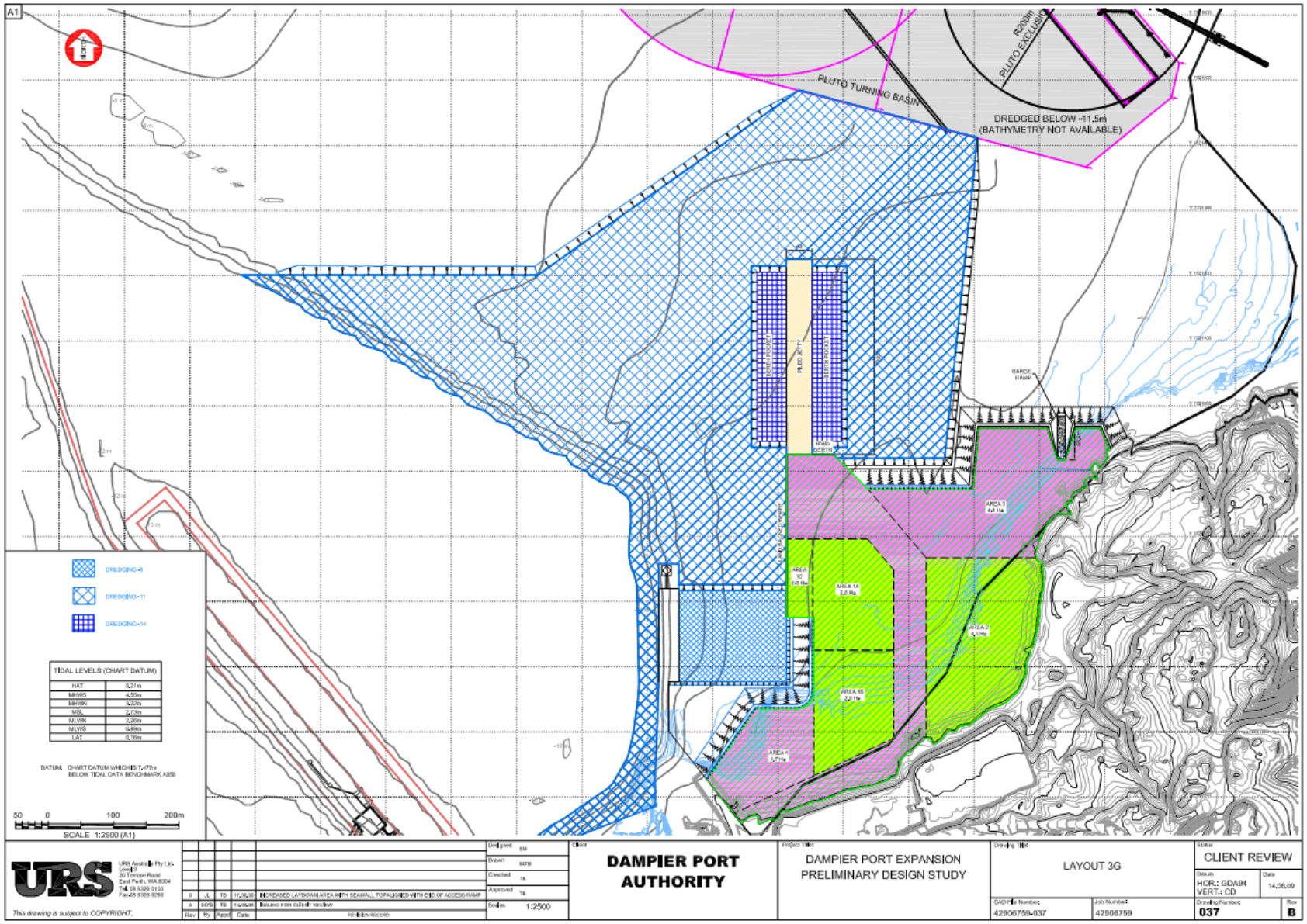

Figure A-1: Proposed development option 3G showing reclamation zones and dredging depths.

APPENDIX B

Estimated Dredge Volumes and Dredge Cut Sequence

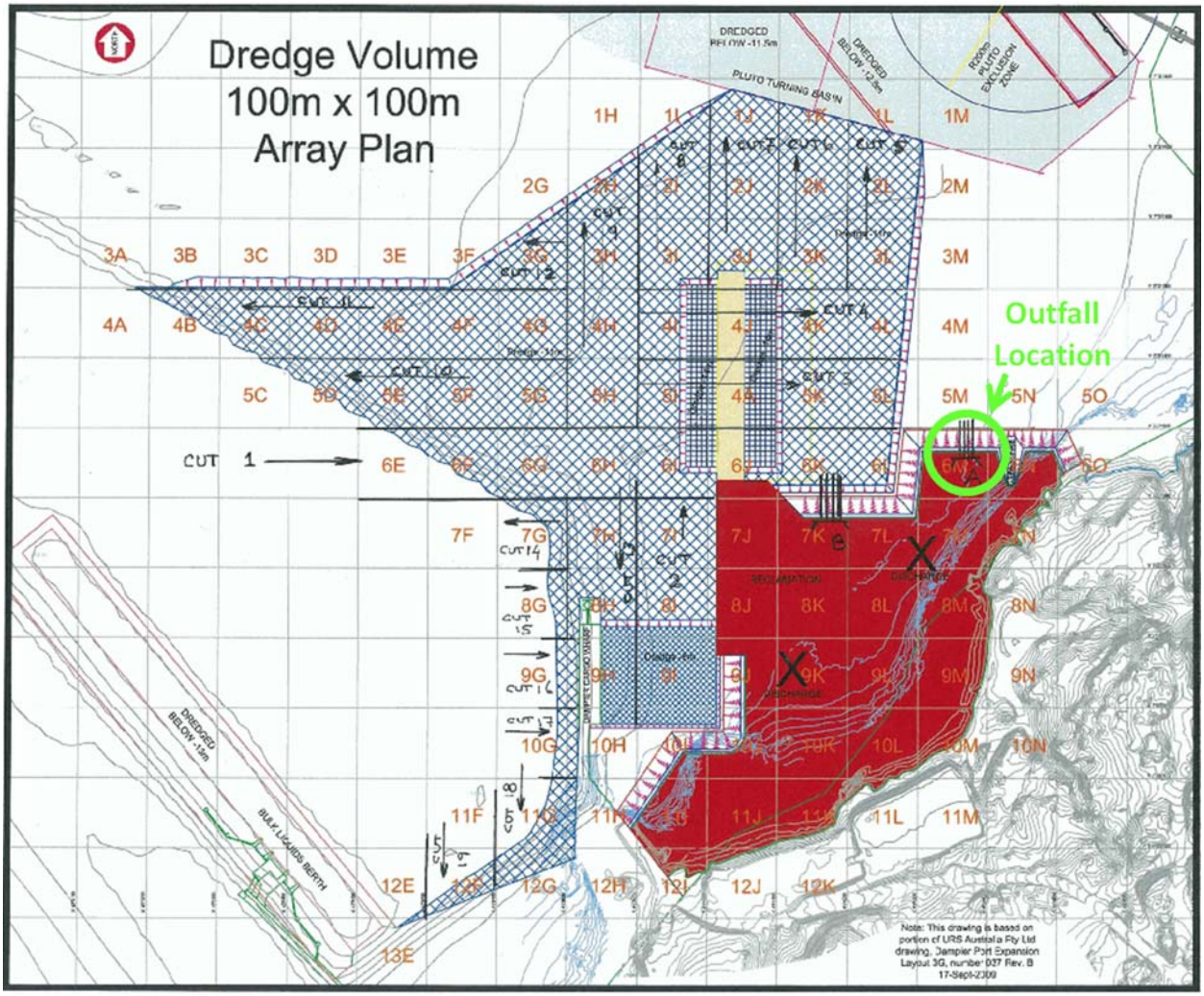

DREDGE CUT SEQUENCE

	CUT DIRECTION →							
CUT	ARRAY							
1	6E	6F	6G	6H	6I	6J	6K	6L
2	9I	8I	71					
3	5I	5J	5K	5L				
4	4I	4J	4K	4L	4M			
5	3L	2L	1L					
6	3K	2K	1K					
7	3J	2J	1J					
8	3I	2I	1I					
9	5H	4H	3H	2H	1H			
10	5G	5F	5E	5D	5C			
11	4G	4F	4E	4D	4C	4B	4A	
12	3G	3F	3E	3D	3C	3B	3A	
13	7H	8H	9H	10H				
14	7G							
15	8G							
16	9G							
17	10G							
18	11G	12G						
19	12F	12E	13E					

Figure B-1: Schematic of the indicative dredge cut sequence and 100 m dredge volume cells (top). Cells included in cuts 1-19 are also indicated (bottom).

Dampier Marine Services Facility Project
Preliminary Calculated Dredge Volumes by 100m x 100m Array
(To be read with reference to Dredge_Volume_Array_Plan_42906759-037-B_R2004.pdf)
(Digital Model: DPA_Port_Expansion_Dredge_Model.pro)

Total 2,103,600 m3

	A	B	C	D	E	F	G	H	I	J	K	L	M	N	O
1								100	17,700	21,800	11,000	1,000			
2							2,500	27,600	44,200	45,000	47,900	46,000	4,000		
3	100	2,000	2,100	2,600	3,000	8,500	34,100	43,800	48,400	53,200	55,700	58,500	5,000		
4	0	7,000	22,000	30,400	33,400	35,900	39,700	45,000	60,400	74,100	58,600	56,300	1,500		
5				10,400	26,800	37,300	43,700	48,600	62,900	76,200	61,000	51,500	0		
6					1,100	17,700	38,700	50,300	61,800	56,500	62,100	43,900			
7							5,000	45,100	57,800	3,600					
8							1,800	33,500	51,300	1,300					
9							1,000	11,500	26,200	900					
10							700	5,700	6,700	1,900					
11							7,900	9,300							
12						8,200	22,400	1,000							
13					200										

Figure B-2: Preliminary calculation of dredge volumes per cell. All volumes shown are in m^3.